Universidad Autónoma de Madrid

Universidad Autónoma de Madrid

Departamento de Biología Molecular

Characterization of Human Adenovirus Assembly: Structural Studies in the Cell and in Purified Incomplete Viral Particles.

- TESIS DOCTORAL –

Gabriela Condezo

Madrid, 2015

Universidad Autónoma de Madrid

Departamento de Biología Molecular

Facultad de Ciencias

Universidad Autónoma de Madrid

Characterization of Human Adenovirus Assembly: Structural Studies in the Cell and Purified Incomplete Viral Particles

Memoria presentada para optar al grado de Doctor en Bioquímica,
Biología Molecular, Biomedicina y Biotecnología (Biociencias Moleculares)

Gabriela Condezo

DIRECTORA DE TESIS:

Dr. Carmen San Martín
Centro Nacional de Biotecnología-CSIC

CNB
CENTRO NACIONAL DE BIOTECNOLOGIA

CSIC

El trabajo recogido en esta memoria ha sido realizado en el Centro Nacional de Biotecnología (CNB-CSIC) bajo la dirección de la Dra. Carmen San Martín Pastrana, y actuando como tutor académico el Dr. Iván Ventoso. Su financiación corrió a cargo de una beca JAE-PreDoc del Consejo Superior de Investigaciones Científicas (CSIC). También se contó con la aportación de diversos proyectos: BFU2007-60228/BMC (MICINN), BFU2010-16382 (MINECO), BFU2013-41249-P (MICINN) y BioStruct-X (número de contrato 283570).

Agradecimientos

En los últimos 6 años he aprendido un montón de técnicas y conocimientos de la mano de personas extraordinarias a nivel profesional y con un gran calor humano. A todos ellos quiero agradecer su apoyo, colaboración y paciencia…

A Carmen muchísimas gracias por permitirme trabajar en tu grupo. Gracias por toda tu ayuda durante este tiempo, eres una excelente jefa y una maravillosa persona. Jamás olvidaré todo lo que has hecho para ayudarme con Extranjería, has evitado que me deporten por lo menos dos veces.

A mis compañeros de laboratorio: Ana, Rosa, Álvaro, María y Marta gracias por vuestros consejos, ayuda y por enseñarme un montón de protocolos. Ustedes han sido colaboradores en el desarrollo de esta tesis, gracias chicos.

Al servicio de microscopía confocal: Silvia, Susana y Ana muchísimas gracias por su ayuda y consejos durante la toma de datos. También quiero agradecer todas esas tardes con buena música y dulces.

Al servicio de microscopía electrónica: Cristina, Javi y Rocío gracias por vuestro apoyo, asesoramiento y colaboración. En especial quiero agradecer la gran cantidad de horas que dedicaron a enseñarme los distintos protocolos empleados en esta tesis, Cristina y Javi muchísimas gracias por vuestra paciencia.

Al laboratorio de estructura celular: Cristina, Laura e Isabel gracias por vuestro asesoramiento, consejos y ayuda durante la elaboración de esta tesis. Vuestras ideas me ayudaron muchísimo en la búsqueda de la factoría de Adenovirus.

Al Lab S0: María José, Michele y Javi gracias por vuestros consejos y por enseñarme sus trucos para preparar las muestras.

Al Lab B13: Roberto, Joaquín, Jesús y José Miguel gracias por vuestro apoyo en el área de informática, sin vuestra ayuda todavía estaría procesando datos o intentando descargar programas. A José María muchas gracia por su apoyo económico para concluir este proyecto. Blanca gracias por todo el papeleo que tuviste que hacer para mi contrato.

Al Lab. 213: Silvia gracias por tu ayuda con el southern blot, el esperma de salmón es en definitiva el reactivo más curioso que he usado, incluso supera la laca de uñas y la gelatina de pollo.

Al servicio de microscopía electrónica del CBM: Maite muchísimas gracias por tu ayuda con las secciones, protocolos y anticuerpos. Los paseos al CBM me servían para despejar la mente; aunque en verano no era tan bonito sobre todo al medio día.

Al CBATEG: Miguel muchísimas gracias por tu colaboración y apoyo constante durante todo este tiempo, estudiar tu mutante Ad5/FC31 ha sido muy interesante, entretenido y a veces estresante, específicamente el extraer el DNA a las partículas ligeras.

A Jane Flint gracias por permitirnos usar el mutante *ts1* como control, el encontrar las mismas estructuras que en Ad5/FC31 nos llevó en la dirección correcta hacia la elaboración del modelo de ensamblaje.

Al departamento de personal y a la oficina de acogida al estudiante extranjero, muchísimas gracias por todo su asesoramiento legal, me ahorraron más problemas con extranjería.

A mis amigas Meriem y Analu muchísimas gracias por vuestro cariño, palabras de aliento en el momento preciso, consejos, risas, paseos, compras; creo que mi estancia en el CNB no habría sino lo mismo sin ustedes. Gracias por estar a mi lado.

Mariale gracias por tu amistad todos estos años, sin tu ayuda y consejos no estaría aquí en España, un beso amigui y mucho ánimo que la próxima defensa es la tuya.

A mi pequeña familia en España: Ana, Sandra, Roxana y Elizabeth gracias vuestro cariño y amistad. Lejos de mi familia me han hecho sentir como en casa.

A mi familia, gracias por estar en todo momento conmigo, con el skype nunca sentí que estaban lejos. A mi padre gracias por presionarme a estudiar, a buscar mi crecimiento profesional. A mi madre gracias por tus consejos, tus historias de animalitos o películas interesantes, en fin por alegrarme las noches. También quiero darte las gracias por preocuparte y estar pendiente de mí en todo momento. A mi hermanita, gracias por tus detalles conmigo, sé que también ha sido duro para ti estudiar en otro país y vivir sola pero ya ves, lo conseguimos.

Presentación

Los Adenovirus (AdV) se encuentran entre los más complejos de los virus icosaédricos carentes de membrana. Incluso después de resolverse su estructura a resolución cuasi-atómica tanto por crio-microscopía electrónica (crio-ME) como por cristalografía de rayos X, la localización de las proteínas minoritarias de la cápside es aún objeto de controversia. La compleja arquitectura de la cápside es producto de un complicado proceso de ensamblaje, del cual muchos aspectos no han sido clarificados. En particular, no se sabe si los procesos de encapsidación del genoma y ensamblaje ocurren de forma secuencial o concertada. Dos estrategias para estudiar el mecanismo de ensamblaje son: el estudio de partículas de baja densidad purificadas (consideradas intermediarios de ensamblaje), y el seguimiento de las proteínas estructurales y el genoma viral hasta su ensamblaje en células infectadas. En la primera parte de esta tesis, se analizan células infectadas con AdV tipo 5 (Ad5) *wild type* (wt) a diferentes tiempos de infección y se comparan con un mutante de Ad5 (Ad5/FC31), con un retraso en el proceso de encapsidación. Se realizaron ensayos de inmuno-fluorescencia e inmuno-microscopía electrónica para determinar la localización del ADN viral y las proteínas de encapsidación, core y cápside en células infectadas. Los resultados indican que todos los factores de ensamblaje se localizan en un área previamente descrita como la zona periférica de replicación, la cual sería la factoría de ensamblaje de AdV. Los intermediarios de ensamblaje observados en esta área apoyan el modelo de ensamblaje y encapsidación concertados. El ensamblaje podría dividirse en dos rutas: una sólo para proteínas de la cápside, y otra sólo para el ADN viral y proteínas del core. Solamente cuando ambas rutas están acopladas por la interacción correcta entre proteínas encapsidadoras y componentes del core, se producen las partículas virales completas. La mutación Ad5/FC31 desacopla estas rutas generando cápsides vacías y cuerpos moteados, que son acumulaciones de cores. En la segunda parte de la tesis, la caracterización molecular y estructural de las partículas ligeras de Ad5/FC31 reveló que estas partículas carecen de genoma viral y proteínas del core, pero habían iniciado la encapsidación y maduración sugiriendo que son productos abortivos de ensamblaje. La estructura de estas partículas ligeras analizadas por crio-ME muestra por primera vez la localización de la proteína L1 52/55 kDa dentro de la cápside, y cómo ésta cambia durante la maduración. Finalmente, estas estructuras ayudan a resolver la controversia actual acerca de la localización de las proteínas minoritarias de la cápside.

Abstract

Adenovirus (AdV) is one of the most complex icosahedral, nonenveloped viruses. Even after its structure was solved at near atomic resolution by both cryo-electron microscopy (cryo-EM) and X-ray crystallography, the localization of minor coat proteins is still a subject of debate. The elaborated capsid architecture is the product of a correspondingly complex assembly process, of which many aspects remain unclear. In particular, it is still not settled if assembly and packaging occur in a sequential or concerted manner. Two strategies to investigate the assembly mechanism are: studying purified light viral particles, which are considered assembly intermediates, and following the structural proteins and viral genome fate until their assembly in infected cells. In the first part of this thesis, cells infected with AdV type 5 (Ad5) wild type (wt) were studied at different post-infection times and compared with an Ad5 mutant (Ad5/FC31), which has a delay in the packaging process. Immunofluorescence and immunoelectron microscopy assays were carried out to determine the localization of viral DNA, packaging, core and capsid proteins in infected cells. The results indicate that all assembly factors can be found in an area previously recognized as the peripheral replicative zone, which could therefore be the AdV assembly factory. Assembly intermediates observed in this region support the concerted assembly and packaging model. The assembly process could be divided in two pathways, one for only capsid proteins and another one for viral DNA and core proteins. Only when both pathways are coupled by correct interaction between packaging proteins and genome, the viral particle is produced. The mutation in Ad5/FC31 decouples these pathways generating empty capsids and speckled bodies, which are accumulations of unpackaged cores. In the second part of this thesis, the molecular and structural characterization of Ad5/FC31 light particles revealed that these particles lack genome and core proteins, but had started packaging and maturation, suggesting that they are assembly dead ends. The cryo-EM structures of the Ad5/FC31 light particles provide the first glimpse on the organization of packaging protein L1 52/55 kDa inside the capsid shell, and how this organization changes during maturation. Finally, the cryo-EM structure also helps to settle the controversy regarding localization of the minor coat proteins.

Abbreviations

3D Three-dimensional

AdV Adenovirus

AdVs Adenoviruses

Ad2 Human adenovirus type 2

Ad5 Human adenovirus type 5

AVP Adenovirus protease

BDMA Benzyl dimethylamine

BrdU Bromodeoxyuridine

CAR Coxsackie and adenovirus receptor

ChIP Chromatin immunoprecipitation

Cryo-EM Cryo electron microscopy

DAS ssDNA accumulation site

DBP Adenovirus ssDNA binding protein

DDSA Dodecenyl succinic anhydride

dsDNA double stranded DNA

EDAS Early ssDNA accumulation site

EM Electron microscopy

EOG Electro-opaque granules

ERS Early replication site

ET Electron tomography

FS Freeze substitution

GONs Group of nine hexons

GOS Group of six

HAdV Human adenovirus

hpi hours post infection

HV Herpes virus

ITR Inverted terminal repeat sequences

IF Inmuno fluorescence

MLP Major late promoter

MNA Methyl nadic anhydride

ND10 Nuclear domain 10

NPC Nuclear pore complex

PAGE Polyacrylamide gel electrophoresis

PML Promyelocytic leukemia protein

PRZ Peripherical replicative zone

ssDNA single stranded DNA

TBS Tris buffer saline

TP Adenovirus terminal protein

VS Virogenic stroma

wt wild type

Ψ Adenovirus packaging domain

Table of contents

1. **Introduction** 3

1.1. Adenovirus 3

1.2. Adenovirus Genome 3

1.3. Adenovirus Structure 5

1.3.1. Minor Coat Proteins 5

1.3.2. Core Components 7

1.4. Adenovirus Infectious Cycle 8

1.5. Adenovirus Assembly 10

1.6. Nuclear Compartmentalization in Adenovirus Infected Cells 11

1.7. Assembly and Cellular Compartmentalization in Other Eukaryotic dsDNA Viruses: Viral Factories 14

1.8. Adenovirus Genome Packaging 16

1.8.1. Packaging Domain 17

1.8.2. Packaging Proteins 17

1.8.3. Adenovirus Incomplete Particles 19

1.9. The Delayed Packaging Mutant Ad5/FC31 21

2. **Objectives** 25

3. **Materials and Methods** **29**

3.1. Viruses and Cells 29

3.2. Antibodies 29

3.3. Virus Propagation and Purification 31

3.4. Quantification of Physical Viral Particles 32

3.5. Quantification of Infectious Viral Particles 33

3.6. Negative Staining Electron Microscopy 33

3.7. Denaturing Protein Electrophoresis 33

3.8. Silver Staining 33

3.9. Western Blot 34

3.10. Extraction of DNA From Purified Viral Particles 34

3.11. DNA Electrophoresis 35

3.12. Viral DNA Detection by Southern Blot 35

3.13. Conventional Electron Microscopy of Infected Cells 35

3.14. Immunofluorescence Microscopy 36

3.15. Immunoelectron Microscopy 37

3.16. Cryo-electron Microscopy and Image Processing 38

4. Results 43

4.1. Study of Adenovirus Assembly Within the Cell 43

4.1.1. Characterization of Cellular Modifications Induced by Adenovirus Using Electron Microscopy of Epon-Embedded Samples. 43

4.1.2. Localization of Factors Involved in Adenovirus Genome Packaging Using Immunofluorescence Microscopy. 47

4.1.3. Possible Localization of Adenovirus Peripheral Replicative Zones in Conventional Electron Microscopy of Infected Cells 53

4.1.4. Localization of Factors Involved in Adenovirus Genome Packaging Using Immunoelectron Microscopy of Freeze-Substituted Samples. 55

4.1.5. Localization of Adenovirus Structural Proteins Using Immunoelectron Microscopy of Freeze-Substituted Samples. 62

4.1.6. The Adenovirus Assembly Factory and the Actual Assembly Site 65

4.1.7. Electro-Opaque Granules, Speckled Bodies and Empty Capsids as Assembly Dead Ends 67

4.2. Study of Incomplete Particles Produced by Ad5/FC31 70

4.2.1. Ad5/FC31 Light Particles Are Not Artefacts Produced During the Purification 71

4.2.2. Molecular Characterization of Viral Particles in L2 and L3 72

4.2.3. Structure of Ad5/FC31 L2 and L3 Particles 74

4.2.4. Comparing the Structures of Ad5/FC31 Light Particles and the Two Alternative Models for Mature Adenovirus Type 5. 76

4.2.5. Differences between mature Ad5 and Ad5/FC31 incomplete particles 78

5. Discussion 83

5.1. Adenovirus Assembly Occurs in the PRZ in a Concerted Manner 83

5.2. Adenovirus Assembly Requires the Coordination of Two Independent Routes 84

5.3. Structures of Incomplete Particles & Implications for Adenovirus Assembly 85

5.4. Origin of Ad5/FC31 Light Particles 89

5.5. Other Contributions of this Thesis 89

5.6. Remaining questions 90

6. Conclusions 93

7. References 99

8. Appendices 109

9. Publications 113

Introduction

1. Introduction

1.1 Adenovirus

Adenoviruses (AdVs) were first isolated in 1953, when searching for etiologic agents of acute respiratory infections (127). They were named *adenoviruses* because the prototype viral strain was isolated from human adenoids. AdVs are responsible for a small portion of acute respiratory morbidity in the general population and for about 5 to 10% of respiratory illnesses in children (11). Since their discovery a large number of AdVs have been detected, infecting a wide range of vertebrates. Currently they are classified into five genera (54).

There are currently over 60 reported human Adenovirus (HAdV) types, grouped in seven species (HAdV A-G), with HAdV-D containing the most members (123). While HAdV generally infects mucosal epithelium, different serotypes differ in their tissue-specificity (gastrointestinal and urinary tract, lung or eyes). Pathogenicity varies according to group and type, but infections are generally well controlled by the host immune system in immunocompetent individuals. However, in the immunosuppresed individuals, AdV infections are frequent cause of morbidity and mortality (74). AdVs have been useful as experimental systems for investigating fundamental processes in the eukaryotic cell life, such as splicing and apoptosis. Recombinant HAdVs are widely studied as vehicles for gene transfer, oncolysis and vaccination (21, 34, 35, 43, 83). Most studies are based on HAdV type 5 (Ad5) and 2 (Ad2), therefore most of the information presented below corresponds to these highly homologous types.

1.2 Adenovirus Genome

The AdV genome is a linear double-stranded DNA molecule of approximately 35 kpb in the viruses infecting humans. It is divided into three main regions according to transcription time: early, delayed early, and late (**Figure 1A**). Each region is further subdivided into transcription units, with five early transcription units (E1A, E1B, E2, E3 and E4), three delayed early transcription units (IX, IVa2 and E2 late), and one late transcription unit that is processed to generate five families of late mRNAs (L1 to L5) (11). Units E1 to E4 are transcribed before the onset of the replication of viral DNA, producing proteins involved in the activation and regulation of transcription and replication, S phase induction of the cell cycle, apoptosis blockage, modulation of the response of the host to infection, and mRNA nuclear exportation. Following the onset of viral DNA synthesis, the expression of genes belonging to the intermediate class (IVa2 and IX proteins) is turned on. IVa2 and IX are structural proteins, but they are also involved in other processes during the infection. IVa2 contributes to activation of the major late promoter (MLP) (147); IX is also a transcriptional activator (81) and sequesters host-cell promyelocytic leukemia protein (PML) (126) which could be involved in nuclear defense mechanisms (87). Units L1 to L5 are transcribed at a later phase, encoding the structural proteins.

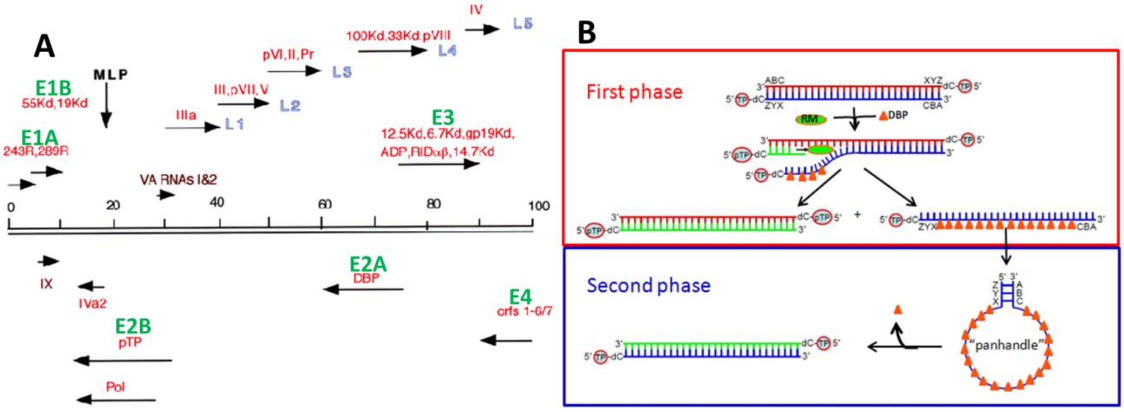
A
MLP
E1B
55Kd,19Kd
E1A
243R,289R
IIIa
L1
III,pVII,V
L2
pVI,II,Pr
L3
100Kd,33Kd,pVIII
L4
IV
L5
E3
12.5Kd,6.7Kd,gp19Kd,
ADP,RIDαβ,14.7Kd
VA RNAs I&2
0
20
40
60
80
100
IX
IVa2
E2B
pTP
Pol
E2A
DBP
E4
orfs 1-6/7
B
First phase
3'
ABC
XYZ
dC
TP
5'
5'
TP
dC
ZYX
CBA
3'
RM
DBP
pTP
dC
+
Second phase
5' 3'
ZYX
ABC
"panhandle"

Figure 1: Transcription and replication of the AdV genome. A. Transcription (128). Early transcripts are outlined in green, late ones in blue. The genes for VA RNA (RNAs that do not translate, their role is combating cellular defence mechanisms) are denoted in brown. Viral proteins in red. Arrows indicate the direction of transcription. MLP, Major Late Promoter. **B.** Replication (image modified from http://cronodon.com/BioTech/Adenovirus.html). Red and blue strands are parental molecules, green strands are daughter molecules. ITRs (ABC and XYZ), precursor TP (pTP), replication machinery (RM), ssDNA binding protein (DBP).

There are two inverted terminal repeat sequences (ITR) (103 to 165 bp, depending on the type) located at each end of the genome (139). The terminal protein binds to these regions, stabilizing the double strand and serving as a primer for viral genome replication (151). The packaging domain (Ψ), located downstream of the left ITR, contains recognition signals for encapsidation of the viral genome (section 1.8.1).

AdV replication takes place in two phases (**Figure 1B**) (77). In the first one, only one of the two DNA strands serves as a template, producing a dsDNA molecule which contains one daughter and one parental strand plus a displaced ssDNA bound to ssDNA binding protein (DBP). This protein is also called E2 DNA binding protein and 72 kDa protein. DBP is a nonstructural protein, and stimulates the initiation and elongation of DNA replication**.** In the second phase, the leftover ssDNA circularizes through annealing of its two ITRs, producing a panhandle structure. This structure can be recognized by the same replication machinery that operates in the first phase, because the panhandle creates the same termini structure of the duplex viral genome.

1.3 Adenovirus Structure

The AdV virion is a nonenveloped, icosahedral particle of approximately 95 nm in diameter, with fibers projecting from the vertices (76, 150). The particle has a mass of approximately 150 MDa, with DNA accounting for 13% of the mass, protein 87%, no membrane or lipid; and trace amounts of carbohydrate (O—linked N-acetyl-glucosamine in fiber) (11). The icosahedral shell surrounds a DNA-containing core. The polypeptides present in the mature virion are designated by roman numbers according to their decreasing apparent molecular weight on denaturing electrophoresis. The AdV capsid shell has a pseudo T=25 triangulation number, and its main components are: 240 hexon capsomers (trimers of protein II, 3x109 kDa) forming most of the capsid surface; 12 penton capsomers (formed by a pentamer of protein III “penton base”, (5x63.3 kDa) and a trimer of IV, “fiber” (3x61.9 kDa)), one at each vertex of the icosahedron (**Figure 2a**). As indicated by their names, penton and hexon capsomers are surrounded by five and six neighbors, respectively. Twelve hexon trimers form each of the 20 facets of the icosahedron. When AdV is subjected to mild dissociation conditions, stable substructures composed by nine hexon trimers (groups of nine, GONs) are reproducibly generated. GONs contain the central hexons in each facet, but not the ones surrounding the penton (peripentonals) (108). The five peripentonal hexon trimers, together with the penton base form a substructure referred to as GOS (Group of Six) (76).

1.3.1 Minor Coat Proteins

Apart from hexon, penton base and fiber, the AdV capsid contains at least four minor coat proteins in the icosahedral shell: polypeptides IIIa, VI, VIII and IX (reviewed in San Martin (131)). These proteins are necessary for correct morphogenesis of the viral particle and have several roles during assembly. The localization of some minor coat proteins is under debate (76, 120). Currently there are two models for the localization of these proteins (**Figure 2A**). One of them is based on cryo-electron microscopy (EM) data and another one in X-ray (XR) diffraction data. Although both studies have similar resolution (3.6 Å for EM and 3.8 Å for XR), the assignation of some proteins in the virus is completely different.

Polypeptides IIIa (in the cryo-EM model, (76)), VI and VIII are located on the inner capsid surface and their precursor forms are cleaved by the viral protease (AVP) during maturation (section 1.5). In the cryo-EM model, five monomers of polypeptide IIIa (precursor form 65.1 kDa) form a pinwheel feature underneath each vertex (60 monomers in the capsid). The N-terminal domain of this protein keeps each GOS together by tethering pairs of peripentonal hexons, and those to penton base. IIIa has also been shown to interact with the putative scaffold protein L1 52/55kDa and promote correct genome packaging (82) (section 1.8.2). Much of this protein (residues 300 to 585) could not be traced in the high resolution cryo-EM structure implying that this region does not follow icosahedral symmetry (76). In the X-ray model, the pinwheel is formed by protein V and VI instead of IIIa (120).

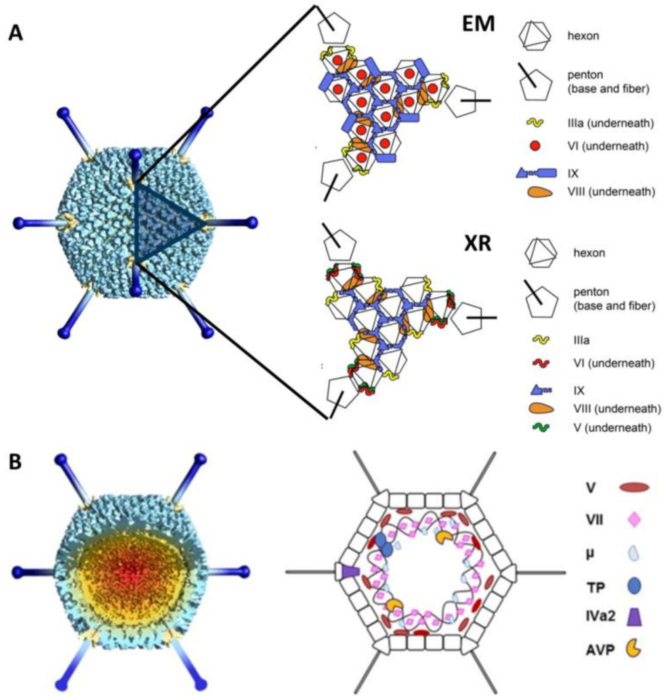

Figure 2: Overall AdV structure and components (131). A. Icosahedral shell organization. The left hand side panel is a model built from a low resolution cryo-EM map, with penton bases highlighted in yellow, and fibers modeled from the crystal structure of the knob and distal shaft (153) in dark blue. The shaded triangle indicates one facet. The schematics in the right hand side indicates the components of the facet as reported in Liu, et al. (76) (electron microscopy model, EM), and in Reddy and Nemerow (120) (X-ray model, XR). **B**. Non-icosahedral components of the AdV particle. A segment has been removed from the cryo-EM map to show the inner capsid contents. The schematics on the right hand side indicate tentative positions, as little is known about the structure and organization of the genome and accompanying proteins. Polypeptide IVa2, which binds to the specific packaging sequence in the viral genome, has been reported to occupy a singular vertex in the capsid (26).

Polypeptide VI (precursor form 26.9 kDa) has been shown to interact with an internal cavity in hexon, establishing a bridge between the icosahedral shell and the core. *In vitro,* the precursor of VI (pVI) binds to hexon with a stoichiometry of 3:3 (47). The copy number of VI is around 360, which does not correspond with the hexon copy number (240 trimers, 720 monomers). The density for pVI is stronger in cryo-EM of the inmature AdV, indicating that before maturation the interaction with hexon is stronger (101, 140) or that pVI is more ordered than its product. Only weak density has been observed for VI in all structural studies of mature AdV (76, 119, 120), indicating that the arrangement of VI within the hexon cavity does not follow icosahedral symmetry. Several roles have been reported for this protein: endosome escape

following cell entry (section 1.4), activation of AdV gene expression, nuclear targeting of hexon during assembly, and finally activation of AVP during maturation (section 1.5).
Polypeptide VIII (precursor form 24.6 kDa) is present in two independent monomers in the icosahedral asymmetric unit (60 copies of VIII in total). One of them is wedged between polypeptide IIIa (in the cryo-EM model) or VI and V (in the X-ray model) and the hexon bases at the periphery of the GOS. The second copy is located around the icosahedral 3-fold symmetry axis.

Finally, polypeptide IX (14.3 kDa, 240 copies in the virion) is the only minor coat protein located on the outer part of the AdV capsid in the cryo-EM model and forms a sort of hairnet on the outer side of the virion, keeping together the hexon trimers in each GON and binding GONs across the icosahedral edges (76) (**Figure 2A**). The N-terminal domains of three IX monomers join via hydrophobic interactions at the icosahedral and local 3-fold axes in the GONs forming triskelion structures. Then the so-called “rope domain” of each monomer runs in a different direction towards the facet edges, where a C-terminal α-helix joins with the C-terminal helices of another three copies of IX, different from those forming the N-terminal triskelion, to create a leucine zipper 4-helix bundle. In the X-ray model however, this 4-helix bundle has been assigned to IIIa. IX has a capsid stabilizing role. The trimeric N-terminal domain of IX is enough to incorporate to the capsid and confer capsid thermostability. It has been proposed that IX may play a role in modulating the viral tropism and/or interfering with the immune response. Also, IX is responsible for interaction with kinesin-1 during the final uncoating stage for translocation of the viral DNA to the nucleus.

1.3.2 Core Components

The AdV core contains four DNA binding proteins (V, VII, X and TP) and the viral genome (**Figure 2B**). Proteins VII, X and TP have precursor forms which are cleaved by AVP. Polypeptides V (41.6 kDa), VII (precursor form 21.9 kDa) and X (precursor form 8.7 kDa) are basic arginine-rich proteins that bind to the viral DNA and likely condense it within the core. V (~157 copies in the virion) can bind to penton base and polypeptide VI, linking the core to the capsid (103). VII (527-833 copies in the virion) (9, 152) is the major core protein and it remains associated with AdV DNA during productive infections (23). Two copies of the TP (precursor form 76.4 kDa) are covalently linked to the 5’ genome ends, circularizing it and acting as a primer for DNA replication (122). Protein X, also called μ (5), has 100-290 copies in the virion (9, 152). The exact localization of these proteins is unknown because they do not follow icosahedral symmetry. However, it is thought that they condense DNA in bead-like structures similar to nucleosomes, called “adenosomes” (154). There is another protein bound to the viral DNA, called IVa2 (50.7 kDa), with a copy number around 5 per virion (26). This protein is part of the packaging machinery (section 1.8.2).

1.4 Adenovirus Infectious Cycle

The AdV replication cycle (11, 40) is divided in two phases, early and late, separated by the onset of viral DNA replication, and is completed after 24 to 36 hours for Ad5 in HeLa cells. The early phase includes adsorption, penetration, movement of partially uncoated virus to the nuclear pore complex (NPC), transport of the viral genome through the NPC into the nucleus, and expression of early transcription units. In HeLa cells, this phase lasts for 5 to 6 hours; afterwards viral DNA replication is detected. Concomitant with the onset of viral replication, the late phase of the cycle begins with the expression of the late transcription units and assembly of viral progeny.

The cycle begins with the interaction of capsid proteins with diverse cellular receptors. In Ad5, fiber protein recognizes a receptor of 46 kDa called CAR (Coxsackie and Adenovirus Receptor) (10), a cell adhesion molecule (63) (**Figure 3, step 1**). Instead of CAR, different HAdV serotypes use other receptors such as: heparin sulfate glycosaminoglycans; desmoglein-2; CD46, CD80 and CD86; vascular cell adhesion molecule-1; MHC1; sialic acid; and other protein and nonprotein receptors (6). Internalization depends on integrins $\alpha_v\beta_3$ and $\alpha_v\beta_5$ binding to the RGD-sequence motif in penton base, triggering integrin-mediated endocytosis (158). Once contact has been established between virus and cell, the phosphatidylinositol-3-OH kinase (PI3K) is activated, which in turn activates Rac and CDC42 GTPases, thus inducing actin polymerization and viral endocytosis into clathrin-coated vesicles (89) (**Figure 3, steps 1 and 2**). As the endosome becomes acidified, the viral particle is destabilized, leading to release of proteins from the capsid. Among these is protein VI, which causes disruption of the endosomal membrane, thereby delivering the remainder of the particle into the cytoplasm (159) (**Figure 3, step 3**). The partially disrupted viral particle attaches to microtubules *via* cytoplasmic dynein-mediated binding (67) and travels along microtubules to the nucleus. When the particle arrives at the nuclear envelope, it docks to the NPC-filament protein CAN/Nup214. The proximity of the capsid to the nuclear pore allows binding of hexon to dynamic histone H1. Importin-β and importin-7 bind histone H1, leading to further disassembly of the capsid (148). Finally, the viral DNA, bound to protein VII, is delivered into the nucleus by the import protein transportin (**Figure 3, step 4**).

In the nucleus, the viral DNA begins its transcription (**Figure 3: step: 5**) at the periphery of ND10s (nuclear domains 10). ND10s are defined by accumulations of proteins that can be interferon-regulated, implicating ND10s as sites of a nuclear defense mechanism. Once the early proteins have been translated (especially: viral polymerase, ssDNA binding protein (DBP) and pTP), (**Figure 3, step 11**), they are imported into the nucleus and viral DNA replication begins (**Figure 3, step 13**). The replication domains are not randomly distributed; they are located close to or at the periphery of ND10s, expanding away from these nuclear domains (65) (section 1.6).

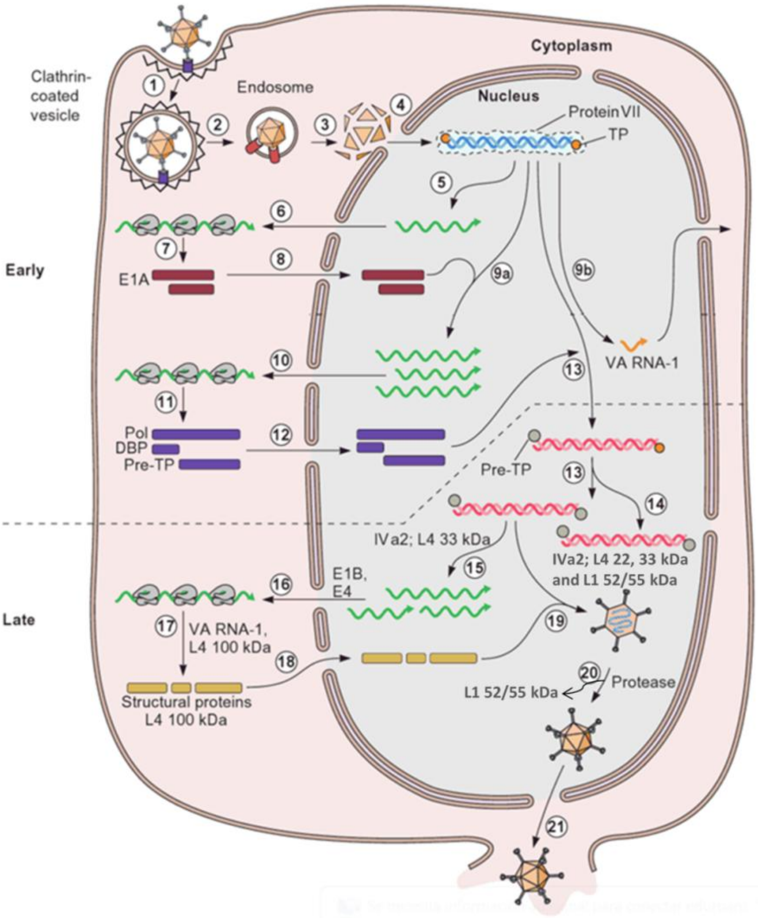
Clathrin-coated vesicle
Endosome
Cytoplasm
Nucleus
Protein VII
TP
①
②
③
④
⑤
⑥
⑦
⑧
Early
E1A
9a
9b
VA RNA-1
⑩
⑪
Pol
DBP
Pre-TP
⑫
⑬
Pre-TP
⑬
⑭
IVa2; L4 33 kDa
IVa2; L4 22, 33 kDa and L1 52/55 kDa
⑮
⑯
E1B, E4
Late
⑰
VA RNA-1, L4 100 kDa
⑱
⑲
Structural proteins L4 100 kDa
⑳
L1 52/55 kDa
Protease
㉑

Figure 3: Single-cell reproductive cycle of human adenovirus (modified from Flint, et al. (40)). Parental DNA in blue, RNA in green (except for VA RNA in orange), newly synthesized DNA in red. The numbers indicate the order of events. Transcription occurs in steps 5, 9 and 15; translation in 7, 11 and 17; replication in 13 and 14; assembly in 19; and maturation in 20.

In the late phase of the cycle, replicated viral DNA molecules serve as templates for further rounds of replication or for transcription of late genes (**Figure 3, steps 13, 14 and 15**). Processed late mRNA species are selectively exported from the nucleus and translated in the cytoplasm. Then, the proteins are imported into the nucleus where the virions will be assembled and matured (**Figure 3, step 19 and 20**) (section 1.5). The viral particles leave the cell by the action of multiple virus gene products involved in several cell death pathways. The

AdV pro-death gene products, such as E1a and E4ORF4, induce apoptosis. On the other hand, E311.6kD, called Adenovirus Death Protein, produces cell lysis and shows no apoptotic characteristics. The exact details of the cell death induced by AdV are unknown (14).

1.5 Adenovirus Assembly

AdV assembly occurs in the nucleus (11); however the trimeric hexon capsomers are assembled from monomers in the cytoplasm. The assembly of hexon trimers requires the 100k protein encoded in L4. The pentameric penton base and trimeric fiber are assembled independently and subsequently join to form a complete penton capsomer. After their production, hexon and penton capsomers are imported into the nucleus. These capsomers, together with the minor coat proteins and the putative scaffold protein L1 52/55 kDa assemble into an empty capsid. The viral DNA is inserted into this structure *via* a so far unclear mechanism (section 1.8). Core proteins are encapsidated with the viral genome to yield noninfectious young virions. These virions contain the precursor version of several capsid (pIIIa, pVI, pVIII) and core proteins (pVII, pμ, pTP). Mature virions are produced upon cleavage of these precursors by AVP (**Figure 4**) (13). The L1 52/55 kDa protein, present in empty capsids but not in mature virions, is also a substrate for AVP (99) (section 1.8.2).

Polypeptide pVI is cleaved at two sites (VI 22.1 kDa). The N-terminal fragment (pVIn) remains bound at the base of peripentonal hexons in mature virions (142). The C-terminal fragment (pVIc) is a cofactor for AVP (84, 157). Polypeptide pVIII has three cleavage sites (VIII 15.4 kDa). In porcine AdV, both pVIII as well as its two largest fragments ($pVIII_N$ and $pVIII_C$) were observed to interact with the packaging protein IVa2 (141). Also the two fragments remain ordered in the mature virion as observed in the cryo-EM structure of Ad5 (76).

Proteolytic maturation is necessary for full viral infectivity because without these cleavages, the AdV particles are unable to uncoat (48, 101). AVP (23 kDa) is a cysteine protease transcribed from the L3 unit, which is activated by the C-terminal peptide derived from protein pVI (pVI_c, Webster, et al. (157)). AVP recognizes (M/I/L)XGX-G and (M/I/L)XGG-X sequence motifs to cleave its substrates. Also, AVP cleaves the L1 52/55kDa protein at multiple sites **(Figure 4)**, many not conforming to AVP consensus cleavage sites. Fragments of different sizes of this protein can be detected from *in vitro* digestion (47, 45, 44, 40, 36, 33, 26, 20 and 17kDa) (99). Apart from pVI_c, AVP also uses viral dsDNA as a cofactor. dsDNA increases the enzymatic activity of AVP by 100 fold, and both cofactors increase the protease catalytic rate by 34000 fold, comparing with AVP alone. (88). AVP enters the capsid with the viral genome (aprox. 50 molecules per virus particle (15)). AVP, partially activated by being bound to DNA, excises pVI. The pVI$_C$ binds to the AVP molecule through a disulfide bond forming the fully active AVP-peptide pVI$_C$ complex bound to DNA. Active AVP slides along DNA via one-dimensional diffusion using pVI$_C$ as a "molecular sled". During this movement, AVP cleaves the protein precursors that are found in its way (13, 46).

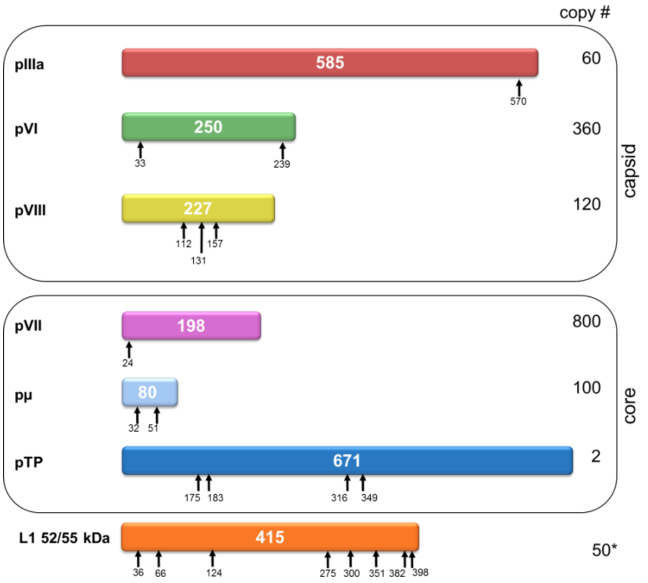

Figure 4: Components of the AdV particle undergoing proteolytic maturation (modified from San Martin (131)). Each Ad5 precursor protein is represented as a bar with the polypeptide length in amino acids indicated in the center. Cleavage sites are denoted by arrows. The prefix "p" denotes the unprocessed precursors. (*) Copy number in young virions.

1.6 Nuclear Compartmentalization in Adenovirus Infected Cells

In an AdV infected cell, the viral DNA is first detected (8 hpi) at the so-called early replicative sites (ERS), close to the ND10s. *In situ* hybridization assays revealed that ERS contain viral ssDNA, dsDNA, and viral replicative activity (**Figure 5, step 1**). *In situ* hybridization (for viral DNA), autoradiography (for tritiated thymidine), inmunocystochemistry (for DBP) and Bromo-deoxyuridine labeling (BrdU, for newly synthesized viral DNA) have been used to characterize nuclear transformations in AdV infected cells from 17 hpi until 41 hpi (12, 66, 71, 97, 107, 114-116). ERSs (**Figure 5, step 1**) give rise to two new structures (**Figure 5, step 2 and Figure 6D**): the ssDNA accumulation site, where a large number of single stranded replicative intermediates are accumulated; and a peripheral replicative zone where viral dsDNA is accumulated and there is continuous replicative activity. This zone surrounds the ssDNA accumulation zone, which has intermittent replicative activity. Later in infection (**Figure 5, step 3**), a single large viral genome storage site is developed. This is the main site of storage for nonreplicating dsDNA viral genomes. It contains also traces of viral ssDNA, and close to this area there are viral particles (12, 109, 114-116). At intermediate times post-infection (17-20 hpi), the ssDNA accumulation site forms a ring-like structure (66, 71, 97) with the peripheral replicative zone located adjacent to both the inner and outher borders of this ring (**Figure 5, step 2 and inset**) (107, 115).

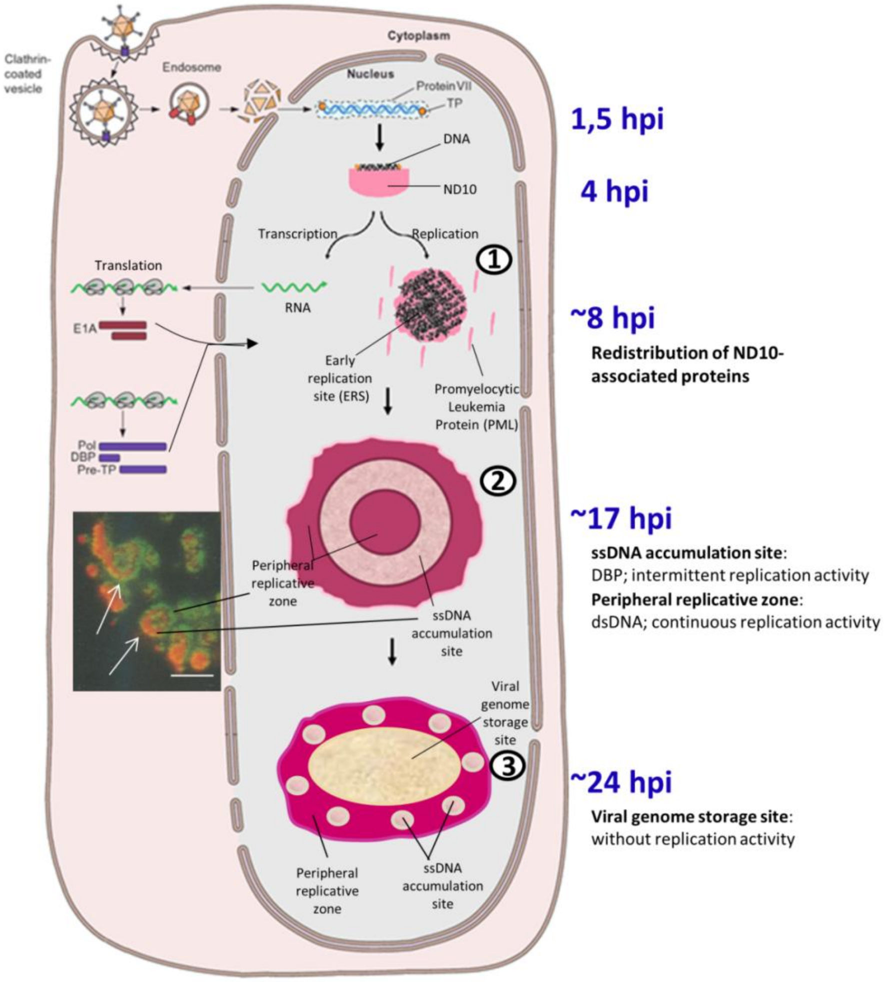
Clathrin-coated vesicle
Endosome
Cytoplasm
Nucleus
Protein VII
TP
DNA
ND10
Transcription
Replication
①
Translation
RNA
E1A
Early replication site (ERS)
Promyelocytic Leukemia Protein (PML)
Pol
DBP
Pre-TP
②
Peripheral replicative zone
ssDNA accumulation site
Viral genome storage site
③
Peripheral replicative zone
ssDNA accumulation site
1,5 hpi
4 hpi
~8 hpi
Redistribution of ND10-associated proteins
~17 hpi
ssDNA accumulation site:
DBP; intermittent replication activity
Peripheral replicative zone:
dsDNA; continuous replication activity
~24 hpi
Viral genome storage site:
without replication activity

Figure 5: Route of viral DNA from the first steps of infection until its accumulation in the nucleus. Parental DNA in blue, RNA in green (modified from Flint, et al. (40), with data from (12, 65, 87, 109, 115-117)). Early, intermediate and late times of infection (1, 2 and 3 respectively) are indicated. The fluorescence image inset shows the localization of DBP/ssDNA (in red) and bitotin-dUTP, newly synthesized viral DNA (in green) (107). White arrows show the pattern reproduced in the cartoon. The bar represents 5 µm.

Apart from the DNA-containing structures, adenovirus infection produces several types of nuclear modifications starting at early times post-infection (~6 hpi) (**Figure 6**). By cellular fractionation and PAGE-autoradiograms it was discovered that several adenovirus early proteins interact with the cellular skeletal framework. Using electron microscopy (EM) of infected cells sections, it was observed that the nuclear membrane of infected cells adopts an irregular outline, perhaps indicating changes in nuclear-cytoplasmic interactions (75). Cellular chromatin is pushed towards the nuclear border (**Figure 6C**). Nucleolar compaction (**Figure 6B**) occurs at 17 hpi, although a few nucleoli remain seemingly unchanged, even at 24 hpi.

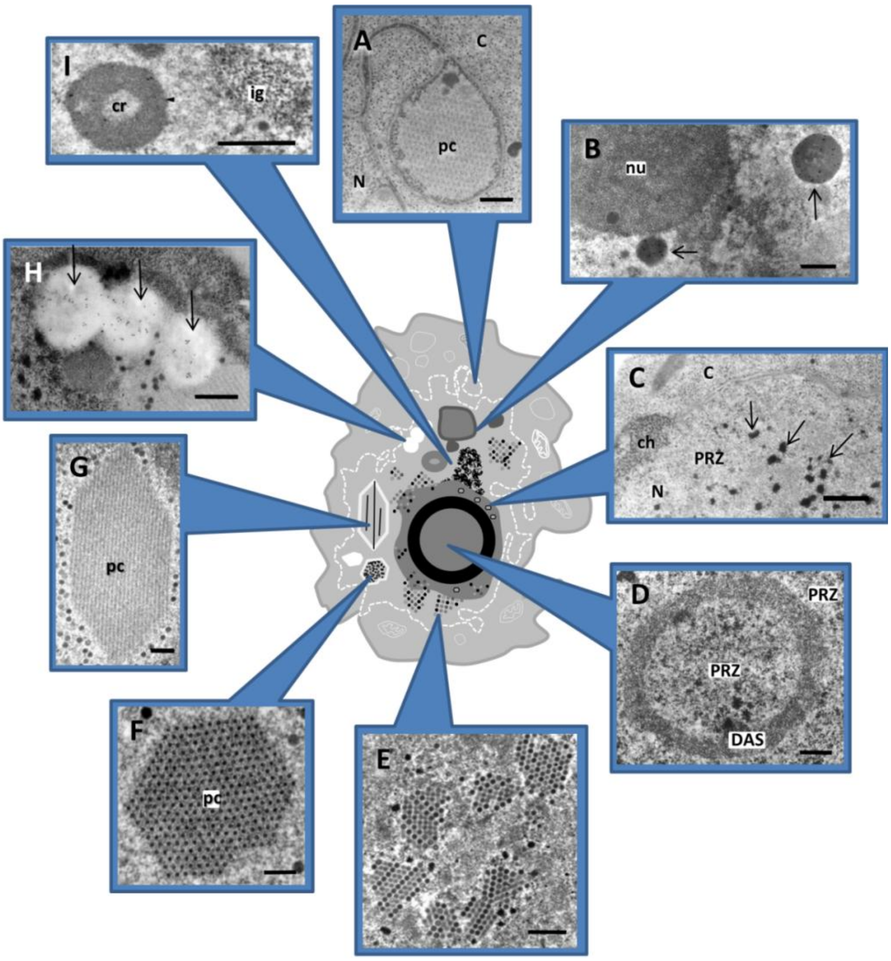

Figure 6: AdV induced alterations in the host cell nucleus during infection. A. Lobule. HeLa cell embedded in Epon at 41 hpi. Protein crystal (pc), nucleus (N) and cytoplasm (C). (111). Bar 2 µm. **B, H-I.** HeLa cell embedded in Lowicryl K4M at 17 hpi. **B.** Nucleolus (nu) and electro-dense inclusion (arrows). Bar 0.5 µm (80). **C.** Electro-opaque granules (arrows) located within the peripheral replicative zone (PRZ). HeLa cell embedded in Epon at 41 hpi. Chromatin (ch) and nucleus (N). Bar 0.5 µm (111). **D.** Peripherical replicative zone (PRZ) and ssDNA accumulation site (DAS). Cellular section embedded in Epon at 17 hpi. Bar 0.5 µm (117). **E.** Section of a paracrystalline array of virus in the nucleus of an infected cell. Bar 0.4 µm (42). **F-G.** Viral protein crystal (pc), cross (F) and longitudinal section (G). HEK 293 cell embedded in Epon at 48 hpi. Bar 0.2 and 0.4 µm respectively (41). **H.** Electron-clear inclusions (arrows). Bar 0.5 µm (112). **I.** Compact ring (cr) and cluster of interchromatin granule (ig). Bar 0.5 µm (110).

In situ hybridization indicated that late viral RNA accumulates in three types of nuclear structures: the peripheral replicative zone (**Figure 6D**); clusters of interchromatin granules (**Figure 6I**), which mostly participate in postsplicing events; and compact rings (**Figure 6I**), which contain unused portions of the primary transcripts resulting from differential polyadenylation site selection (110, 117, 118). Two types of inclusions, of yet unknown function, are found at late times by EM: electron-dense and clear inclusions (**Figure 6B and H**). In fiber-deleted viruses, unused hexon and penton base proteins have been detected by inmunogold labeling in the clear inclusions (113), while protein IVa2 has been detected in electron-dense inclusions and compact rings (80). Also, protein IX has been detected in clear amorphous inclusions (125). At late times (~24 hpi) protein crystals (**Figure 6F-G**) and virus particles (**Figure 6E**) appear. The protein crystals contain penton capsomers (penton base and fiber), which could associate into dodecahedrons disposed in parallel rows (41, 61).

At later infection times (41 hpi), viruses appear in the cytoplasm, some of them located next to nuclear pores. Abnormally large portions of the nuclear envelope (forming lobes, **Figure 6A**) devoid of underlying condensed chromatin, and proliferation of either the inner or both membranes of the nuclear envelope can also be seen. A new structure, called electro-opaque granules (**Figure 6C**) containing viral RNA, can be found by *in situ* hybridization in the clusters of interchromatin granule and peripheral replicative zone (111).

In spite of the large amounts of experimental work summarized above, it is still not clear where and how AdV assembly occurs in the nucleus of infected cells, and if it occurs in a particular environment forming a viral factory.

1.7 Assembly and Cellular Compartmentalization in Other Eukaryotic dsDNA Viruses: Viral Factories

Viral factories represent subcellular scaffolds where replicated genomes and capsid proteins spatially intersect in an efficient and coordinated manner to assemble virions (37). Depending on the virus and its replication and assembly site, it is possible to group eukaryotic dsDNA viruses in three classes: those with replication and assembly in the cytoplasm; those with replication in the nucleus and final assembly in the cytoplasm; and those with replication and assembly in the nucleus. Factories have been extensively studied for viruses assembling in the cytoplasm, but they are less well characterized in viruses with nuclear assembly due to the limited comprehension of the functional architecture of the nucleus (31).

For the first group, which includes *Poxviridae, Phycodnaviridae, Iridoviridae, Asfarviridae and Mimiviridae,* replication and assembly occur in classical cytoplasmic viral factories (91). These factories are elaborate structures whose formation involves massive rearrangement of host cytoskeleton and membranes. Assembly of these viruses is complex due to the need to recruit one or several envelopes. For example, the Mimivirus factory (90) originates from several fused replication centers. Cellular vesicles fuse forming multivesicular bodies next to the replication center, which rupture to form large open membrane sheets that act as precursors for the inner Mimivirus membrane. The Mimivirus factory is organized in three zones: replication; membrane assembly; capsid assembly and DNA packaging zone (**Figure 7A**). An icosahedral vertex is generated on the top of the open membrane sheets by recruting of structural Mimivirus capsid proteins (**Figure 7B**). During capsid assembly, the inner membrane layer is shaped into icosahedral morphology. It has been proposed that membrane overhangs consisting of open membrane sheets prevent premature closure of the icosahedral capsids, thus enabling the formation of a DNA-encapsidating portal (**Figure 7B**). A similar mechanism has been described for African swine fever virus (ASFV) assembly (143).

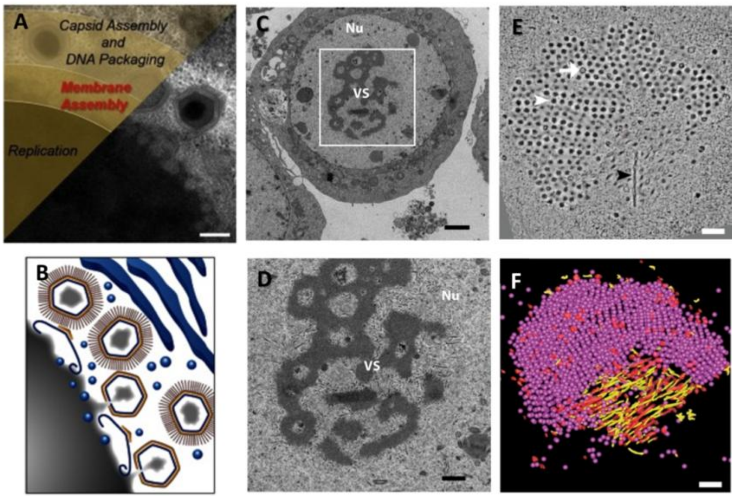

Figure 7: Examples of each eukaryotic dsDNA virus class according to the localization of its factory. A. Viral assembly zones of Mimivirus factory overlying the EM image. Scale bar 500 nm (90). **B.** Model of Mimivirus membrane and capsid assembly in its factory (90). **C.** Autographa californica nucleopolyhedrovirus (AcMNPV)-infected Sf9 cell. Scale bar 1 µm (18). **D.** Higher magnification image of the region boxed in panel (C). Virogenic stroma (VS), nucleus (Nu). Scale bar 500 nm (18). **E.** Electron tomography reconstruction section of Polyomavirus nuclear factory. A tubular structure appears in the plane (black arrowhead). Empty (white arrow) and full (white arrowhead) virions are identified in the virus cluster. Scale bar 200 nm (37). **F.** 3D model of (C) showing ~2000 full assembled virions (pink spheres) and 2% empty virions (red spheres) in a 300 nm thick section. The tubular structures are either filled with electron-dense material (yellow cylinders) or empty (red cylinders). Scale bar 200 nm (37).

For the other two groups, the term “nuclear factories” is employed to denote the location where viral DNA is synthesized, late genes transcribed, capsid assembled and DNA packaged (91). Herpesvirus (HV) and Baculovirus are representative of the second group (replication in the nucleus and final assembly in the cytoplasm). In HV, the nuclear factory consists in nuclear globular structures, also called replication compartments. Specialized machinery for late gene expression has been detected in these compartments. After synthesis of the capsid proteins, they move into the nucleus, where capsid assembly and DNA packaging occur. The following steps of tegumentation and envelopment continue in the cytoplasmic factory (91).

In Baculovirus (**Figure 7C and D**), the nuclear factory consists in a virogenic stroma (VS). VS is an electron dense, chromatin-like structure surrounding multiple translucent spaces that is found near the center of the nucleus in infected cells. The VS structure appears to be composed of RNA and protein with discrete concentrations of DNA that border intrastromal spaces, the sites of virion assembly (124).

Finally, Polyomavirus (PyV), which is included in the third group (replication and assembly in the nucleus), presents a new structure as center of assembly. Erickson *et al* (2012) used EM and electron tomography (ET), to identify tubular structures in close physical association with progeny virions in the nucleus of PyV-infected mouse fibroblasts (**Figure 7E and F**). These structures have virions apparently “shed” or “budding” from their ends. In comparison with virions in the same sections, the density surrounding the tubes corresponded to the density of the outer capsid of the virions, while the dense core was similar to the virion interior. Immunohistochemistry assays suggested that genome replication may be occurring adjacent to, but nor directly at the site of the factories.

1.8 Adenovirus Genome Packaging

Genome packaging is one the least understood steps in AdV assembly. Unlike in HV or bacteriophage, there is no *in vitro* assembly system for AdV. Numerous studies on the viral DNA, packaging proteins and the interactions between them have been reported (see below), and two models have been proposed relating capsid assembly and packaging: sequential and concerted. In the sequential model, a motor complex would transfer the DNA into a preformed capsid, using the energy derived from ATP hydrolysis. A difficulty that this model has to circumvent is how to package DNA bound to proteins. Chatterjee, et al. (23) found that VII and its precursor form (pVII) were associated with the viral DNA throughout infection (2-51 hpi). This result was obtained by analyzing the nuclear content of cells infected with ^{32}P-labelled Ad2, which were irradiated with ultraviolet light (to induce cross-linking between proteins and DNA), at various points along the infectious cycle. However, chromatin inmunoprecipitation assays (ChIP) suggested that VII is removed gradually from at least certain regions of the genome by interaction with other proteins during the early phase (56, 70). Also, remodeling factors, chaperones and histones bind to viral DNA from early times of infection (~1 hpi for histones) (70, 130). At late times (16 hpi), the pVII levels increase on the newly synthesized DNA while the amount of bound histones declines (30, 33). In conclusion, the viral DNA is always bound to proteins (cellular and/or viral proteins) during the infectious cycle. If the DNA translocation is with the protein pVII, it would be a novel mechanism of motor driven protein-DNA packaging which has not been previously described. If instead the naked DNA is transferred, the protein pVII would have to be first removed from the DNA, then penetrate the capsid freely so that it can be associated with the packaged DNA again (**Figure 8A**). In this case, an interesting question would be how the DNA packaging motor or an unknown viral factor strip protein pVII off to make the DNA ready for packaging. In the concerted model, pVII and DNA would form a chromatin-like structure first, and the viral capsid proteins would assemble around it (**Figure 8B**). In this case, an initiator for genome condensing would be required instead of a motor. In the next sections, previous studies about AdV packaging are summarized.

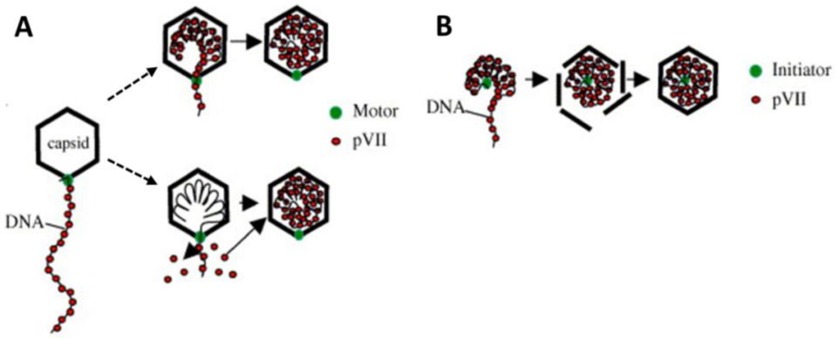

Figure 8: Models for packaging the AdV DNA-pVII complex (image modified from Zhang and Arcos (166)). A Sequential model. **B** Concerted model.

1.8.1 Packaging Domain

Adenovirus packaging begins from the left-end of the genome, where the specific packaging sequence (Ψ) is located (53, 145). This domain comprises nucleotides 200 to 397 (in Ad5) from the left end, between the ITR and the E1A transcription unit, and is composed by 7 repeated regions called "A-repeats" (**Figure 9**)(44, 53, 60, 136). These regions have a characteristic sequence motif 5'-TTTGN$_8$CGXG-3', which is conserved between different serotypes (44, 60, 136). The A-repeats exhibit differences in the ability to support viral packaging, with elements I, II, V and VI as the most critical repeats (136). Changes in spacing between the two conserved parts of the consensus motif (TTTG and CGXG) compromised DNA encapsidation, rather than changes in spacing between different A repeats (136). Although Ψ is at the 5'-end of the genome, it can be moved to the 3'-end and still be functional, as long as it is inserted within the first 600 nucleotides, approximately, of the genome end. If this distance is larger, the DNA is not packaged (60).

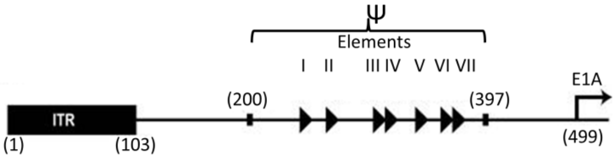

Figure 9: Arrangement of the left end of the Ad5 genome. The A-repeats, represented as triangles, are located between nucleotides 200 and 397, upstream of the transcription start site of the E1A promoter, shown as a right-facing arrow (image modified from Tyler, et al. (149)).

1.8.2 Packaging Proteins

Several AdV proteins are required for genome packaging to occur: IVa2, L1 52/55 kDa, L4 22 kDa, L4 33 kDa, and IIIa. When these proteins are modified (thermo-sensitive mutants) or deleted, only empty capsids are produced, demonstrating that they are not necessary for capsid assembly but are required for DNA packaging (27, 28, 50, 93, 163, 164). Among these proteins, IVa2 and L4 22 kDa bind directly to Ψ (94, 167). L4 22 kDa and L4 33 kDa are products of the same transcription unit. They share a common N terminus but have different C termini.

Bioinformatic analyses show conserved motifs associated with binding and hydrolysis of ATP in the IVa2 sequence (72). This finding supported the idea of IVa2 acting as a packaging motor protein in AdV, similarly to the packaging motors in dsDNA bacteriophage (22). Also, it has been reported that IVa2 is present at a single vertex in the virion (26). All these evidences favor the sequential model. However, although ATP binding assays demonstrated binding to the nucleoside triphosphate, ATP hydrolysis by IVa2 has not been proved so far (95). *In vitro*, higher-order IVa2-containing complexes form on adjacent packaging repeats. These complexes are thought to be required to form the hypothetic packaging motor (96), by analogy with motor complexes of bacteriophage which are formed by oligomeric protein complexes. However, it is not clear how the DNA bound to proteins (in nucleosome-like structures) would be translocated by a packaging motor. This kind of mechanism has not been observed previously.

Coimmunoprecipitation studies showed that IVa2 and L1 52/55kDa interact during the course of AdV infection (51). L1 52/55kDa is a phosphoprotein that migrates as a doublet on denaturing electrophoresis gels. This protein is present in empty capsids, assembly intermediates and young virions (section 1.8.3), but mostly absent in mature virions, suggesting a scaffolding role (58, 99). However, a mutant incapable of expressing L1 52/55 kDa (H5pm8001) produces empty capsids, indicating that this protein is not a classical scaffolding protein (50). L1 52/55 kDa is released from the viral particle by proteolytic processing, which leads to loss of interaction of this protein with itself, core and capsid proteins (99). The large size of the L1 52/55 kDa proteolytic fragments (over 15 kDa) suggests that cleavage, packaging and scaffold release may be happening simultaneously before the viral particle is sealed (supporting the concerted model). The available evidence suggests that L1 52/55 kDa is required to mediate the stable association between the viral DNA and the empty capsid to produce a full particle. *In vivo*, IVa2 and L1 52/55kDa proteins bind to the packaging domain and each protein-DNA interaction is independent of the other (102). *In vitro,* IVa2 protein binds strongly to Ψ, however no interaction has been observed for L1 52/55 kDa (102). This observation suggests that the L1 52/55 kDa protein-DNA interaction may be mediated by an intermediate protein. This result is corroborated in recent studies (164), where binding of both L4 22 kDa and IVa2 proteins to Ψ is required to recruit the L1 52/55 kDa protein *in vivo*.

Electrophoretic mobility shift assays showed that L4 22 kDa alone did not interact with the A-repeats, but it did form complexes on them in the presence of the IVa2 protein (38). Also, the authors suggested that L4 22 kDa enhances binding of IVa2 to Ψ. It has been proposed by Yang and Maluf (165) that a single IVa2 loads onto a single CGXG site and a single L4-22k loads onto a single TTTG site of the A-repeats. By analytical sedimentation velocity and equilibrium methods it was demonstrated that L4 22 kDa binding promotes cooperative assembly of IVa2 onto Ψ, and that saturating levels of L4 22 kDa diminish this cooperativity. Under no limiting conditions of L4 22k or IVa2 a large complex would be formed (165). ChIP assays demonstrated that L4 22kDa and IVa2 are dependent on each other for binding to Ψ *in vivo* (164).

Another protein involved in packaging is L4 33kDa. The role of L4 33 kDa remains obscure. Even when propagated in a L4 33kDa complementing cell line, a L4 33kDa mutant (with amber mutation) only produced empty capsids, demonstrating the role of L4 33k in packaging although it neither binds to Ψ nor influences the interaction of other packaging proteins with Ψ *in vivo* (163). Studies using packaging protein mutants are complex because some of them have other roles at early times of infection; for example, IVa2 is a transcription factor of the MLP (147), L4 33k is an alternative RNA splicing factor (146), and L4 22 kDa actives the expression of late genes (7). It is interesting to notice that packaging proteins are found both in empty capsids and binding to Ψ, suggesting that there may be two separate pools of these proteins where capsid-associated components may be poised as a portal vertex (ready to receive viral DNA for encapsidation). A second pool of these proteins may be bound to packaging sequences and promote an interaction between the viral DNA and capsid components (82).

Finally, polypeptide IIIa, a component of the icosahedral shell (section 1.3.1), interacts with L1 52/55kDa *in vitro* and associates with the viral packaging domain *in vivo*, indicating how the viral genome may be tethered to the capsid during the encapsidation process (82). L1 52/55 kDa and IIIa proteins are involved in serotype specificity of Ad packaging, whereas IVa2 or L4 22k proteins are not (82, 162). These observations suggest that the specificity is due to protein-protein interactions rather than to protein-DNA interactions.

1.8.3 Adenovirus Incomplete Particles

When Ad5 is purified using standards protocols, at least 2 bands are routinely observed in CsCl gradients. The low density band contains light particles lacking the viral genome, while the high density band contains mature virions. The light particles are considered precursors of mature virions (assembly intermediates) because in pulse-chase experiments they appear earlier (144), contain protein precursors (64, 160), and do not have DNA or only fragments (17, 29, 145, 160). This evidence is the second pillar supporting the sequential packaging model: existence of a procapsid. However, assays at long periods of chase (13h) indicate that light particles are very stable structures (68), their quantity is constant, and they do not become mature virions. The light particles of *ts4* and *ts369* mutants (thermo-sensitive mutations in IIIa and L1 52/55 kDa respectively) could not be chased into mature virions when the infected cells were shifted to the permissive temperature (59, 68), suggesting that these particles are not assembly intermediates but defective assembly products.

Interestingly, more than two bands appear when variations in the protocols are used for purification, or for other AdV types. Some extra bands correspond to light particles, but others are denser than the mature virion (17). Particles in the light bands contain both uncleaved protein precursors and their cleavage products, and proteins present in light particles but not in mature virions, that is, L1 52/55 kDa. The particles heavier than the mature virion represent particles that have not completed their maturation, and are called young virions (36, 64).

For AdV type 2 and 12, up to five discrete types of particles are produced. Each contains a specific-sized fragment of AdV DNA, and the labeled DNA signal (radioactivity) increased with the band density (17). Tibbetts (1977) observed the same for light particles of AdV type 7. For AdV type 16, four light bands were observed, and each band carried a different size of DNA (160). The presence of different lengths of packaged DNA has been taken as evidence for a sequential packaging model, although the actual origin of these DNA fragments is not well understood. Daniell (29) characterized the DNA contained in light particles by restriction enzyme analysis and by electron microscopy and heteroduplexing techniques. He found viral DNA fragments heterogeneous in length, ranging in size from 15% of the viral genome to full length. Daniell (1976) presented an adenovirus replication model to explain the heterogeneous nature of incomplete genomes isolated. The model assumes that breaks may occur in the displaced single strands of DNA during the replication. The resulting truncated molecules are unable to reform panhandle structures of the regular kind, but they may undergo some sort of illegitimate base pairing that enables them to serve as their own primer-templates. For the light particles of AdV type 2 and *ts4* mutant, the DNA was extracted and analyzed by agarose gel electrophoresis, restriction endonuclease cleavage and blot hybridization. In this case the DNA consisted in a heterogeneous population of subgenomic-size molecules ranging from about 200 to 1000 base pairs. It was proposed that the fragmentation of DNA is through endonuclease cleavage or mechanical shear during extraction and purification. However, it is possible also that some of the fragments of DNA arise due to errors in DNA replication (69). Edvardsson, et al. (36) demonstrated that cores were released from a population of light particles when they are purified on CsCl gradient without fixation, suggesting that some light particles could be artifacts produced during purification.

There is a correlation between punctual inhibition of DNA synthesis and reduced virus assembly under conditions where viral protein synthesis is virtually unaltered (156). Mature virions are not produced despite the presence of viral DNA accumulated previously to the inhibition. Pulse-chase experiments for DNA with *ts3,* thermo-sensitive mutant in hexon (57), indicated that only DNA being synthesized is packaged into mature virions. Also, ssDNA and DBP have been detected, by *in situ* hybridization and inmunolabeling assays, close to virions in cellular sections (111, 114). These results suggested that DNA synthesis is coupled to virus assembly (156), favoring the concerted packaging model.

Although many kinds of AdV light particles have been described, their structure and the conformational changes that happen during packaging remain a mystery. Only recently, Cheng, et al. (25) reported cryo-EM maps at 4.5 - 5 Å resolution of two types of bovine AdV type 3 light particles. One of them was lacking the GOS, while the other lacked penton bases and contained more DNA than the first one (observations from cryo-ET, and protein composition). Unfortunately, these particles came from a purification where no heavy band was obtained, therefore raising doubts regarding whether they consisted of assembly intermediates or virions degraded during purification. In these maps, no density was attributed to protein L1 52/55 kDa, a characteristic component of AdV light particles.

1.9 The Delayed Packaging Mutant Ad5/FC31

As described in section 1.8.2, several mutants for packaging proteins have been reported that produce only light particles (28, 50, 59, 93, 163, 164). An alternative mutation related to packaging was described by Alba, et al. (3), and denoted as Ad5/FC31. Ad5/FC31 (1) was generated by insertion of two exogenous sequences, *attB/attP*, flanking Ψ in an Ad5 E1/E4 deleted genome. These sequences are the targets for the recombinase of bacteriophage Φ31. To facilitate tracing of virus amplification, Ad5/FC31 has a green fluorescent protein cassette (GFP) between Ψ and the *attP* sequence (**Figure 10A**). Ad5/FC31 was designed as a possible helper vector for gene therapy. When propagated in cells expressing the Φ31 recombinase, the packaging signal would be excised and only the vector genome containing transgenes would be packaged. However, it was observed that even in cells not expressing the recombinase, this mutant produced a low amount of mature virions (<99.9%) compared to the control virus at 36 hpi, but it reached the same virus production yield than the control at 56 hpi (**Figure 10B**). Therefore, this mutant has a delay of 20 h in its cycle. Further, it was shown that the *attB* insertion was enough to induce this delay (**Figure 10B**). Replication and packaging studies were carried out to determine the cause of this delay. The viral protein and DNA production levels were similar in Ad5/FC31 and in control virus (**Figure 10C and D**). However, the analysis of packaged viral genomes showed that only 1-5% of Ad5/FC31 genome was packaged into virus at 36 hpi (**Figure 10D**), suggesting that low production levels at this time of infection were due to packaging problems (3). Electrophoretic Mobility Shift Assays (EMSA) showed that one or several nuclear proteins were binding to the *attB* sequence (1) and not to *attP*. This interaction could be interfering with correct interaction of viral packaging proteins and Ψ, hindering packaging of genomes synthesized until the interfering proteins are depleted. In Ad5/FC31 purifications, at 36 hpi the only visible band in a first CsCl gradient is the light band, while at 56 hpi the light and heavy bands are visible but the light band is still the most abundant. In a second gradient, the light band further separates into three bands (1, 2).

In this thesis, the Ad5/FC31 mutant and its comparison with wild type (wt) Ad5 were used to investigate the assembly of AdV in the cell and also to characterize the structure of light viral particles, possible assembly intermediates.

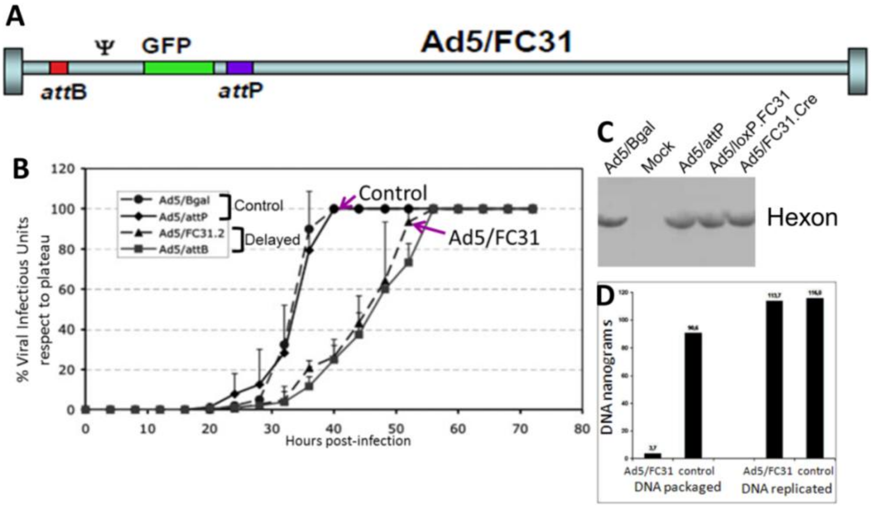

Figure 10: Ad5/FC31 mutant. A. Scheme of the Ad5/FC31 mutant genome showing the location of *attB/attP* insertions (1). **B.** Viral cycle of *attB/attP*-modified and control adenovirus. Infectious Units (IU) were determined every 4 h and compared to the IU value at the end of each viral cycle (3). **C.** Western blot against hexon produced by AdV controls and Ad5/FC31 at 24 hpi (1). **D.** Packaged and replicated DNA of Ad5/FC31 and control at 36 hpi (MOI=5) (1).

Objectives

2. Objectives

The general aim of this thesis is the study of AdV assembly within the cell, and the structural modifications produced by genome packaging in the AdV capsid.

In particular, the following objectives were pursued:

1. To follow the AdV assembly key players (DNA and proteins) within the cell, and compare their distribution in wt and the delayed packaging mutant Ad5/FC31.
2. To characterize the molecular composition and structure of incomplete particles generated by the Ad5/FC31 mutant.

Materials

and

Methods

3. Materials and Methods

3.1 Viruses and Cells

The viruses used in this study were:

Virus	Description
Ad5GL	Nonreplicative, E1 deleted, structurally wild type (wt) Ad5. Contains GFP and firefly luciferase genes (designated by the suffix "GL") (138)
Ad5/FC31[1]	Nonreplicative, E1 and E3 deleted Ad5 variant. Delayed packaging mutant. Contains an *attB/attP* insertion flanking Ψ and a GFP cassette following Ψ (3). There is a delay of 20 h in its viral cycle.
Ad2 *ts1*[2]	Replicative at 32°C and nonreplicative at 39°C. Contains a thermo-sensitive mutation in the AVP gene (57). At 39°C produces only young virions.

[1] The initial seed was kindly provided by our collaborator Dr. Miguel Chillón (Centro de Biotecnología Animal y Terapia Génica "CBATEG", Universidad Autónoma de Barcelona).

[2] Kindly provided by Dr. Jane Flint (Department of Molecular Biology-Princeton University, New Jersey).

The cell lines used were:

Cell line	**ATCC**	**Description**
HEK 293	CRL-1573	Human Embrionic Kidney cell line transformed with sheared Ad5 DNA (45). Complements for propagation of E1 deleted Ad5 variants.

3.2 Antibodies

The primary antibodies used in fluorescence, electron microscopy and western blot were:

Antibody	**Type**	**Dilutions used**			**Antigen**
		Fluorescence microscopy	**Electron microscopy**	**Western blot**	
Rat anti-BrdU (abcam Cat # ab6326)	Monoclonal	1:250	1:25	---	BrdU in ssDNA
Rat anti-VII[1]	Serum	---	1:50	1:3000	pVII (Ad5)

(55)					
Mouse anti-IVa2[2]	Serum	1:200	1:10	---	IVa2 (Ad2)
Mouse anti-IVa2 cocktail[2]: 6C9, 3H7, 9F4, 8H11, 3F3, 2B9 (4)	Hybridoma supernatants	---	---	1:20	IVa2 (Ad2)
Mouse anti-DBP[2] (121)	Monoclonal	1/20	---	---	DBP (Ad5)
Rabbit anti-L1 52/55 kDa[3] (96)	Serum	1:300	1:60	1:2000	L1 52/55 kDa full length (Ad5)
Mouse anti-V[2] (79)	Monoclonal	---	---	1:500	V (Ad2)
Rabbit anti-VI[4] (16)	Serum	---	---	1:500	VI (Ad2)
Rabbit anti-fiber[5] (62)	Serum	1:300	1:100	---	Fiber knob (Ad5)

Antibodies were kindly provided by [1]Kyosuke Nagata (University of Tsukuba), [2]Jane Flint (Department of Molecular Biology-Princeton University, New Jersey), [3]Patrick Hearing (State University of New York), [4] Urs Greber (Institut of Molecular Life Sciences-University of Zurich), and [5]Robert Gerard (University of Texas).

The secondary antibodies used were:

Antibody	Source	Cat #	Use[1]	Dilution
Alexa Fluor®488 Goat Anti-Mouse	Invitrogen	A-11029	IF	1:500
Alexa Fluor®546 Goat Anti-Mouse	Invitrogen	A-11030	IF	1:500
Alexa Fluor®555 Goat Anti-Rat	Invitrogen	A-21434	IF	1:500
Alexa Fluor®594 Goat Anti-Rat	Invitrogen	A-11007	IF	1:500
Alexa Fluor®594	Invitrogen	A-11032	IF	1:500

Goat Anti-Mouse				
Alexa Fluor®594 Donkey Anti-Rabbit	Invitrogen	A-21207	IF	1:500
Alexa Fluor®647 Goat Anti-Rabbit	Invitrogen	A-21245	IF	1:500
Pacific Blue™ Goat Anti-Rabbit	Invitrogen	P-10994	IF	1:500
Pacific Blue™ Goat Anti-Mouse	Invitrogen	P-31582	IF	1:500
Gold-conjugated Goat Anti-Rabbit (10 nm)	BB International	EM-GFAR10	EM	1:40
Gold-conjugated Anti-Mouse (10 nm)	BB International	EM-GFAF10	EM	1:40
Gold-conjugated Goat Anti-Rat (15 nm)	BB International	EM-GAT15	EM	1:40
Peroxidase-conjugated Goat Anti-Rabbit	Jackson ImmunoResearch laboratories	111-035-003	WB	1:100000
ECL™ peroxidase-conjugated Sheep Anti-Mouse	GE Healthcare Life Sciences	NA931VS	WB	1:5000
ECL™ peroxidase-conjugated Goat Anti-Rat	GE Healthcare Life Sciences	NA935V	WB	1:5000

[1] Immunofluorescence (IF), electron microscopy (EM), western blot (WB).

3.3 Virus Propagation and Purification

HEK293 cells were propagated in Dulbecco's modified Eagle's medium (DMEM, Sigma Cat# D6429) supplemented with 10% fetal bovine serum (FBS, Biological Industries Cat# 04-001-1A), 10 units-10 µg/ml penicillin-streptomycin (Sigma Cat# P4333), 0.05 mg/ml gentamicin (Sigma Cat# G1397), 4 mM L-Glutamine (MERCK Cat# 3520) and 1X non essential amino acid solution (Sigma Cat# M7145), and maintained at 37°C in a humidified incubator with 5% CO_2. Cells were seeded in p100 tissue culture dishes (BD Falcon Cat# 353003) at a density of 2.8x10^6 cells in 10 ml of medium. When the cell monolayers reached about 70% confluence, the purified virus was thoroughly mixed with fresh medium (this had FBS 2% instead of 10%) and added to the cells at a multiplicity of infection (MOI) of 5 infectious particles per cell. The cells were collected after 36 hpi for Ad5GL and 56 hpi for Ad5/FC31.

Infected cells from 60 p100 tissue culture plates were collected and centrifuged in a Heraeus 1.0R megafuge for 40 min at 4000 rpm and 4°C. The cells were resuspended in 42 ml of medium (from the supernatant) and lysed by four freeze-thaw cycles. Cell lysates were clarified to remove cellular debris by centrifugation in a Heraeus 1.0R megafuge at 4000 rpm for 30 min at 4°C.

For double CsCl gradient ultracentrifugation, the supernatant was distributed in 6 tubes containing a discontinuous gradient of 1.25 g/ml and 1.40 g/ml CsCl in TD1X buffer (137 mM NaCl, 5.1 mM KCl, 0.7 mM $Na_2HPO_4.7H_2O$, 25 mM Tris-HCl pH 7.4) (2,5 ml of each CsCl buffer and 7 ml of supernatant) and centrifuged at 35700 rpm for 90 min at 18°C in a Beckman Optima L-100 XP ultracentrifuge using a Beckman SW41Ti swinging bucket rotor. The low and high density virus bands from each tube were collected (1 ml of band by tube) and independently pooled. In the second gradient, the high and low density pooled material (6 ml) was laid onto 6 ml of a CsCl 1.31 g/ml solution in TD1X buffer and centrifuged for 18 hours at 35700 rpm and 18°C in a Beckman SW41Ti swinging bucket rotor. Bands containing viral particles from each tube were collected and transferred into Econo-Pac 10DG disposable chromatography columns (Biorad Cat#732-2010) with molecular weight cutoff of 6000 Daltons for buffer exchange to HBS (20 mM HEPES, 0.15M NaCl pH7.8). Aliquots were collected, and those with higher concentration of viral particles (estimated by absorbance at 260 and 280 nm) were stored at -80°C after adding glycerol to a final concentration of 10%. The density of CsCl solutions was determined by weighing a known volume. The viral particle density was determined by the same method, weighing a known volume of each band.

3.4 Quantification of Physical Viral Particles

Capsid protein concentration was quantified using the hexon fluorescence emission spectra obtained in a Hitachi Model F-2500 FL Spectrophotometer. Sample volumes of 0.150 ml were examined in sealed quarz cuvettes. The sample was excited at 285 nm, and the emission was monitored from 310 to 375 nm using excitation and emission slit widths of 10 nm. The spectra were corrected by subtraction of the buffer spectrum. The maximum emission intensity for each spectrum was found at 333 nm and recorded. The concentration was determined from a calibration curve calculated from a known concentration sample.

3.5 Quantification of Infectious Viral Particles

The end point dilution assay was used to measure virus infectious titer. Serial dilutions of a virus stock were prepared and inoculated onto replicate cell cultures, in 96 well plastic plates. The number of cells infected displaying GFP signal was determined for each virus dilution. Serial dilutions 1:10 were used and the initial inoculum volume was 100 µl. The cells with GFP signal were counted after 36 hpi. The final infectious titer was determined by calculating the average of the titers of the last three dilutions showing GFP signal, using the next formula:

$$\left[\frac{(\text{Number of cells with GFP signal x dilution factor})}{infection\ volume\ in\ ml}\right] = Number\ of\ infective\ particles\ per\ ml$$

3.6 Negative Staining Electron Microscopy

A drop of 5 µl of the sample was incubated on glow discharged collodion/carbon coated grids for 5 min to allow sample adsorption. Excess fluid was removed by touching on the edge of the grid with a piece of Whatman paper, without allowing it to become completely dry (blotting step). Then the grid was incubated with staining agent 2% (w/v) uranyl acetate, for 30 sec. After staining the grids were blotted and air dried on a filter paper in a Petri dish. The grids were examined in a JEOL JEM 1230 transmission electron microscope at 100 kV.

3.7 Denaturing Protein Electrophoresis

Samples were denatured in loading buffer (1% SDS, 1% β-mercaptoethanol, 10% glycerol, 50 mM Tris-HCl pH 6.8, 1.6% bromophenol blue) and incubated at 95°C for 10 min. Gradient gels (4-20% of acrylamide, Mini-PROTEAN TGX precast gels # 456-1096 from BioRad) were run in a minigel Biorad electrophoresis system. Molecular weight markers used were P7708S from New England BioLabs. Electrophoreses were performed at 100 V for approximately 100 min in TBE buffer (89 mM Tris base, 89 mM boric acid and 2 mM EDTA) at room temperature.

3.8 Silver Staining

After electrophoresis, the gels were fixed in 20 ml ethanol, 5 ml acetic acid and milli-Q water up to 50 ml for at least 30 min. Gels were sensitized by soaking for 30 min in 15 ml ethanol, 2 ml sodium thiosulfate (5% w/v), 3.4 g of sodium acetate and water up to 50 ml. Gels were rinsed three times in milli-Q water, 3 min for each wash, then incubated in silver nitrate 0.25% (w/v) for 20 min for staining, and rinsed twice for 30 seconds per wash in milli-Q water. Gels were transferred into the developer solution (1.25 g Na_2CO_3, 20 µl of formaldehyde 37%, up to 50 ml with milli-Q water), and transferred to stop solution (40 mM EDTA-$Na_2.2H_2O$) for at least 10 min, when the adequate degree of staining was achieved, then washed in milli-Q water.

3.9 Western Blot

Proteins were transferred from the gels to a nitrocellulose membrane (BioRad Cat# 162-0115) on a Bio-Rad semidry transfer apparatus (Bio-Rad Cat# 170-3940) for 25 min at 15 V, then blocked for 1 h at room temperature in 5% skim powdered milk in Tris buffer saline ("TBS" 0.09% NaCl, 0.01% Tween 20, 0.1 M Tris-HCl pH 7.5). The membrane was then probed overnight at 4°C with the primary antibody diluted in 0.5% skim powdered milk in TBS. After this incubation, the membrane was washed three times in TBS and probed for 1 h at room temperature with the appropriate horseradish peroxidase (HRP) conjugated secondary antibody. The signal was detected using LiteAblot kit (Gentaur Cat# EMP10004).

3.10 Extraction of DNA From Purified Viral Particles

Samples (200 µl) were heated for 10 min at 70°C, then incubated for 1 hour at 37°C after addition of 400 µl of lysis buffer (10 mM Tris-HCl, 0.1M EDTA, 0.5% SDS pH 8.0). Then, proteinase K (100 µg/ml) was added and the incubation continued overnight at 50°C. After cooling at room temperature, 1 volume of phenol:chloroform:isoamyl alcohol 25:24:1 (Sigma Cat# P3803) was added, and the samples were swirled and centrifuged for 10 min at maximum velocity in an Eppendorf Centrifuge 5424. The aqueous phase was collected and 1 volume of chloroform was added, swirled and centrifuged again. Two volumes of ethanol and 0.4 volumes of 5M NaCl were added to the aqueous phase collected, and the tube was swirled until the solution was thoroughly mixed. After incubating overnight at -20°C, the samples were centrifuged for 10 min at maximum velocity, and the precipitated DNA was washed with 70% ethanol, centrifuged and resuspended in 50 µl of milli-Q water. DNA concentration and purity were estimated by absorbance at 260 nm and 260/280 ratio respectively.

3.11 DNA Electrophoresis

Samples were mixed with loading buffer (0.1% xylene cyanol, 0.1% bromophenol blue, 30% glycerol, 10 mM EDTA) and loaded into a 0.8% agarose gel. Electrophoreses were performed at 80 V for 2 hours in TAE buffer (40 mM Tris-base, 1.14% acetic acid, 1 mM EDTA). DNA was visualized with 0.3 µg/ml ethidium bromide. Promega 1 kb ladder (Cat# G5711) and New England Biolabs lambda DNA-Hind III digest (Cat# 174N3012S) were used as molecular weight markers.

3.12 Viral DNA Detection by Southern Blot

The detection of viral DNA by Southern blot was performed according to the protocol recommended by GE Healthcare in its Amersham Hybond-N+ product (nylon membrane), specifically the protocol for capillary blotting. DraIII-digested Ad2 *ts1* DNA was used as a probe after labeling with alkaline phosphatase following the protocol of Amersham Gene Images AlkPhos Direct Labelling and Detection System (GE Healthcare Life Sciences Cat# RPN3680). This protocol was followed by hybridization, post-hybridization, signal generation and detection with CDP-Star (GE Healthcare Life Sciences Cat# RPN3682).

3.13 Conventional Electron Microscopy of Infected Cells

HEK293 cells were grown in a p100 culture plate to 70% confluence, then infected with Ad5/FC31 or Ad5GL with MOI = 5. At the desired time post infection, the medium was removed and the cells were fixed with 2% glutaraldehyde and 1% tannic acid in 0.4 M HEPES pH 7.2 during 1.5 h at room temperature. All solutions were prepared in buffer 0.4 M HEPES pH 7.2 and the washes were done with this solution unless otherwise indicated. The cells were collected and centrifuged for 5 min at 4000 rpm. The cross-linking solution was removed and 1 ml of HEPES was added. When needed, samples were stored at 4°C until further processing. When all samples had been fixed, they were washed 3 times with HEPES for 15 min at 4°C and centrifuged at 4000 rpm during 5 min. 300 µl of 1% osmium tetroxide and 0.8% potassium ferricyanide were added to the samples and incubated for 1 hour at 4°C. After three washes with HEPES, 300 µl of 2% uranyl acetate in milli-Q water were added and the samples were incubated for 40 min at 4°C, then washed three times with milli-Q water. Dilutions of dry acetone SecSol at 50%, 70%, and 90% v/v in water were prepared. Samples were dehydrated by sequential incubation with increasing concentrations of acetone SecSol (50%, 70%, 90%, and twice 100% in incubations of 15 min at 4°C). Epon resin was prepared by mixing 4.8 g 812-resin, 1.9 g DDSA, 3.3 g MNA and 5 drops BDMA (812 Epon Embedding Kit, Electron Microscopy Sciences #14120). Samples were incubated overnight in a mix of acetone:Epon resin (1:1) at room temperature in an Eppendorf tube rotator. The next day the cells were centrifuged (10 min at 8000 rpm), the mix acetone:Epon was removed and new Epon resin was added for incubation during 6 hours at room temperature. Then, cells were centrifuged again to remove the Epon, fresh resin was added, and embedding proceeded overnight at room temperature. A last Epon resin change was done the next day and the cells were transferred to beem capsules (that were filled with Epon). Capsules were placed in an incubator during two days at 60°C for polymerization. Ultrathin sections (~70nm) were obtained using a Leica EM UC6 Ultramicrotome and collected on Formvar-coated nickel grids (200 mesh, 0.25% Formvar). The sections were stained with saturated uranyl acetate during 25 min, floated on 4 drops of milli-Q water, stained on lead citrate drops during 1 min, and washed in 4 drops of milli-Q water. The grids were examined in a JEOL JEM 1230 transmission electron microscope at 100kV.

The electron density of viral particles in sections was analyzed using the software package XMIPP (32). Image frames (50x50 px) containing single viral particles were extracted from micrographs and normalized. The average electron density was calculated within a mask of radius 25 px, corresponding to the size of the viral particle.

3.14 Immunofluorescence Microscopy

Cover glasses (diameter: 12 mm) were incubated on poly-L-lysine (Sigma-Aldrich Cat # P4707) for 30 min at 37°C, then placed in 24 well culture plates (Thermo Scientific Nunc^{TM} Cat# 142475) and washed with PBS (137 mM NaCl, 2.7 mM KCl, 10 mM Na_2HPO_4, 1.8 mM KH_2PO_4 pH 7.4). HEK293 cells at 70 – 80% confluence were diluted 1:5 in DMEM medium and seeded on the cover glasses. After 24 hours, cells were infected with Ad5/FC31 or Ad5GL with MOI = 50 in inoculums of 200 µl. The infection was synchronized by incubating the cells for 30 min at 4°C and then 30 min at 37°C. The inoculums were removed and DMEM was added. For BrdU labeling, at 18 hpi at 37°C the medium was changed by medium containing 25 µg/ml BrdU (5-Bromo-2’-deoxyuridine, Sigma Cat#B5002-1G), followed by another change at 25 hpi. Incubation with BrdU proceeded at 37°C.

After the desired post-infection time, the medium was removed and 4% paraformaldehyde in PBS was added to the cells during 10 min. After 3 rinses with PBS, cover glasses were incubated with a mixture of 0.5% saponin and 10% FBS in PBS for 10 min. Samples were rinsed twice with PBS and incubated with primary antibody (section 3.2) in 0.5% saponin and 2% FBS in PBS during 45 min. After three more rinses, incubation with secondary antibodies was carried out in darkness. The secondary antibodies (section 3.2) were diluted in 0.5% saponin and 2% FBS in PBS. Samples were rinsed 3 times with PBS before adding DAPI (Sigma Cat#32670) or Topro-3 (Invitrogen Cat# T3605) for DNA staining (15 min, dilution 1:200 in PBS). After a final rinse with PBS, cover glasses were mounted on glass slides using ProLong (Invitrogen Cat# P36930) drops (4µl). The antifade reagent was allowed to dry overnight before sample observation. All incubations were carried out at room temperature. Images were taken using a confocal multispectral Leica TCS SP5 system.

The following modifications to the protocol described above were applied for anti-BrdU labeling: fixed samples were washed three times with saponin 1% in PBS (5 min 3x), then subjected to DNA denaturing treatment: 1N HCl during 10 min at 4°C, followed by 2N HCl during 10 min at room temperature, and finally 20 min at 37°C. Borate buffer (4 g NaOH; 23.5 g borate acid to 500 ml pH 8.2) was added to neutralize during 12 min at room temperature. After that, the protocol continued with the block-permeabilization described above, but with 1% saponin instead of 0.5%.

For double labeling assays, the primary antibodies were used together in the same incubation except for the antibodies against IVa2 and L1 52/55kDa, because the first one had lower affinity than the second antibody for its antigen. Therefore, a new modification was used for this assay: anti-IVa2 was incubated first, then 4% paraformaldehyde was used to fix the antibody during 5 min, and then anti-L1 52/55kDa was added. The secondary antibodies were incubated together. Immunofluorescence image analyses were carried out with Image J (137).

3.15 Immunoelectron Microscopy

BrdU labeling of newly synthesized DNA was carried out as described for immunoflurescence (section 4.14), for HEK293 cells grown in p100 culture plates without cover glasses. Infected and control cells were fixed with 4% paraformaldehyde in PBS after medium removal. After rinsing three times with PBS, glycerol was added drop by drop up to 15% concentration. After 15 min at 4°C, glycerol was increased to 30%. After 15 more min at 4°C, the cells were harvested and centrifuged for 10 min at 5000 rpm. The pellets were placed on small squares (0.2 x 0.2 cm) of Whatman paper and frozen by plunge freezing in liquid ethane using a Leica CPC plunger. Freeze substitution was carried out in a Leica EM automatic freeze-substitution system (AFS). Samples were transferred from liquid nitrogen into capsules precooled in the AFS chamber, and then the capsules were filled with 0.5% uranyl acetate in dry methanol

SecSol. After 6 hours of incubation at -90°C, the solution was replaced by a new one and incubated overnight at the same temperature. These steps were repeated for two more days. The last day the system was programmed to increase the temperature to -40°C; this increment was done in 7 hours during the night. Samples were rinsed three times (3 x 1 h) with dry methanol SecSol, then incubated with methanol: resin 3:1 (1 hour), methanol: resin 1:1 (1 h), methanol: resin 1:3 (1 h), resin 100% (15min) and finally resin 100% overnight. On the fifth day, the resin was changed twice, once in the morning and once in the afternoon. For polymerization, samples were irradiated at -40°C for 48 hours with ultraviolet light, then at 20°C for 48 hours more. The resin used was Lowicryl HM20, prepared as follows: for 20 g of resin, mix 2.98 g crosslinker D, 17.02 g monomer E and 0.1 g initiator C. All solutions or materials were cooled in the AFS for 15 min prior to entering in contact with the samples. The ultrathin sections were collected in the same way as indicated in section 3.13.

For immunolabeling, grids carrying freeze-substitution ultrathin sections were placed on TBG (30 mM Tris-HCl pH 8, 150 mM NaCl, 0.1% BSA and 1% gelatin) drops with the sections in contact with the solution for 10 min, and then incubated with the primary antibody in TBG at the required dilution (section 3.2) for 30 min. The grids were washed 3 times with PBS, and then floated on 4 TBG drops (5 min per drop). Gold-conjugated secondary antibodies (section 3.2) were diluted in TBG, and samples incubated for 30 min. Then, grids were washed 3 times with PBS and milli-Q water, and stained in the same way described in section 3.13 except that lead citrate was not used. All incubations were carried out at room temperature.

For anti-BrdU labeling, an additional step was required. Sections were treated with 0.2 mg/ml proteinase K (Roche Cat# 3115879) for 15 min at 37°C, then washed with milli-Q water and denatured with 2N HCl for 25 min. After several (~4) rinses in milli-Q water, the protocol continued with the TBG incubation. To unmask protein VII, sections were floated on three drops of DNase buffer (10 mM Tris-HCl pH 8.2, 10 mM NaCl, 5 mM $MgCl_2$) (5 min per drop), then incubated with 50 µg/ml DNAse (Sigma Cat# D5025) for 1 hour at 37°C, rinsed in milli-Q water and transferred to TBG to start the immunogold labeling protocol. Incubation with the anti-VII primary antibody was performed overnight at 4°C.

3.16 Cryo-electron Microscopy and Image Processing

Purified viral particles of Ad5/FC31 (light particles L2 and L3, section 4.2) at initial concentration $5.18x10^{11}$ vp/ml were concentrated (9 times for L3 and 10 times for L2) by spinning at 4°C in an Amicon Ultra centrifugal filter of 100000 MWCO (Millipore

Cat#UFC510096), applied to Quantifoil R2/4 300 mesh Cu/Rh glow discharged grids and vitrified in liquid ethane using a Leica CPC plunger. Low dose cryo-EM images were acquired on a FEI Tecnai FEG200 electron microscope operated at 200 kV using a 4K x 4K Eagle CCD camera, at a nominal magnification of x50000 and a defocus range of 0.5-4 µm (as estimated using XMIPP). The camera has a pixel size of 15 µm, giving a nominal sampling rate of 2.16 Å/px in the sample.

All images were preprocessed using the software package XMIPP (32). Micrographs (889 for L2, 580 for L3) were screened for minimal drift and astigmatism, and corrected for the phase oscillations of the CTF (phase flip). Only complete particles were manually picked, extracted into box frames of 516 px, and normalized. Particle images (11344 for L2, 11962 for L3) were scaled down to 256 px frames (4.35 Å/px) for computational efficiency. All 2D and 3D classifications and refinements were performed using RELION (133). The 2D classification was used to discard low quality particles. The 2D classification was run for 25 iterations, with 100 classes, with an angular sampling of 10°, and a regularization parameter T =2. The 3D classification was run for 50 iterations, with four classes, starting with an angular sampling of 3.7° and sequentially decreasing to 0.2°, and a regularization parameter T = 4. The initial reference for 3D classifications and refinements was a Ad5 density map created from the cryo-EM high resolution map (PDB: 3IYN (76)) using pdb2mrc (78), and low-pass filtered to 60 Å resolution. The class giving the best resolution (containing 6743 particles for L2 and 6679 particles for L3) was individually refined and used for further analyses. Reported resolutions are based on the gold-standard FSC = 0.143 criterion as implemented in RELION auto-refine and post-process routines (24, 134).

Reference density maps for comparison with the two alternative high resolution models for mature Ad5 were calculated from the corresponding deposited structures (PDB IDs 3IYN for cryo-EM (76) and 4CWU for X-ray crystallography (120)) using pdb2mrc and low-pass filtered to the same resolution as the Ad5/FC31 maps. Atomic models were fitted to the experimental maps using UCSF Chimera (104), after refining the scale of the experimental map by cross-correlation with each reference map. Difference maps were calculated by subtracting the Ad5 map from those of the Ad5/FC31 light particles after filtering all to the same resolution, refining the scale of the experimental map as described above, and normalizing. These subtractions were calculated, and the corresponding figures were obtained, with UCSF Chimera, using the HideDust tool for clarity when required.

For comparison with the Ad2 *ts1* map, a previously published dataset (100) at 2.8 Å/px was reprocessed with RELION auto-refine and post-process procedures. The final 10210 particle map (at 7.7 Å gold-standard resolution) was low-pass filtered at 12.3 Å. The Ad5/FC31 L2 and L3 cryo-EM maps are deposited in the Electron Microscopy Data Bank (EMDB, http://www.ebi.ac.uk/pdbe/emdb; accession numbers EMD-3003 and EMD-3004).

Results

4 Results

4.1 Study of Adenovirus Assembly Within the Cell

There is a considerable amount of inmunofluorescence and EM studies on AdV infection (section 1.6), but there are few specific studies about the viral particle assembly in the cell. Most of the structural studies focus on the replication centers and the nuclear modifications induced by AdV at early times post-infection (the first 24 hours). In the present study, the packaging factors have been followed at late times of infection. The labeling pattern of these factors and the nuclear modifications induced by the wt virus and the delayed packaging mutant Ad5/FC31 were compared in an attempt to obtain new information on the packaging process.

4.1.1 Characterization of Cellular Modifications Induced by Adenovirus Using Electron Microscopy of Epon-Embedded Samples.

The changes in cellular, and particularly, nuclear structure induced by Ad5 wt and Ad5/FC31 at late times post-infection (24, 36, 48 and 56 hpi) were analyzed and compared by EM observation of thin sections of infected cells embedded in Epon. In general, the same modifications reported in the bibliography were found for both wt and Ad5/FC31. In the first 24 hpi (not shown), lobulations of the nuclear envelope could be observed and the cellular DNA was condensed at the periphery of the nucleus. At this time, the nuclei of infected cells presented: clear and electron dense inclusions, compact rings, protein crystals (small at this time of infection) and virus particles. At 36 hpi, the nucleus occupied a large part of the cell (**Figure 11 A and H**) and the cytoplasm was reduced compared to uninfected cells (**Figure 11M**). Compact rings were also observed, some of them looking like typical rings, others looking rather like spheres with holes (**Figure 11B**). At 36 hpi, protein crystals (**Figure 11 D, F, I and K**) and nuclear lobes (**Figure 11 G and L**) increased in number and size; more viruses could be observed in the nucleus (**Figure 11 A and H**), and even some in the cytoplasm (**Figure 11A**); in the nucleus the virus particles formed close-packed arrays (**Figure 11 C and J**).

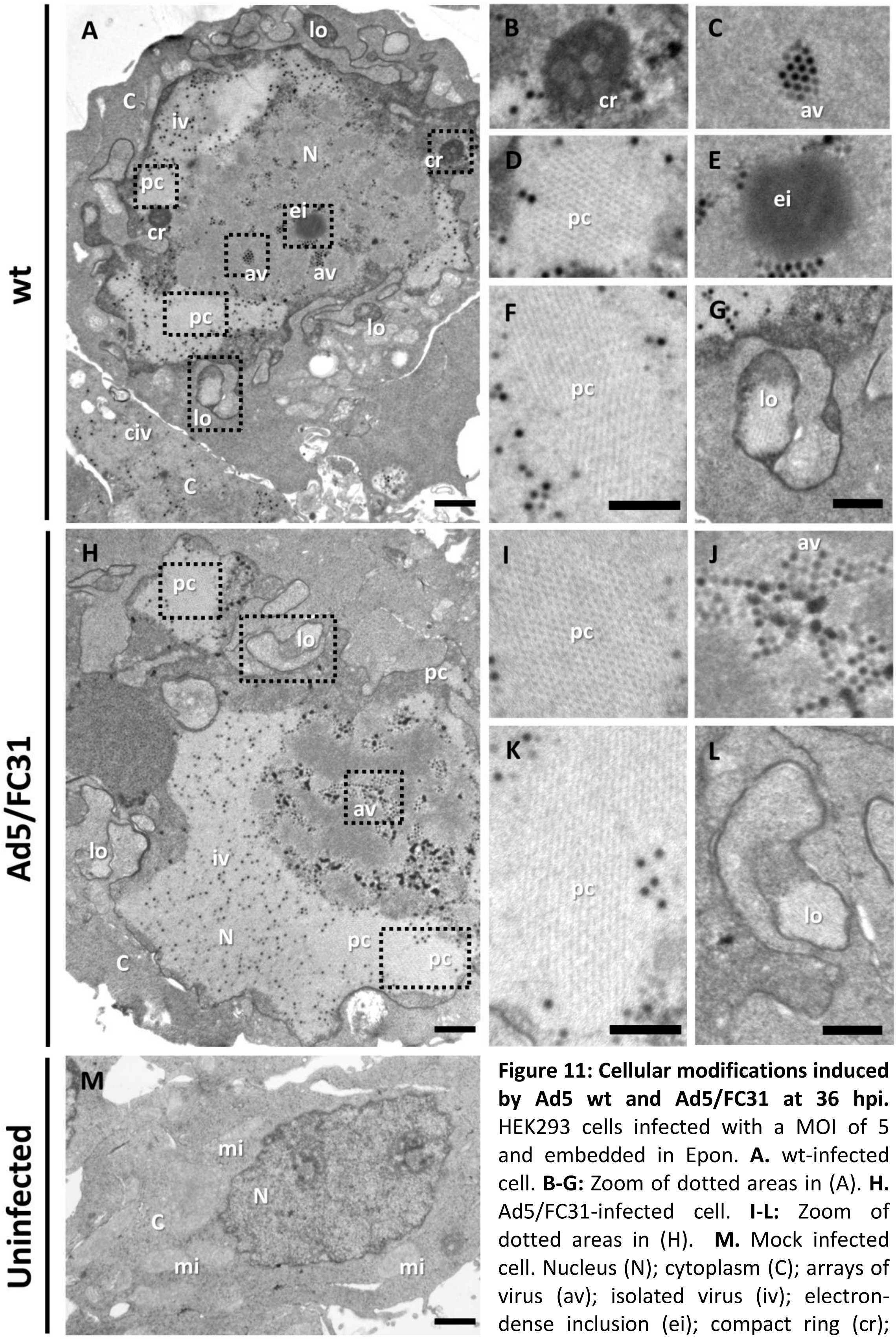
wt
A
lo
C
iv
N
cr
pc
cr
ei
av
av
pc
lo
lo
civ
C
B
cr
C
av
D
pc
E
ei
F
pc
G
lo
Ad5/FC31
H
pc
lo
pc
av
lo
iv
N
C
pc
pc
I
pc
J
av
K
pc
L
lo
Uninfected
M
mi
N
C
mi
mi

Figure 11: Cellular modifications induced by Ad5 wt and Ad5/FC31 at 36 hpi. HEK293 cells infected with a MOI of 5 and embedded in Epon. **A.** wt-infected cell. **B-G:** Zoom of dotted areas in (A). **H.** Ad5/FC31-infected cell. **I-L:** Zoom of dotted areas in (H). **M.** Mock infected cell. Nucleus (N); cytoplasm (C); arrays of virus (av); isolated virus (iv); electron-dense inclusion (ei); compact ring (cr); lobes (lo); protein crystal (pc); cytoplasmic isolated virus (civ); mitochondria (mi). Scale bars: **A, H and M.** 1 µm. **B, C, D, E, F, I, J, K and G, L.** 500 nm.

At 48 hpi, large protein crystals (up to ~8 µm larger dimension), inclusions, compact rings and viral particles could be observed, and the nucleolus appeared more compact (**Figure 12B**) that at early times post-infection. Also, phagocytic vacuoles started to appear. Finally at 56 hpi, phagocytic vacuoles were present in both wt and Ad5/FC31, but cellular damage was much more evident for wt than for Ad5/FC31 (**Figure 12 F and G**). Some cells infected with wt were completely lysed with only the cytoskeleton remaining (not shown). In most cells infected with wt the nuclear envelope was broken, the cytosol was disorganized and contained abundant viral particles (**Figure 12F**).

Interestingly, apart from the modifications described above, a new structure consisting of dots with very high electron density embedded in a high electron dense background was detected in infections with Ad5/FC31, and was called "speckled body" (SB) due to its appearance (**Figure 12C-E**). The possibility that this structure corresponded to compact nucleolus was ruled out because the electron dense dots of SBs are larger (70 ± 11 nm, n=50) than the typical dots of nucleolus (eukaryotic ribosomes around 25-30 nm). The size of SB dots is more similar to that of the viral particles (**Figure 12A**, insets). SBs were observed in Ad5/FC31 infected cells from 36 hpi. At this time of infection many SBs had a lobular, loose organization (**Figure 12C**), while at later times they appeared more compact and circular (~3 µm) (**Figure 12 E and G**). Occasionally, ring shaped SBs were also found (**Figure 12D**). Extensive search revealed that SBs were also present in Ad5 wt infected cells, but their appearance was extremely rare. A summary of the cellular modifications induced by both virus types is presented in **Table 1**.

Table 1: Time of appearance of the main cellular alterations observed after infection of HEK 293 cells with Ad5 wt or Ad5/FC31 (MOI = 5).

Feature	wt	Ad5/FC31
Protein crystals	24hpi	24hpi
Arrays of virus	24hpi	24hpi
Lobes	24hpi (few)	24hpi
Cytoplasmic virus	36hpi	36hpi
Phagocytic vacuoles	48hpi	48hpi
Speckled bodies	36hpi (Very unusual)	36hpi

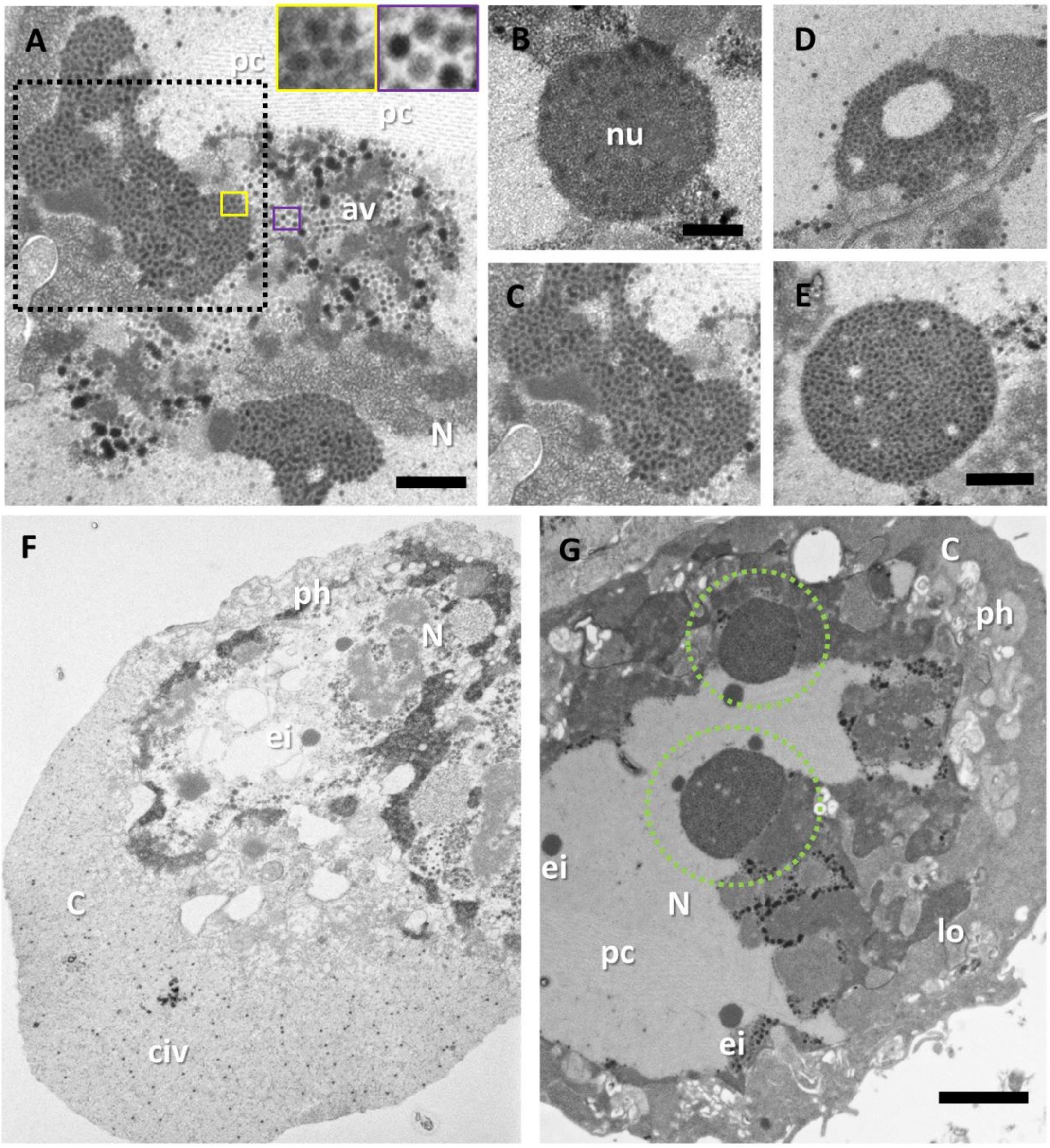

Figure 12: Differences in cell modifications induced by Ad5 wt and Ad5/FC31 at very late times post-infection. Cells infected with a MOI = 5 and embedded in Epon. **A.** Ad5/FC31 at 48 hpi. The insets show zooms in a speckled body (yellow area) and viral particles (purple area). **B.** Nucleolus from cell infected with Ad5 wt at 48 hpi. **C.** Speckled body, zoom of dotted area in (A). **D-E.** Other speckled bodies found in Ad5/FC31 infections at 36 and 56 hpi respectively. **F and G.** Cells at 56 hpi infected with Ad5 wt and Ad5/FC31 respectively. Green dotted circles highlight speckled bodies. Nucleus (N); cytoplasm (C); isolated virus (iv); cytoplasmic isolated virus (civ); electron-dense inclusion (ei); lobes (lo); protein crystal (pc); phagocytic vacuoles (ph). Scale bars: **A.** 700 nm. **B-E.** 500 nm. **F-G.** 1.5 µm.

In conclusion, the most noticeable differences between wt and Ad5/FC31 regarding modifications induced in the cell were found starting at 36 hpi, in agreement with differences in the viral cycle and genome packaging previously observed (1). At 48 hpi, the presence of the Ad5/FC31 SBs was most noticeable. Further, at 56 hpi cell damage was extensive in wt infections. Therefore, subsequent experiments aiming to localize the packaging factors in the cells were carried out at 36 or 48 hpi.

4.1.2 Localization of Factors Involved in Adenovirus Genome Packaging Using Inmunofluorescence Microscopy.

To obtain information on the nuclear region where AdV packaging happens, newly synthesized viral DNA and packaging factors IVa2 and L1 52/55 kDa were localized by inmunofluorescence microscopy in wt or Ad5/FC31 infected cells at 36 hpi.

To label viral DNA, two doses of BrdU were supplied to infected cells at 18 and 25 hpi (section 3.14). This strategy ensures that all DNA synthesized at late times post-infection is labeled, and that only viral DNA is labeled, since at 18 hpi cellular DNA replication no longer occurs (52). Viral DNA label in both Ad5/FC31 and wt showed a diffuse ring pattern (**Figure 13A-F**). Analyzing these rings in orthogonal views, it was found that they had an ellipsoidal shape with a maximum axis 6.8 ± 1.8 µm and minimum axis 5.0 ± 1.2 µm (n=40). These rings are similar to those previously reported for early replication foci (71). When the patterns of the two types of infection were compared, more DNA signal was detected in Ad5/FC31 than in wt infected cells (more cells infected with Ad5/FC31 have BrdU signal, **Figure 13 B and E**). This observation is consistent with that reported by Alba, et al. (3), where this mutant had a normal DNA replication but its packaging was delayed. The packaging defect would produce the DNA accumulations observed in fluorescence microscopy. Occasionally, in Ad5/FC31 infections a concentric ring pattern (maximum axis 6.8 ± 1.5 µm and minimum axis 3.7 ± 1.0 µm, n=19 for external ring) was also observed (**Figure 13 G and H**). This kind of pattern has previously been described by Pombo et al (1994) at early times post-infection and also corresponds to replication centers.

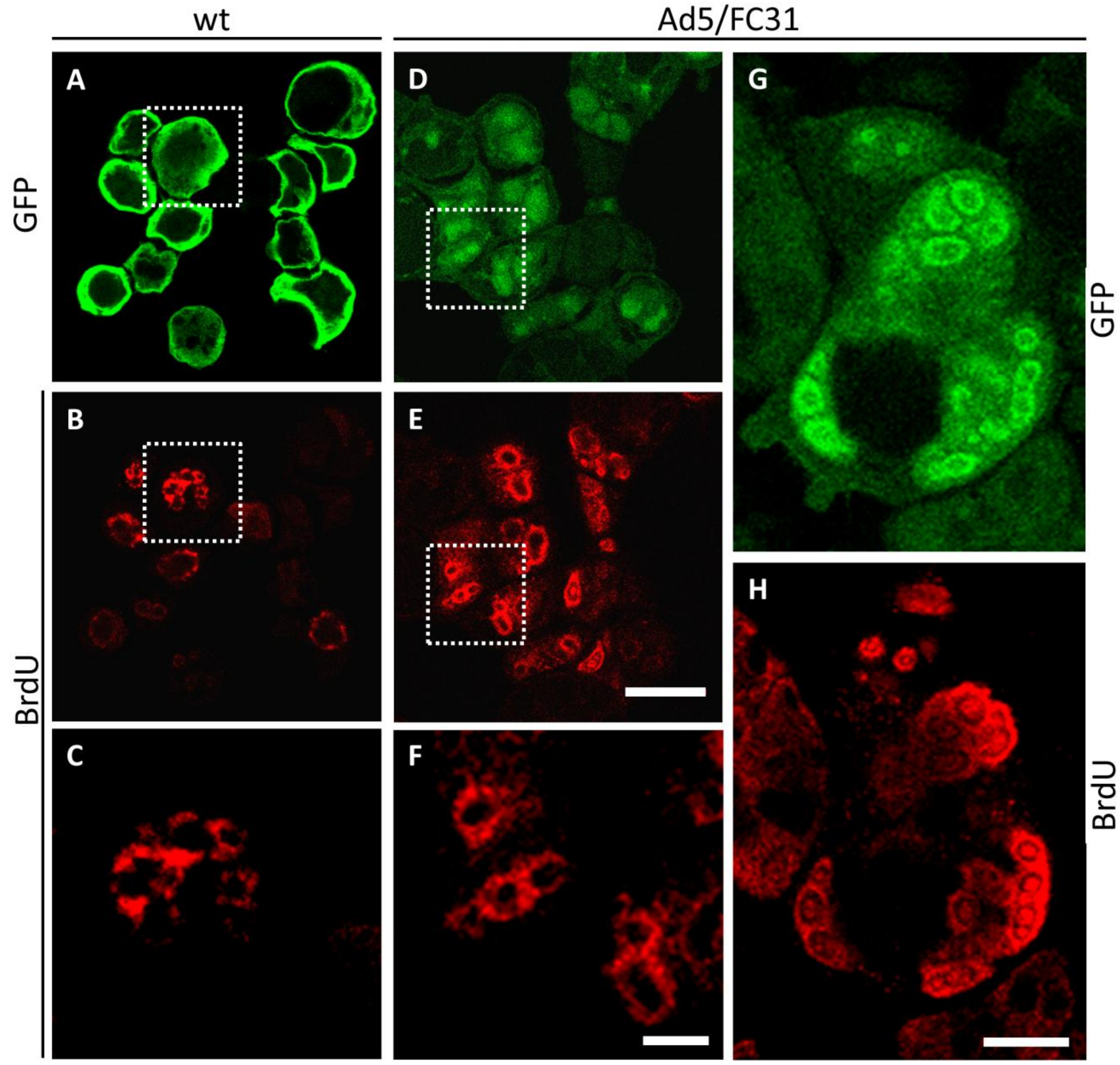

Figure 13: Viral DNA in cells infected with Adenovirus (MOI=50) at 36 hpi. Confocal planes (0.38 µm thick for wt and 0.29 µm thick for Ad5/FC31) showing representative labeling pattern in Ad5 wt (**A-C**) and Ad5/FC31 (**D-F**). **G-H.** Extreme DNA accumulation in an Ad5/FC31 infected cell showing a concentric ring pattern. **A, D and G.** GFP signal (green) indicates the expression of early viral genes in these cells. The signal in (D and G) is low because the acid treatment required for BrdU labeling affects GFP (section 3.14). In (A) anti-GFP was used to increase the signal. **B-C, E-F and H**. BrdU signal (red). **C and F.** Zoom in areas highlighted with white squares in (B) and (E), respectively. Scale bars: **A-B and D-E.** 20 µm. **C and F.** 5 µm. **G-H.** 10 µm.

In AdV replication centers, dsDNA produced by continuous replication accumulates around ssDNA areas with little replication activity (section 1.6). The diffuse ring BrdU label at late times post-infection could correspond to a center of replication and accumulation of viral dsDNA. In that case the area labeled with BrdU would be the peripheral replicative zone (PRZ) and the unlabeled areas in the wt and Ad5/FC31 pattern (inside the ring) could correspond to the ssDNA accumulation site (DAS) where the replication is not continuous and the ssDNA is accumulated. To test this hypothesis, the presence of AdV ssDNA binding protein (DBP) was investigated using double labeling against BrdU and DBP.

Unlike the sharp rings described for DBP at early times post-infection (20 hpi) (107) (**Figure 5**, inset), at 36 hpi the DBP labeling pattern is diffuse. However there are zones where this protein is accumulated (**Figure 14**). These accumulations are adjacent to or surrounded by BrdU-labeled zones, and sometimes they overlap, possibly indicating ssDNA engaged in active replication. The DBP regions (without BrdU signal) would correspond to ssDNA synthesized at early times post-infection before addition of the first BrdU dose. Therefore, these areas could be called early ssDNA accumulation site (EDAS), and from now on the term EDAS will be used instead of DAS. These results support the idea that BrdU labeling is revealing AdV replication centers at late times post-infection.

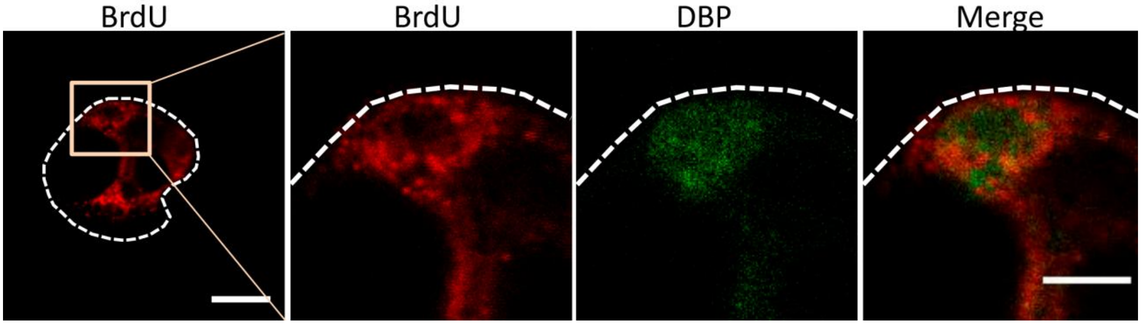

Figure 14: Localization of Viral dsDNA and ssDNA in replication centers. Confocal plane (0.29 µm thick) showing a HEK 293 cell infected with Ad5/FC31 (MOI = 50, 36 hpi) and labeled with anti-BrdU and anti-DBP. Scale bar for first image: 10 µm; last image: 5 µm. The dashed white contour indicates the periphery of the infected cell.

Next, the localization of the packaging proteins IVa2 and L1 52/55 kDa was analyzed. No difference was observed between wt and Ad5/FC31 infections for the L1 52/55 kDa and IVa2 inmunofluorescence labeling pattern. In all cases, these proteins showed diffuse signal around unlabeled areas in the nucleus. Also, both IVa2 and L1 52/55 kDa appeared in amorphous clusters and small rings (maximum axis 1.6 ± 0.3 µm and minimum axis 1.2 ± 0.3 µm, n=37) (**Figure 15**), although label in clusters for IVa2 was less noticeable than for L1 52/55 kDa. In general, label for IVa2 was weak, perhaps correlating with the low copy number of the protein in the virions, or with limited antibody reactivity.

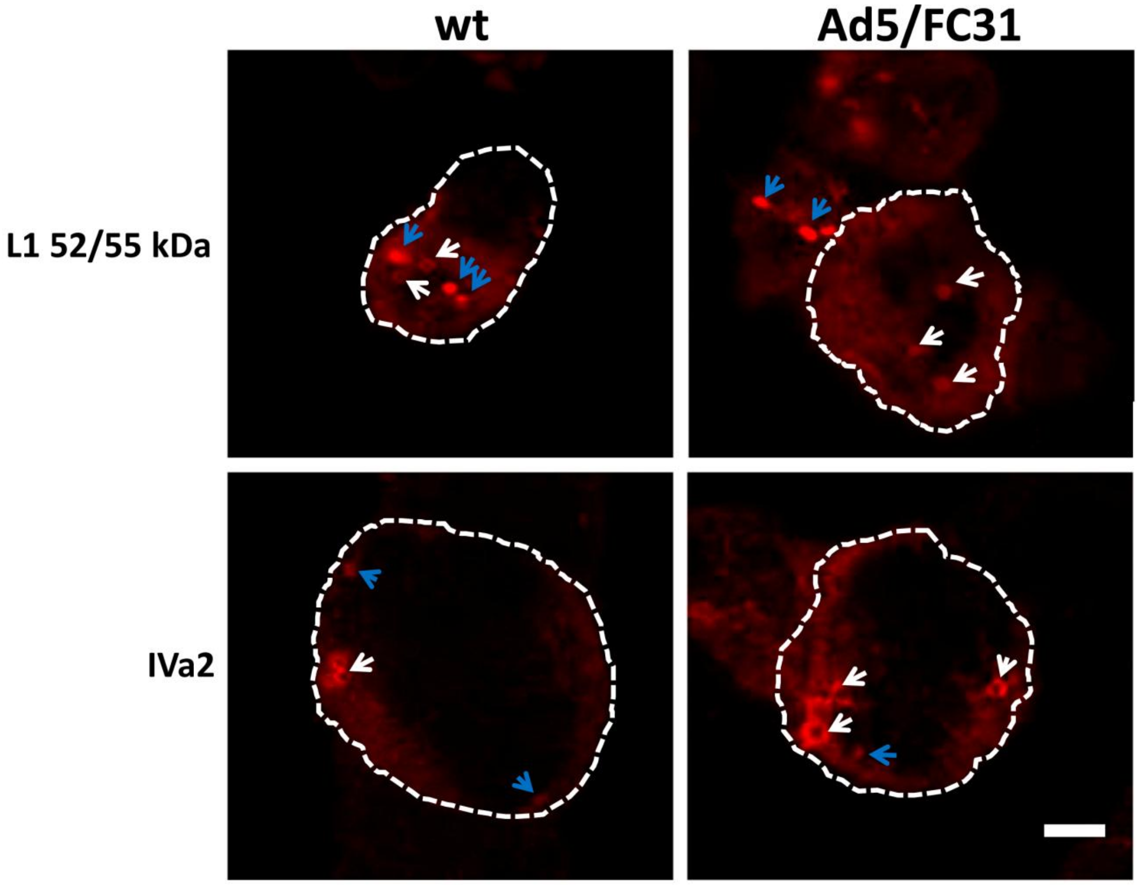

Figure 15: Adenovirus infected cells (MOI=50, 36hpi) labeled with antibodies for L1 52/55 kDa and IVa2. Rings are indicated with white arrows, and clusters are indicated with blue arrows on confocal planes 0.29 µm thick. Scale bar 4 µm. The dashed white contours indicate the periphery of the infected cell.

In view of the similar pattern presented by IVa2 and L1 52/55 kDa, double labeling was carried out to determine if they colocalize. This assay revealed that both proteins were present in the small rings (**Figure 16 D, H and L**) while they occasionally appeared together in amorphous clusters (**Figure 16 B, C, F, G, J and K**). It must be noted that the size difference and lack of BrdU label rule out the possibility that the small rings correspond to replication centers.

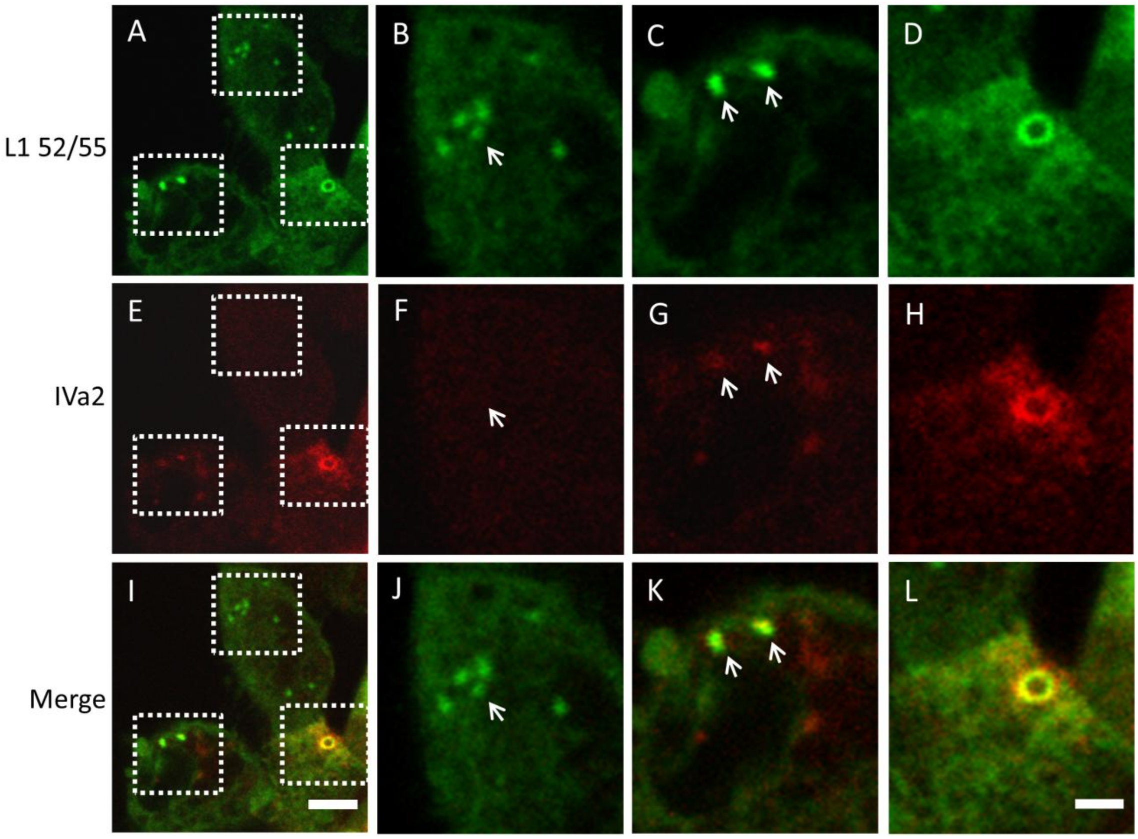

Figure 16: Double labeling against L1 52/55 kDa and IVa2 in Ad5 wt infected cells (MOI=50, 36hpi). A, E and I. Confocal plane (0.21 µm thick) showing a general view in a sample labeled with anti-L1 52/55 kDa, anti-IVa2 and simultaneous display of label for both proteins, respectively. Bar: 5 µm. **B-D, F-H and J-L.** Zoom of dotted areas in A, E and I respectively. Bar: 2 µm. Arrows point to label in clusters.

The diffuse label around nuclear unlabeled zones for L1 52/55 kDa and IVa2 was reminiscent of the BrdU labeling in the PRZ of replication centers (**Figure 13**). To test the possibility that the packaging proteins were located at the PRZs, double labeling assays for viral DNA and L1 52/55kDa or IVa2 were carried out. In these experiments, no label for IVa2 was observed, indicating that the reactivity of the anti-IVa2 is sensitive to the acid treatment required to label DNA with BrdU (section 3.14). For both viruses, L1 52/55kDa was detected in the periphery of replication centers labeled with BrdU (**Figure 17**), where both signals intermingled. There was no label for L1 52/55 kDa in the BrdU-unlabeled areas corresponding to the EDAS. The presence of L1 52/55 kDa in the PRZ could indicate that DNA packaging occurs in this area.

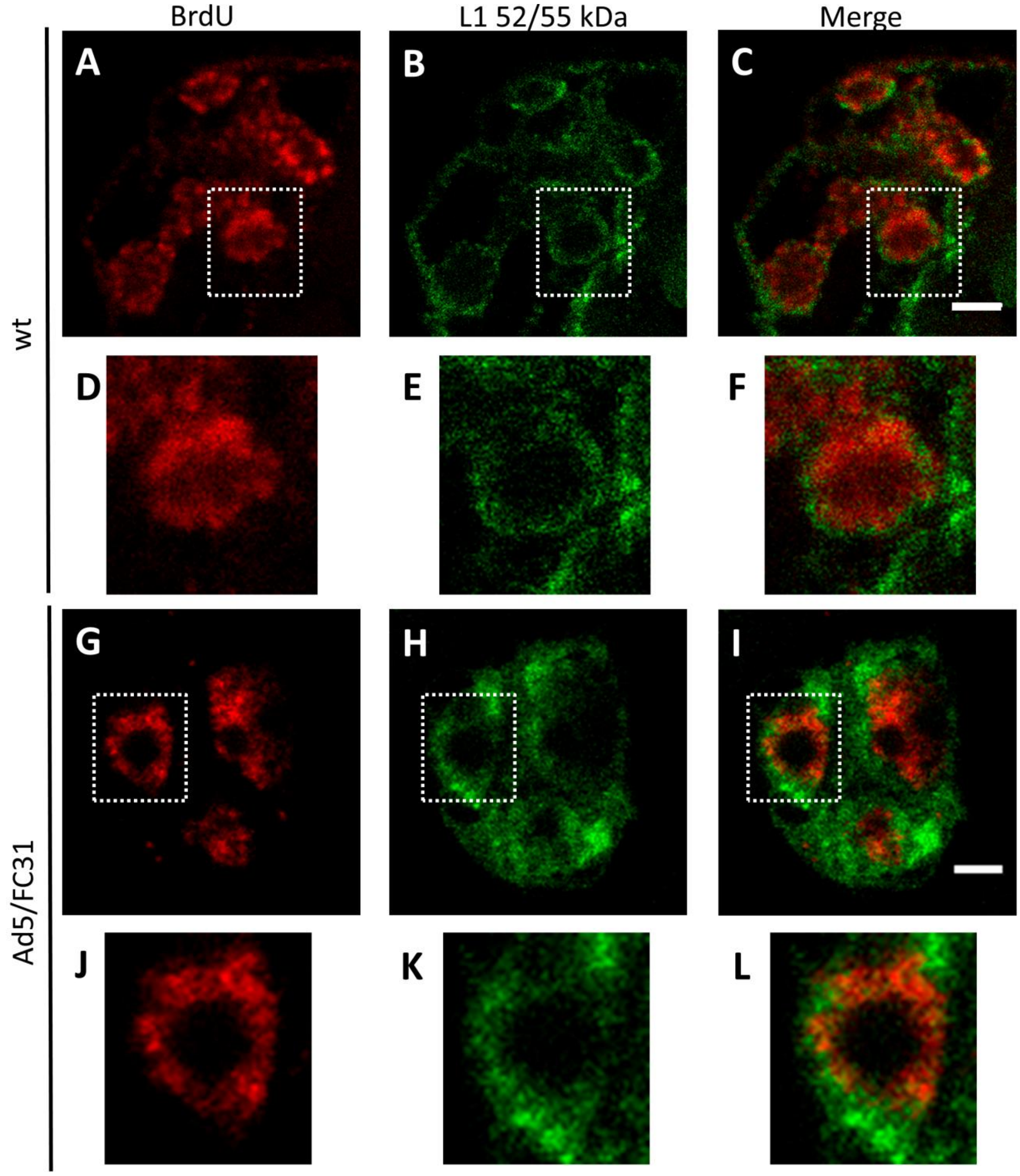
BrdU
L1 52/55 kDa
Merge
A
B
C
D
E
F
G
H
I
J
K
L
wt
Ad5/FC31

Figure 17: Double labeling against viral DNA and L1 52/55 kDa in Ad5 wt and Ad5/FC31 infected cells (MOI 50, 36 hpi). A-F Cell infected with wt (confocal plane 0.29 µm thick). **D-F.** Zoom of the dotted areas in A, B and C. **G-L.** Cell infected with Ad5/FC31 (confocal plane 0.21 µm thick) **J-L.** Zoom of the dotted areas in G, H and I respectively. Scale bars 3 µm.

4.1.3 Possible Localization of Adenovirus PRZs in Conventional EM of Infected Cells

To obtain more detail on the possible packaging site of AdV in infected cells, EM was used. First, sections from Epon embedded cells were analyzed for regions in the nucleus that could correspond to PRZs. Previous EM studies (12, 109, 114-116) indicated that PRZs were ring-shaped moderately electro-dense regions, surrounding electro-clear areas corresponding to EDAS. Also, it had been described that PRZs contained electron-opaque grains (EOGs) and viral particles. Regions corresponding to these characteristics, and in a size range compatible with that of PRZs at late times post-infection (as observed by the IF assays presented here) were identified in both Ad5 wt and Ad5/FC31 infected cells (**Figure 18**). Interestingly, it was observed from 36 hpi that EOGs seemed to originate from loose electron-dense material, which was tentatively called DNA bundle because of its texture (**Figure 18 G**).

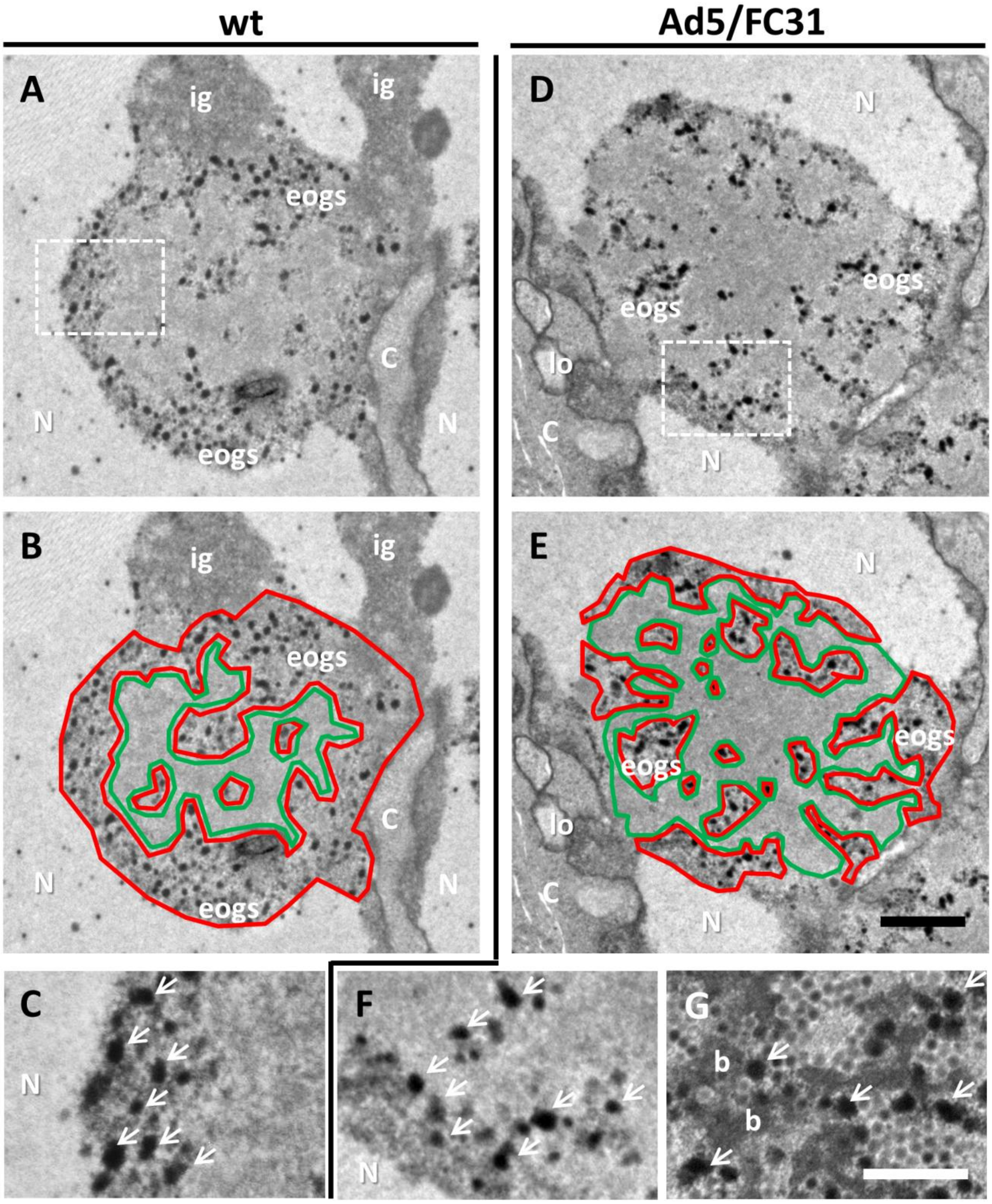
wt
Ad5/FC31
A
ig
ig
eogs
C
N
N
eogs
B
ig
ig
eogs
C
N
N
eogs
D
N
eogs
eogs
lo
C
N
E
N
eogs
eogs
lo
C
N
C
N
F
N
G
b
b

Figure 18: Possible AdV replication centers at late times post-infection observed in Epon sections. Cellular sections infected with Ad5 wt (**A-C**) and Ad5/FC31 (**D-G**) at 36 hpi (MOI = 5). **B and E.** Red and green contours indicate the possible PRZ (red) and EDAS (green) regions. The contour colors are chosen for comparison with the BrdU/DBP double labeling shown in Fig. 14. **C and F.** Zoom of the dotted areas in A and D respectively. White arrows indicate EOGs. **G.** Section of a cell infected with Ad5/FC31 at 48 hpi (MOI = 5). The EOGs are in direct contact with loose electron-dense material which could be DNA by its texture (DNA bundles, b). Numerous viral particles are also present. Nucleus (N); cytoplasm (C); lobes (lo); electron-opaque grains (eogs); cluster of interchromatin granules (ig). **A-B and D-E** Scale bar 1 µm**. C, F and G.** Scale bar 500 nm.

4.1.4 Localization of Factors Involved in Adenovirus Genome Packaging Using Immuno-Electron Microscopy on Freeze-Substituted Samples.

To corroborate the identity of the possible PRZs, infected cells were treated with BrdU and processed for immuno-EM by freeze substitution (FS), to preserve both structure and immunoreactivity. In FS samples, the possible PRZs and EDAS regions were identified on the basis of their electron-density and the presence of EOGs and viral particles (**Figure 19A-B and E-F,** red and green contours indicate PRZ and EDAS regions respectively). Label for BrdU was specifically found in the possible PRZ area confirming its identity (**Figure 19 B and F**). Label in the PRZ was frequently associated to full particles (virions) (F**igure 19 B and G**, arrows), EOGs (**Figure 19 D and H**) and the loose electro-dense material ("bundles", labeled with b in **Figure 19 B, C, F and G**), confirming that they contained viral DNA. The different electron density levels of these structures could indicate different degrees of DNA condensation, from most relaxed (bundles) to most compact (virions and EOGs). The signal of BrdU in EOGs indicated the presence of viral DNA, and not only RNA as it had been reported by other studies (111) (section 1.6). The observed EOGs had various sizes but they were generally larger than the viral particles. No significant BrdU label was observed outside the viral replication center or in the cytosol. The electro clear area proposed to be the EDAS showed weak label (**Figure 19 B and F**), in agreement with the IF results and previous reports indicating low replicative activity in this region. Labeling with anti-DBP antibody was unsuccessful, suggesting that even under FS conditions the reactivity of the DBP epitopes was not preserved.

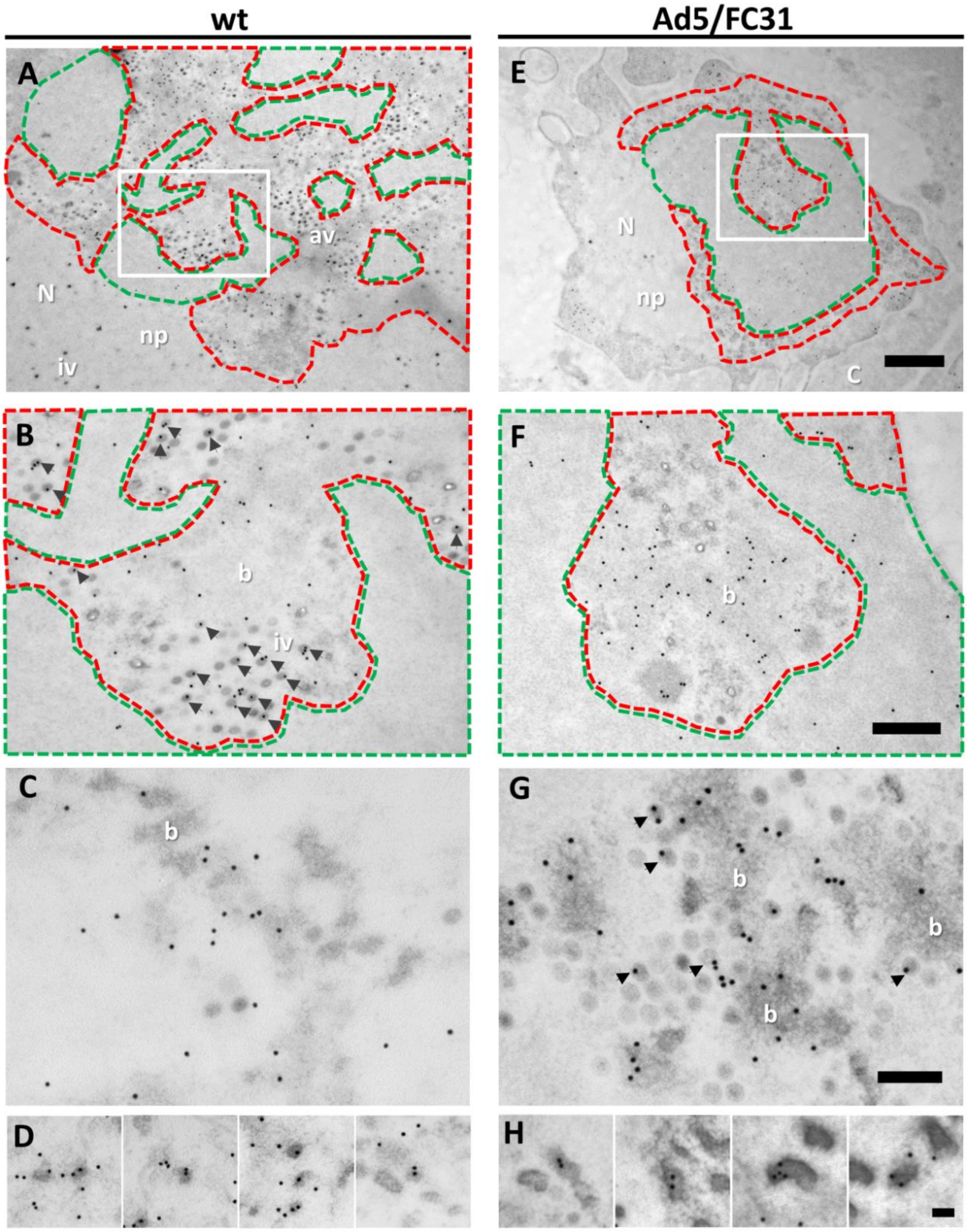

Figure 19: Localization of newly synthesized viral DNA in infected cells processed by freeze-substitution. Viral DNA replication and accumulation centers labeled with anti-BrdU and 15 nm gold particles in HEK293 cells infected with Ad5 wt (A-D) and Ad5/FC31 (E-H) (MOI=50, 48 hpi). Cellular sections treated with proteinase K before immuno-labeling. **A and E** show low magnification views of replication centers with the EDAS area (electro-clear) highlighted in green and the PRZ in red. **B and F.** Zoom of highlighted areas in (A) and (E) respectively. **C and G.** Details of other PRZs showing BrdU signal on bundles, indicating that they contain viral DNA. **D and H.** EOGs produced by Ad5 wt and Ad5/FC31 respectively. Scale bars: 1 µm **(A and E);** 0.4 µm **(B and F);** 200 nm **(C and G)** and 100 nm **(D and H).** Nucleus (N); cytoplasm (C); isolated virus particles (iv); DNA bundles (b); nucleoplasm (np). Arrowheads indicate viral particles with BrdU signal.

Next, the localization of packaging protein L1 52/55 kDa was analyzed. Scattered label for this protein was observed throughout the infected nuclei, including the PRZ (**Figure 20 A and B**). However, very few gold particles were observed in the EDAS, supporting the specificity of the label. It is interesting to highlight that the L1 52/55 kDa signal in the PRZ is usually associated to the electro-dense material present in this area (EOGs and the bundles previously described for BrdU labeling, **Figure 20 A-B and Figure 21 F and L**). Sections labeled for L1 52/55 kDa were also scanned for substructures outside the PRZ that could correspond to the clusters and rings observed by IF (**Figure 15**). Very abundant label was found in electron dense, smooth inclusions (**Figure 21 A and G**), which by size (diameter 1.1 µm ± 0.4 µm, n=16) and amount of label could correspond to the clusters observed by IF. No label was detected in ring-like structures, even in compact rings (**Figure 21 B and H**), which were the obvious candidates by both shape and size. As expected, L1 52/55 kDa was detected in viral particles, particularly in those with lower electron density which probably have not completed packaging (**Figure 21 C-D and I-J**). Label in viral particles sometimes presented an arch pattern suggesting a shell of this protein inside the capsid. These observations support the idea of two pools of L1 52/55 kDa protein during assembly (82), one binding to the viral DNA (signal in bundles and EOGs) and another binding to capsid proteins (signal in electro clear capsids). Interestingly, groups of gold particles also forming little arches were found near the PRZs (**Figure 21 E and K**), suggesting L1 52/55 kDa shell fragments on their way to assemble with capsid proteins. This interpretation would be supported by the previously reported homo-oligomerization capacity of L1 52/55 kDa (99). Another interesting observation is the arch pattern present in EOGs (**Figure 21 F and L**), suggesting the formation of an L1 52/55 kDa shell on the electron dense material they contain. Since L1 52/55 kDa has been shown to bind to the packaging signal in the viral DNA *in vivo*, this observation supports the hypothesis that EOGs could be DNA condensations, specifically viral genomes.

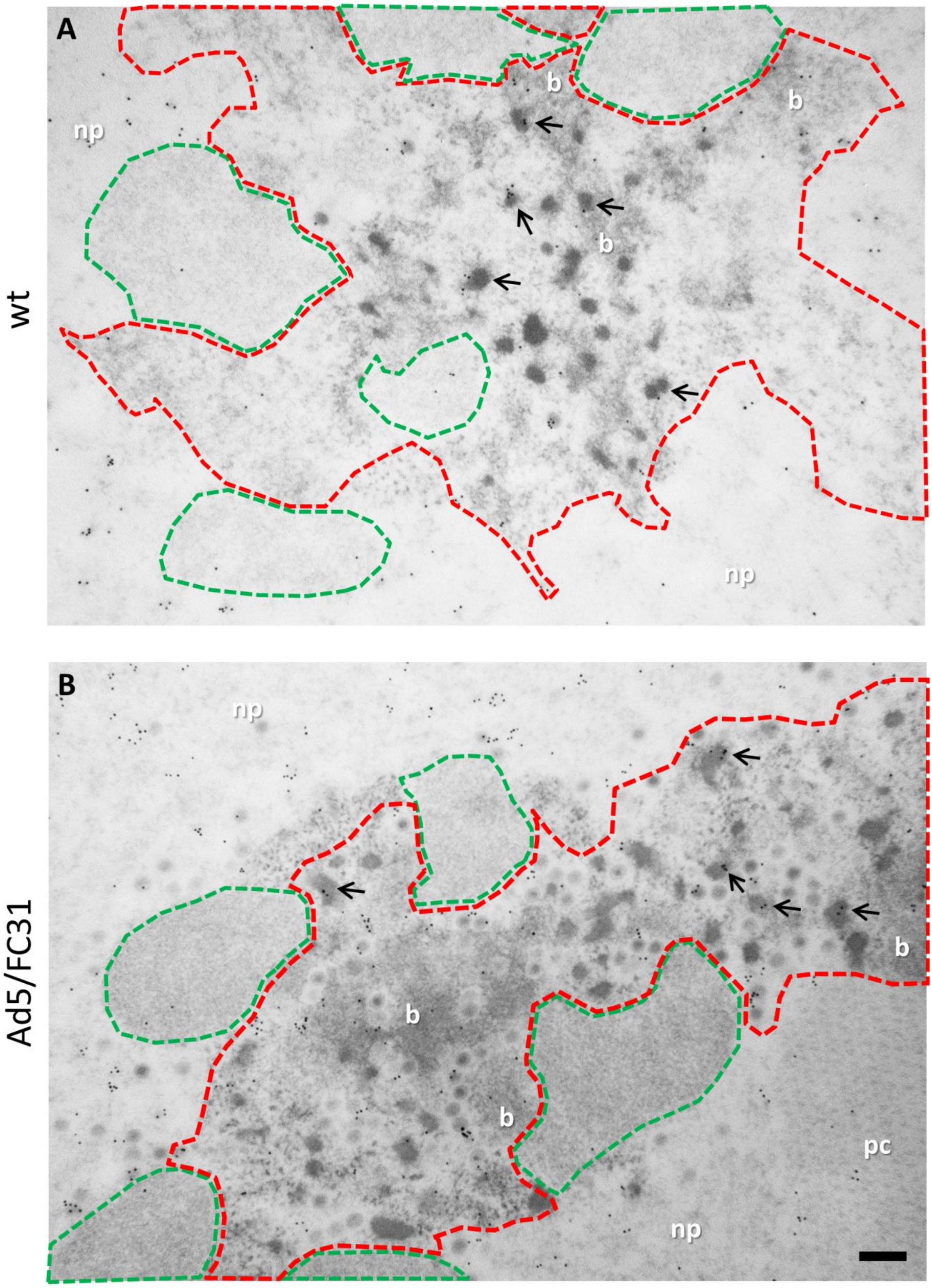
A
wt
np
b
b
b
np
B
Ad5/FC31
np
b
b
b
pc
np

Figure 20: Immunolabeling against L1 52/55 kDa protein. HEK 293 cells infected with Ad5 wt (A) and Ad5/FC31 (B) (MOI = 50, 48 hpi). Arrows indicate the presence of L1 52/55 kDa in EOGs. Nucleoplasm (np); protein crystal (pc); DNA bundles (b). Green area: EDAS; red area: PRZ. Scale bar 200 nm.

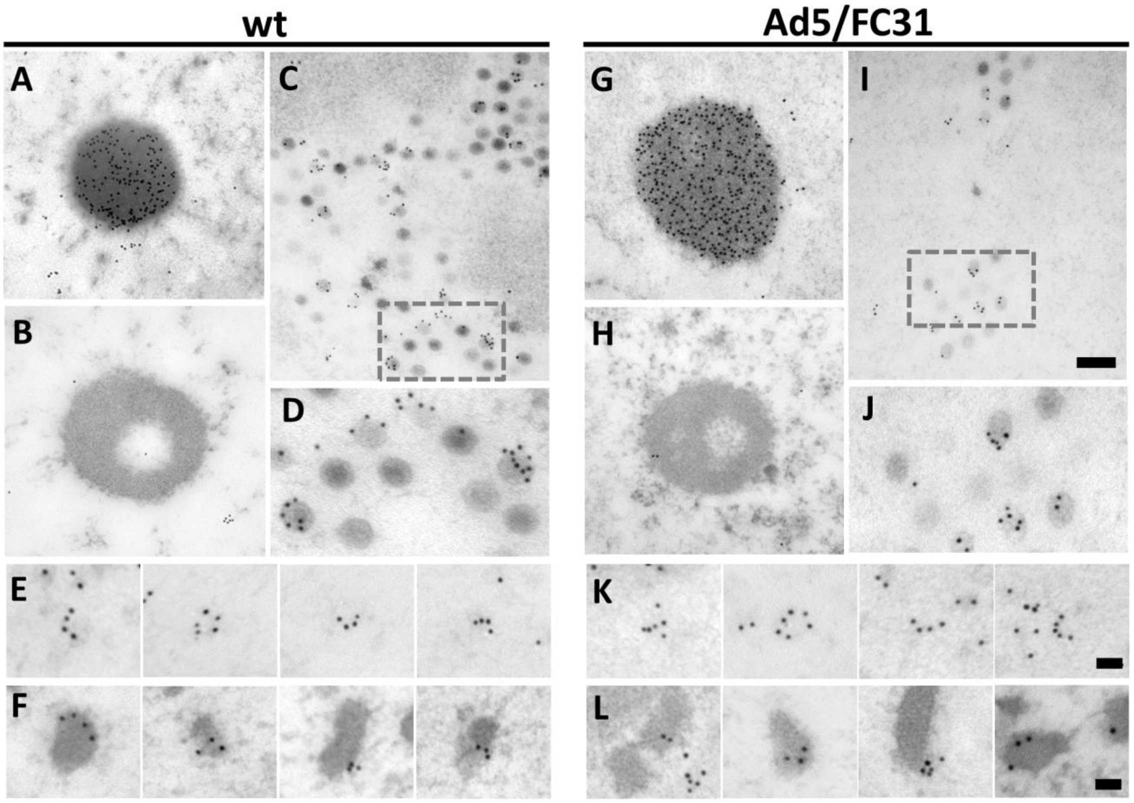

Figure 21: Structures observable in Ad5 wt and Ad5/FC31 infected cells labeled for L1 52/55 kDa. A and G. Electron dense inclusions. **B and H.** Compact rings. **C and I.** viral particles. **D and J.** Zoom on the dotted areas in C and I respectively. **E and K.** Arch-shaped labels in the nucleoplasm close to PRZs. **F and L.** Electro-opaque grains. Scale bars: 200 nm in **A-C** and **G-I**; 50 nm in **E-F** and **K-L**.

The label for packaging protein IVa2 was very similar to that for L1 52/55 kDa, but weaker as previously observed in IF. Signal was observed scattered throughout the nucleus, but was practically absent from EDAS (**Figure 22 A and B**). It was most abundant in electron dense inclusions (**Figure 23 A and E**), supporting the hypothesis that these corresponded to clusters labeled for IVa2 in IF. Surprisingly, IVa2 was not detected in compact rings (**Figure 23 B and F**), in contradiction with previous findings (80). Therefore, it is not possible at this point to correlate the small rings labeled for IVa2 and L1 52/55 kDa in IF with any structure observed by immune-EM. IVa2 was not easily detected in viral particles (**Figure 23 C-D and G-H**); only a few capsids had signal. This result is consistent with its low copy number (6-8) and highly localized position at a single vertex (26). There would be very little chance of exposing just the adequate vertex in a resin section. Finally, signal for IVa2 was observed in the PRZ on electro dense material (bundles and some EOGs) (**Figure 22 A-B, Figure 23 D and H**), again supporting the idea that these structures contain viral genomes.

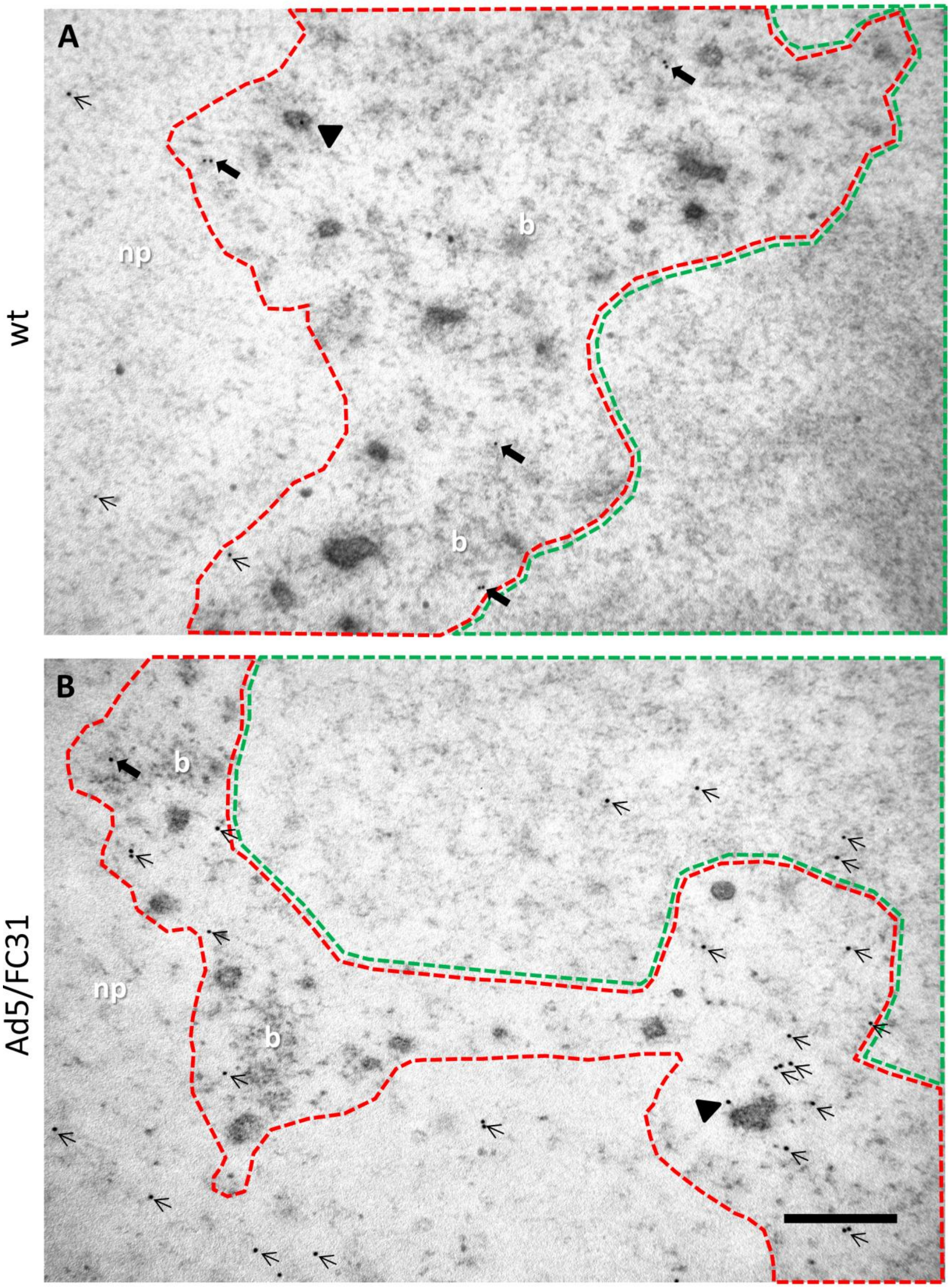

Figure 22: Immunolabeling against IVa2 protein. Cellular sections treated with DNase before the immuno-labeling in an attempt to unmask IVa2 protein epitopes. **A and B.** HEK 293 cell infected with Ad5 wt and Ad5/FC31, respectively, at 48 hpi. Scale bar 300 nm. Green area: EDAS. Red area: PRZ. All arrows indicate the presence of gold particles; closed black arrows and black arrowheads specify the presence of IVa2 in DNA bundles (b) and EOG respectively.

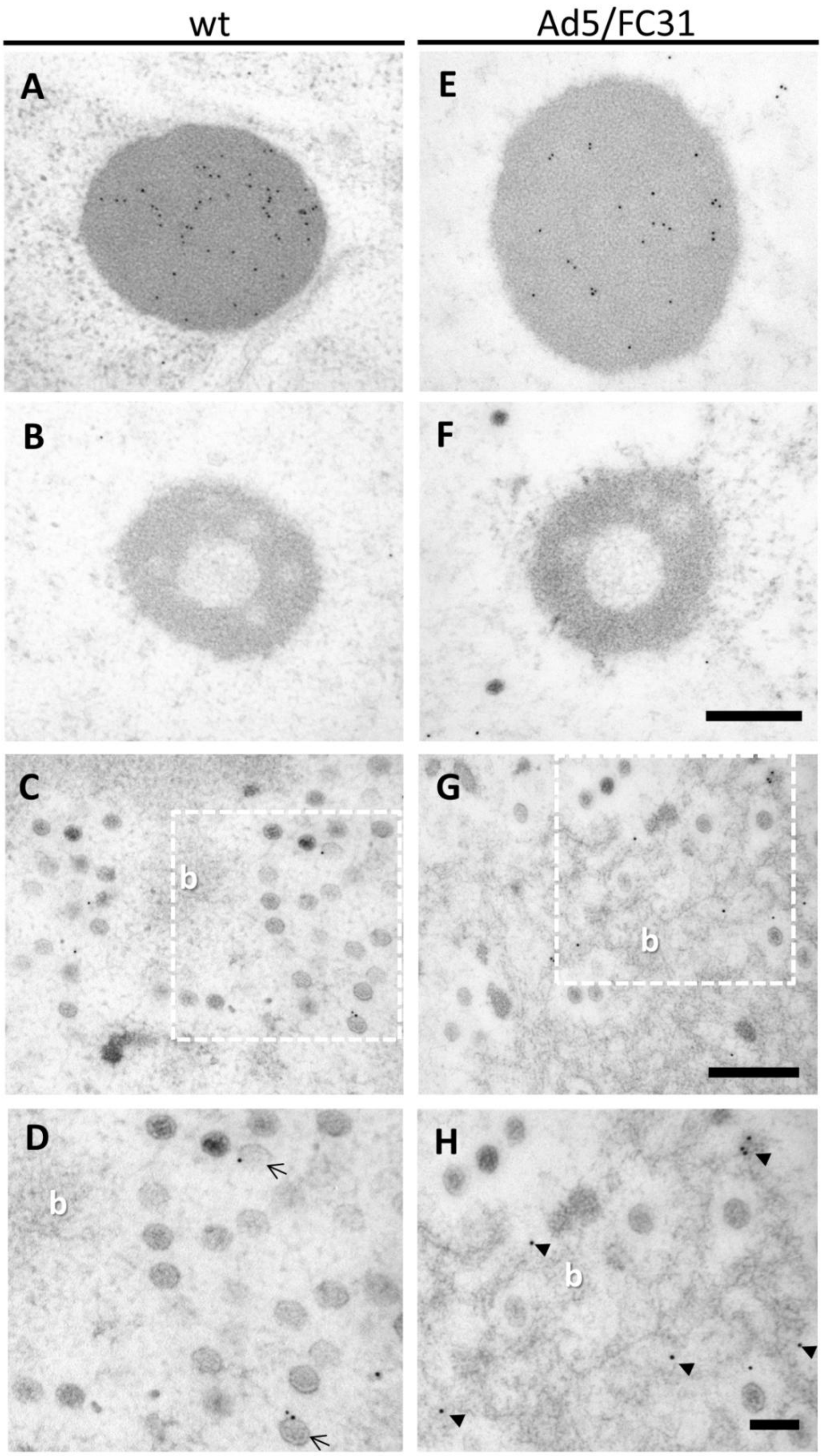

Figure 23: Immunolabeling against IVa2 protein. Structures produced by Ad5 wt (**A-D**) and Ad5/FC31 (**E-H**) labeled for IVa2. Cellular sections treated with DNase before the immunolabeling in an attempt to unmask IVa2 protein epitopes. **A and E.** Electron dense inclusions. **B and F.** Compact rings. **C and G.** Virus particles surrounded by DNA bundles (b). **D and H.** Zoom of the dotted areas in E and I respectively. Arrows and arrowheads indicate the presence of IVa2 in viral particles and DNA bundles respectively. Scale bars: **A-B and E-F.** 300 nm. **C and G**. 200 nm. **D and H.** 100nm.

Summarizing, immuno-EM confirmed that the PRZ contained loose bundles of viral DNA synthesized after 18 hpi, and both packaging factors L1 52/55 kDa and IVa2. PRZs also contained viral particles, and EOGs that by their electron density, texture and label for BrdU and packaging proteins are consistent with condensed viral genomes. Further, label for L1 52/55 kDa protein in EOGs sometimes formed a shell. These results suggest that the PRZ could be the location in the nucleus where AdV packaging takes place. To test this hypothesis, further experiments were undertaken.

4.1.5 Localization of Adenovirus Structural Proteins Using Immune-Electron Microscopy of Freeze-Substituted Samples

To further assess the hypothesis that the PRZ is the AdV assembly zone, the presence of core and capsid proteins was analyzed. Protein VII was selected to study its localization as core protein. This protein binds to the viral DNA and helps condense it in nucleosome-like structures (154). Label for VII was exclusively observed in the PRZ, frequently in EOGs (**Figure 24 A-B and D-E**) and also in DNA bundles but in lower amounts (**Figure 24F**). This result corroborates the idea that the bundles and EOGs are viral DNA condensed to different degrees by core proteins. Also, protein VII was detected in viral particles (**Figure 24 C and F**).

An antibody against fiber was used to study the localization of capsid proteins. Analyzing capsid protein localization in AdV infected cells is not straightforward, since this virus produces a large excess of both hexon and fiber (105, 106). For fiber, this excess production is thought to have a role in facilitating virus spread throughout the epithelium (155). Fiber was detected in protein crystals (**Figure 25 A and F**), as previously shown (41), and in electron-dense inclusions (**Figure 25 B and G**). It is intriguing that fiber is also detected in these inclusions as well as L1 52/55 kDa and IVa2. This observation could indicate that these inclusions are deposits for excess or misfolded viral proteins. This idea is supported by the observation of a similar structure produced by the Vaccinia virus E6R mutant (20). This mutant fails to properly package the Vaccinia viroplasm (formed by core wall, lateral body and nucleocapsid proteins) into viral membranes, resulting in an accumulation of empty immature virions and large aggregates of viroplasm “aggregated virosomes”, which look like the electron dense inclusions observed in AdV infections. It is not clear if the proteins contained in these structures could be used later in the AdV assembly or if they are final deposits.

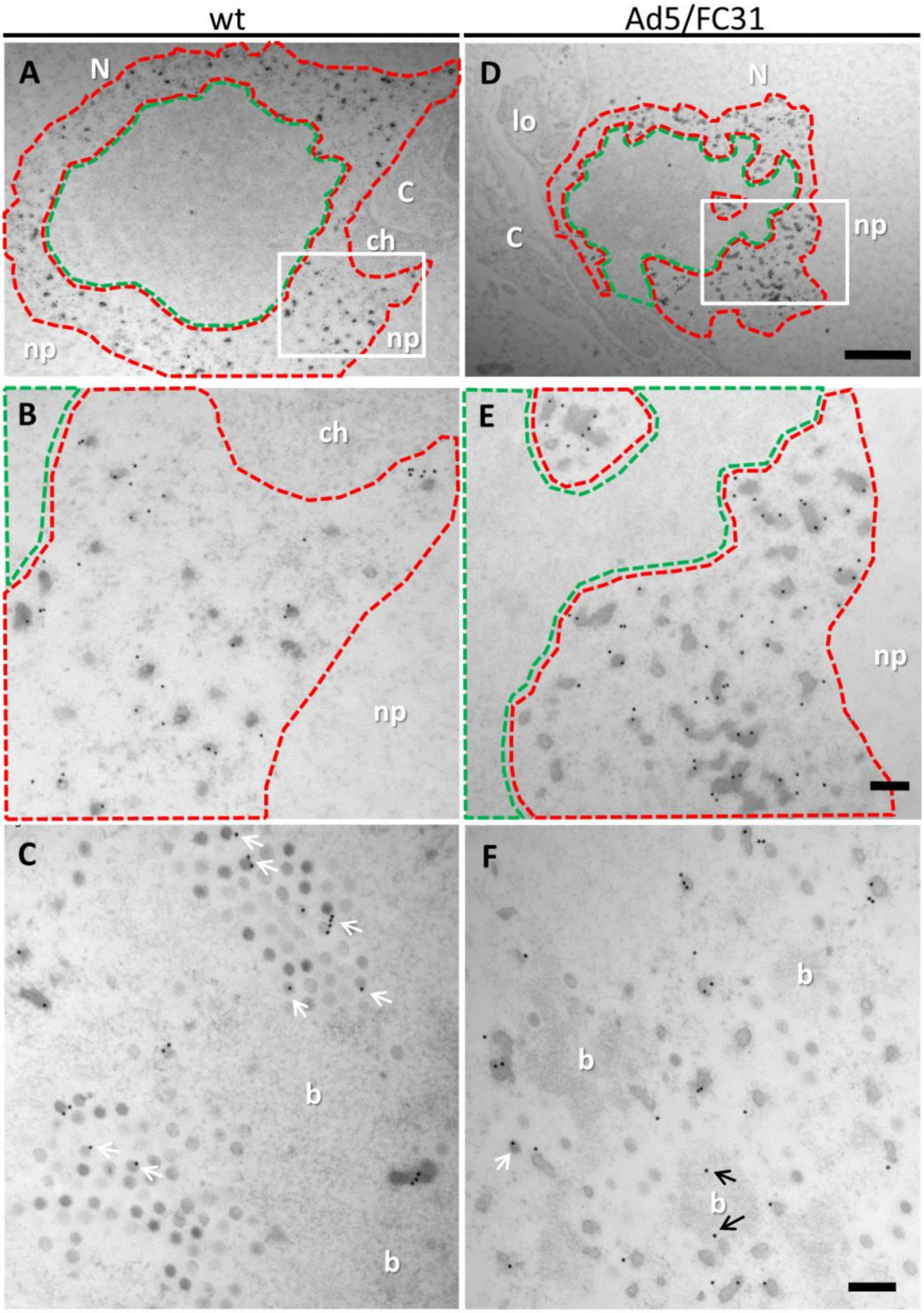

Figure 24: Presence of core proteins in the putative AdV assembly zone. DNA replication and accumulation center labeled against protein VII in HEK293 cells infected with Ad5 wt or Ad5/FC31 (MOI=50) at 48 hpi. Cells were treated with DNase before immuno-labeling to unmask VII epitopes. **A-C** Ad5 wt infected cells. **B.** Zoom of square area in (A). **D-F.** Ad5/FC31 infected cells. **E.** Zoom of square area in (D). Green area: EDAS; red area: PRZ. White arrows indicate signal in viral particles and black arrows indicate signal in DNA bundles. Nucleoplasm (np); nucleus (N); cytoplasm (C); chromatin (ch); DNA bundles (b); lobes (lo). Scale bars: **A and C.** 1 µm. **B, C, E and D.** 0.2 µm.

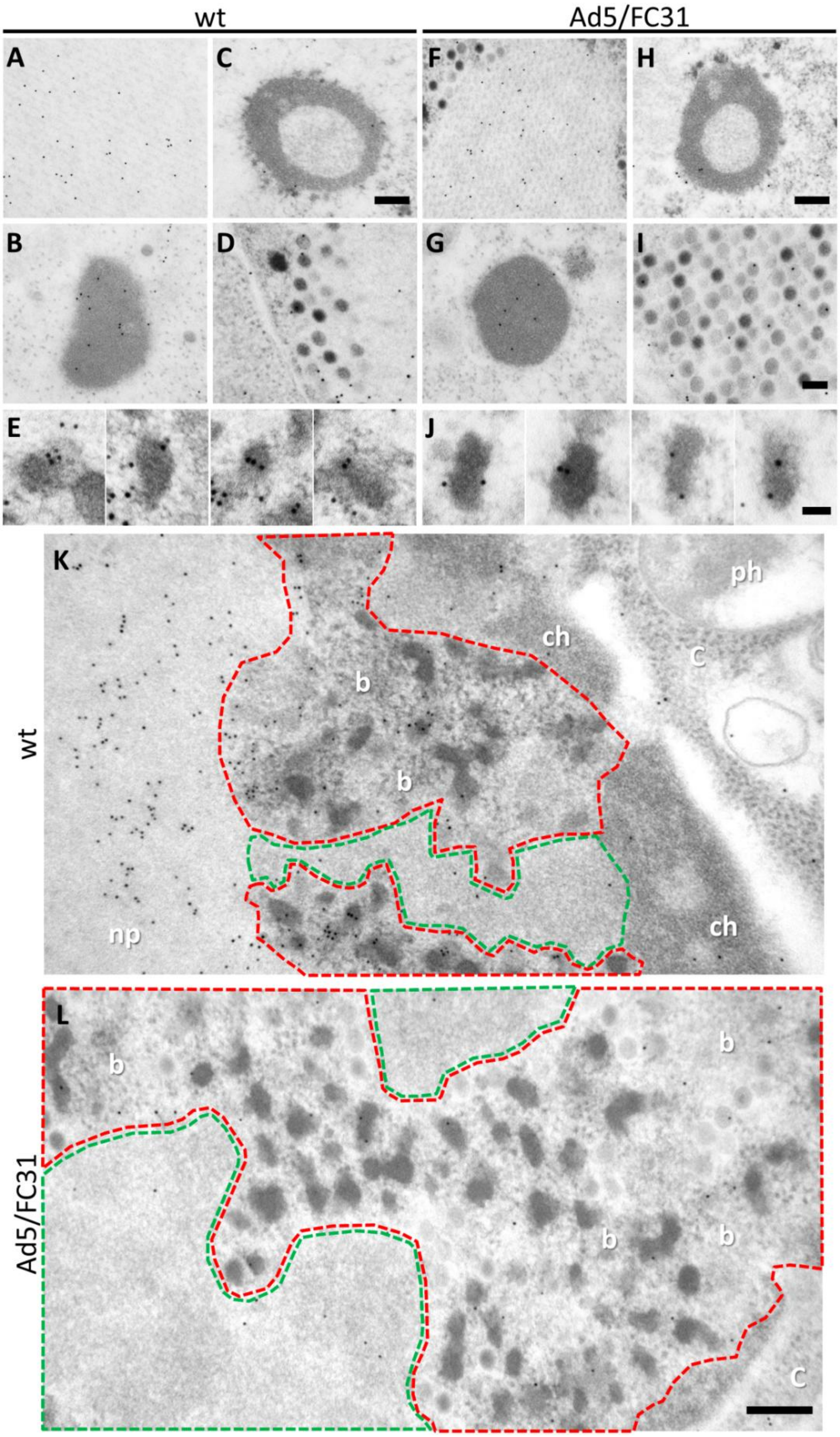

Figure 25: Immunolabeling against fiber protein. A-E and K. HEK 293 cells infected with Ad5 wt (MOI = 50 at 48 hpi). **F-J and L.** HEK 293 cells infected with Ad5/FC31 (MOI = 50 at 48 hpi). **A and F.** Protein crystal. **B and G.** Electron dense inclusions. **C and H.** Compact rings. **D and I.** Viral particles. **A-D and F-I.** Scale bar 200 nm. **E and J.** Electron-opaque grains. Scale bar 50 nm. **K and L.** DNA replication and accumulation center. Scale bar 200 nm. Green area: EDAS. Red area: PRZ. Cytoplasm (C); nucleoplasm (np); chromatin (ch); phagocytic vacuoles (ph) and DNA bundles (b).

Label for fiber was not significant in compact rings (**Figure 25 C and H**). Low signal was observed in viral particles (**Figure 25 D and I**). Finally, fiber was detected in the PRZ (**Figure 25 K and L**), in particular in EOGs (**Figure 25 E and J**) and DNA bundles (**Figure 25 K and L**). Only weak signal was observed in the EDAS (**Figure 25 K and L**), supporting the specificity of the label.

4.1.6 The Adenovirus Assembly Factory and the Actual Assembly Site.

The presence of core and capsid proteins in the PRZ, together with newly synthesized viral DNA and packaging factors, supports the idea that this zone is the AdV assembly site, and not only the DNA replication and accumulation zone as previously described (12, 114-116). This localization of the AdV assembles site is consistent with the work of Weber, et al. (156), where they found that replication and assembly are coupled. Therefore, these processes have to happen in the same place: the PRZ. With this in mind, the term "nuclear factory" could be applied to this structure, making reference to the factories produced by others viruses. Within the AdV factory, the results presented here suggest that the EOGs could be the genome condensation/capsid recruitment sites where assembly occurs, because all assembly factors are present in this structure (viral DNA, packaging, core and capsid proteins). Also, EOGs are frequently observed close to viral particles (**Figure 26 A-C**), which would support this idea. On the other hand, it is important to highlight that the bundles have the same labeling than EOGs, therefore it is possible that it is in this structure where AdV assembly occurs. Viral particles are also found in the vicinity of the bundles (**Figure 26 C**). Detailed observation of FS samples in search for possible assembly intermediates revealed that half capsids could occasionally be observed engulfing viral DNA budding from the loose DNA bundles (**Figure 26D**), indicating that these are indeed the assembly site. It is interesting to note that finding this kind of assembly intermediates or capsid fragments was extremely hard, indicating that assembly is a highly cooperative (all or nothing) process in AdV.

Exhaustive examination of all FS samples yielded a possible sequence of events in AdV assembly (**Figure 27 and 40**). First, small condensations of viral DNA protrude from the DNA bundle periphery. These condensations are often more electron-dense than the bundle, suggesting the condensing action of core protein VII (**Figure 27B**). We propose that these protrusions are budding viral cores. These protrusions, containing one of the two L1 52/55 kDa pools (the one bound to the packaging sequence, see section 1.8.2) would be the recruitment spot for the other L1 52/55 kDa pool (the one bound to capsid fragments, **Figure 40**). These capsid fragments would then assemble around the budding core (**Figure 27C**), and gradually grow (**Figure 27D**) until the complete particle is formed (**Figure 27E**) and finally detaches from the DNA bundle (**Figure 27F**). Presumably, maturation and L1 52/55 kDa ejection would be happening simultaneously with capsid growth (99). The presence of half capsids assembling around budding cores would support the model of concerted rather than sequential assembly and packaging.

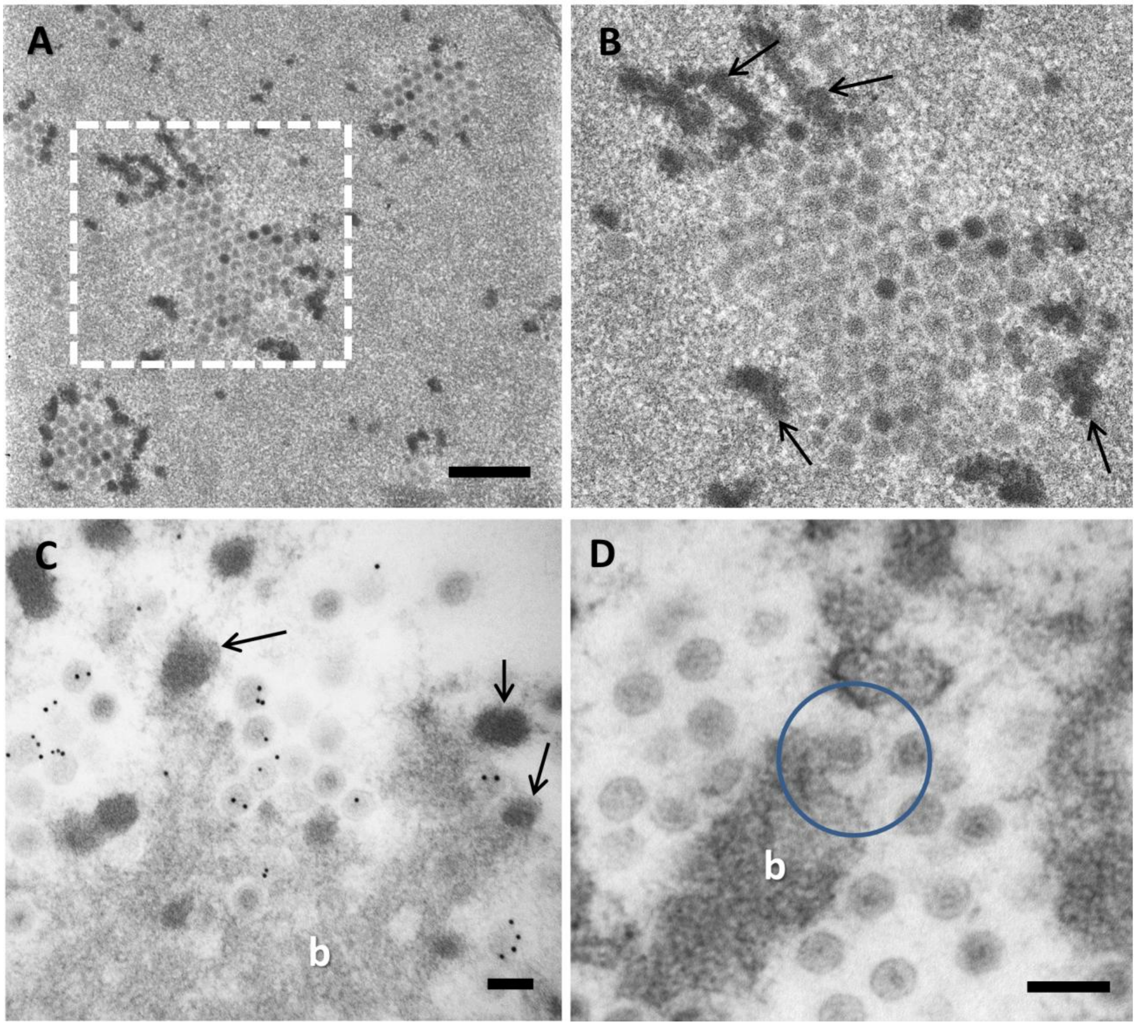

Figure 26: Possible assembly sites within the AdV factory. A-C. Viral particles of Ad5/FC31 close to EOGs. **A** Epon section at 56 hpi. **B.** Zoom of dotted area in (A). **C-D.** Freeze-substituted HEK293 cell infected at 48 hpi. **C.** labeled for L1 52/55 kDa. EOGs arise from DNA bundles (b). **D.** A blue ring highlights a partially formed capsid bound to a bud in a DNA bundle**.** Scale bars: 400 nm (A); 100 nm (C-D).

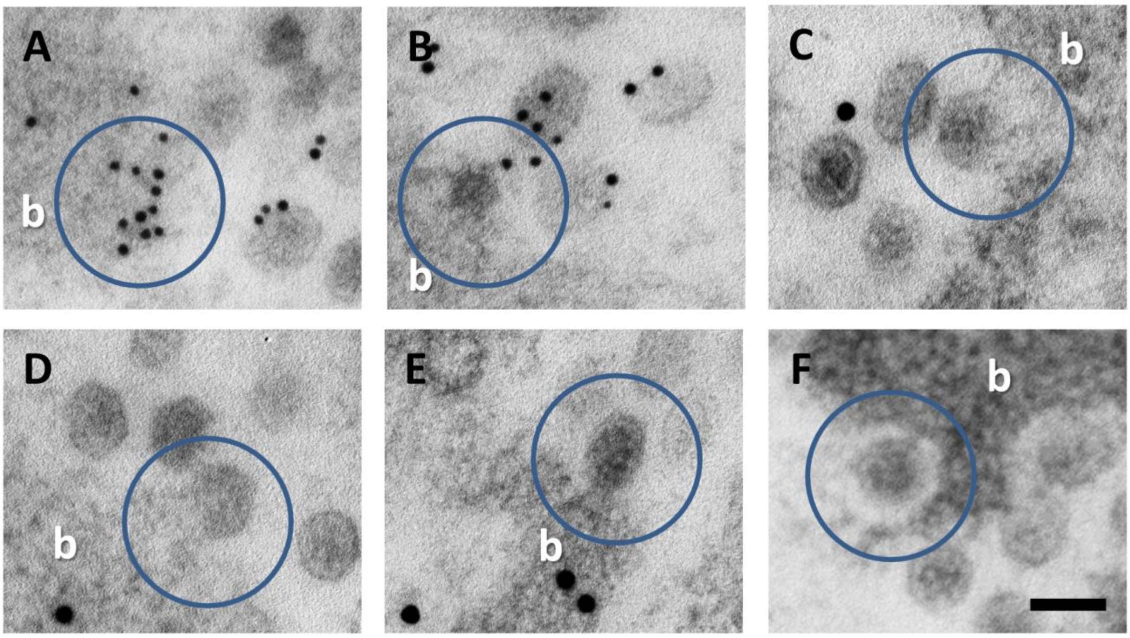

Figure 27: Possible sequence of events in AdV assembly. Freeze-substituted HEK 293 cells infected with Ad5/FC31 (MOI=50) at 48 hpi. **A-B.** L1 52/55 kDa label. **C-E.** BrdU label. **F.** No label. **A.** L1 52/55 kDa is accumulated on electron dense areas in the periphery of a DNA bundle (b). **B.** A small condensation arises from the surface of the DNA bundle. **C.** The capsid starts to assemble around the DNA condensation. **D.** Capsid growth around the budding core. **E.** When the capsid is almost ready the link with the DNA bundle is small. **F.** The viral particle is sealed and separated from the bundle. Scale bar 100 nm. More examples of these events can be found in Figure 40.

4.1.7 Electro-Opaque Granules, Speckled Bodies and Empty Capsids as Assembly Dead Ends.

EOGs were also observed to arise from the DNA bundles, and were labeled for structural and packaging factors, but they adopted variable shapes and sizes different from those expected for a viral particle or subassembly (**Figure 26C**). They can be interpreted as failed assembly events, budding cores where association with capsid fragments was unsuccessful. It is interesting to notice that EOGs are more abundant in Ad5/FC31 than in wt factories (**Figure 28**), correlating with the packaging defect of the mutant (1). The fact that Ad5/FC31 also generates a larger amount of light density particles than wt ((2), section 1.9) suggests that both EOGs and genome lacking particles are dead ends in assembly, appearing as a consequence of uncoupling between core budding and shell recruiting.

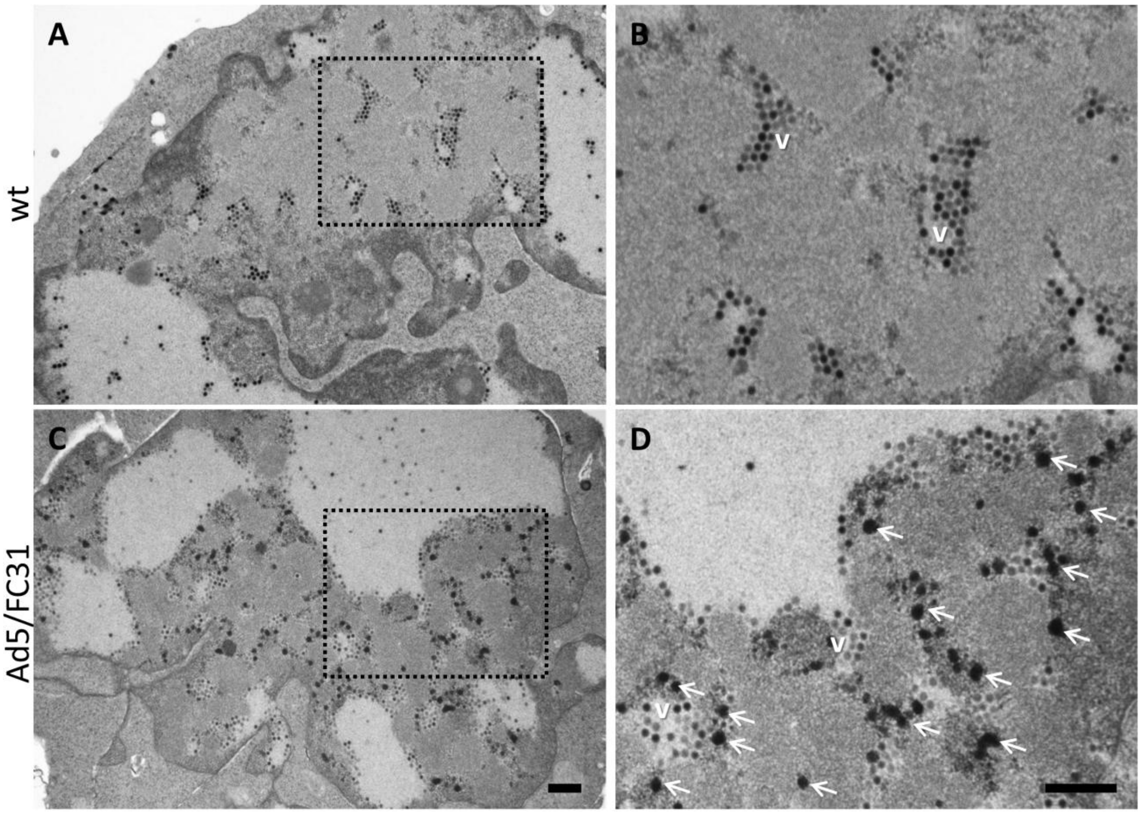

Figure 28: **EOGs are produced in greater amounts in Ad5/FC31 than Ad5 wt AdV factory. A-D.** Infected cells (MOI=5) embedded in Epon at 24 hpi. Scale bar 500 nm. **A-B.** wt. **C-D.** Ad5/FC31. **B and D.** Zoom of dotted areas in (A) and (C) respectively. White arrows indicate the presence of EOGS in the nuclear factory. Viral particles (v).

Apart from the amount of EOGs, the most notable difference found between Ad5/FC31 and wt was the presence of SBs in the mutant (section 4.1.1). After having determined that AdV assembly occurs in the PRZ, the SBs were reexamined. These structures are often close to or adjacent to the PRZ (**Figure 12 A and G**). Because of their size and texture, the speckles of the SBs are reminiscent of viral cores (**Figure 12A**). Now, after the inmuno-labeling results in electron microscopy, the site where the cores are assembled is known. This process occurs in the PRZ. Therefore, it is possible that SBs are PRZs containing viral condensed genomes; these genomes would not have been packaged due to the Ad5/FC31 mutation. This idea is also supported by the observation of some SBs with ring shape (**Figure 12D**), similar to the PRZ shape. To corroborate this idea, the presence of two core components (viral DNA and protein VII) in SBs was tested. In the initial immunolabeling experiments, no signal was observed for BrdU (viral DNA) and the signal for VII was low (**Figure 29A**). The possibility that the VII epitopes were masked by the tight complex between the condensing protein and the DNA was considered. For this reason, a DNase treatment was performed before using the antibody. This treatment increased the signal for VII (**Figure 29B**), indicating that SBs contain VII but also DNA, because DNase treatment was necessary to unmask the VII epitopes. Therefore the SBs contain viral cores. The effect of the DNase treatment indicated DNA presence, but the SBs did not have BrdU signal. This result is possible if the DNA in the SBs comes from DNA produced in the first 18 hpi prior to incorporation of BrdU. Therefore the cores contained in SBs are early cores, which have lost their opportunity to be packaged due to the Ad5/FC31 mutation that interferes with the packaging proteins and Ψ interaction. It can then be proposed that SBs are early collapsed PRZs, which have suffered extreme condensation producing these compact structures.

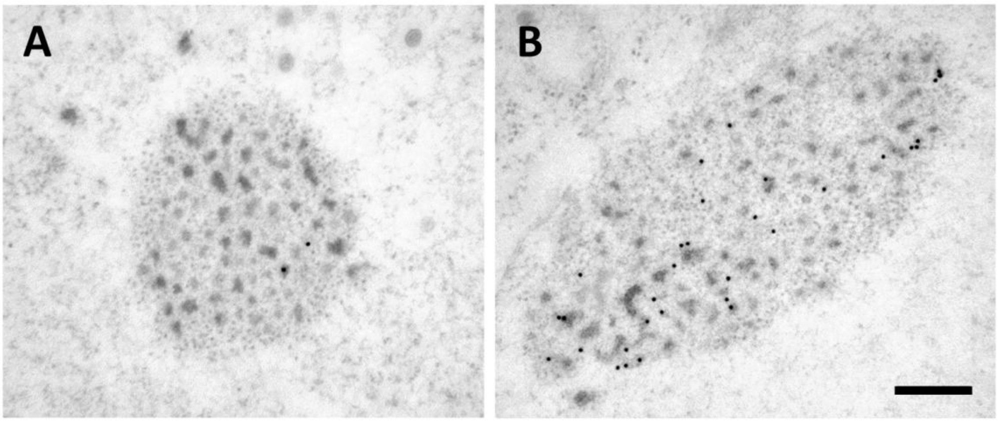

Figure 29: Labeling with anti-VII in SBs produced by Ad5/FC31. A. Label without DNase treatment. **B.** Label after DNase treatment. Scale bar 300 nm.

Antibodies against L1 52/55 kDa and fiber sometimes labeled the SBs but this labeling was not significant because the signal was similar to the background (not shown).

4.2 Study of Incomplete Particles Produced by Ad5/FC31

During AdV purification in CsCl gradients it is common to observe two bands, one heavy band (high density) which contains mature particles and another one with lower density, light band, which contains particles lacking viral genome. Studies on this kind of particles (section 1.8.3) (17, 29, 64, 144, 145, 160) suggested that light particles are assembly intermediates. However, other studies indicated that perhaps these particles are defective assembly products (59, 68). There is no structural information on wt light particles, as they are often heterogeneous and low amounts are produced. The only structural study was done by Cheng, et al. (25) on bovine AdV (BAdV3) light particles, but the results were unclear because in the BAdV3 purification no heavy band was obtained. Therefore the analyzed particles could be degradation products. Also, no density was assigned to L1 52/55 kDa, which is present in high copy number in the light particles.

In the first part of this thesis (section 4.1.7), it was suggested that light particles were dead end products, produced by a decoupling in the capsid and core assembly pathways. This idea is supported by the higher amount of light particles present in Ad5/FC31 purifications, with respect to the Ad5 wt ones (2). This high amount of light particles could be exploited for structural studies. Light density particles of Ad5/FC31 produced at 56 hpi were purified in two consecutive CsCl gradients. After centrifugation in a first CsCl gradient, two bands were obtained (light and heavy band) (**Figure 30A**). For Ad5/FC31, the concentration of viral particles (as estimated by intrinsic fluorescence) was $2x10^{12}$ vp/ml for the light band, and $4.8x10^{11}$ vp/ml for the heavy band. For Ad5 wt the concentration of light and heavy bands was $1.4x10^{11}$ and $1.5x10^{12}$ vp/ml respectively. In a second gradient, the light band separated into three bands (L1, L2 and L3), as expected (2) (**Figure 30B**). However, band L1 was found to have little reproducibility, as its composition varied between purifications, and was not further analyzed. Bands L2 and L3 have very close buoyant density, 1.26 and 1.28 g/ml respectively (1.33 g/ml for the heavy band). These bands contained approximately $1x10^{12}$ viral particles (vp)/ml (section 3.4).

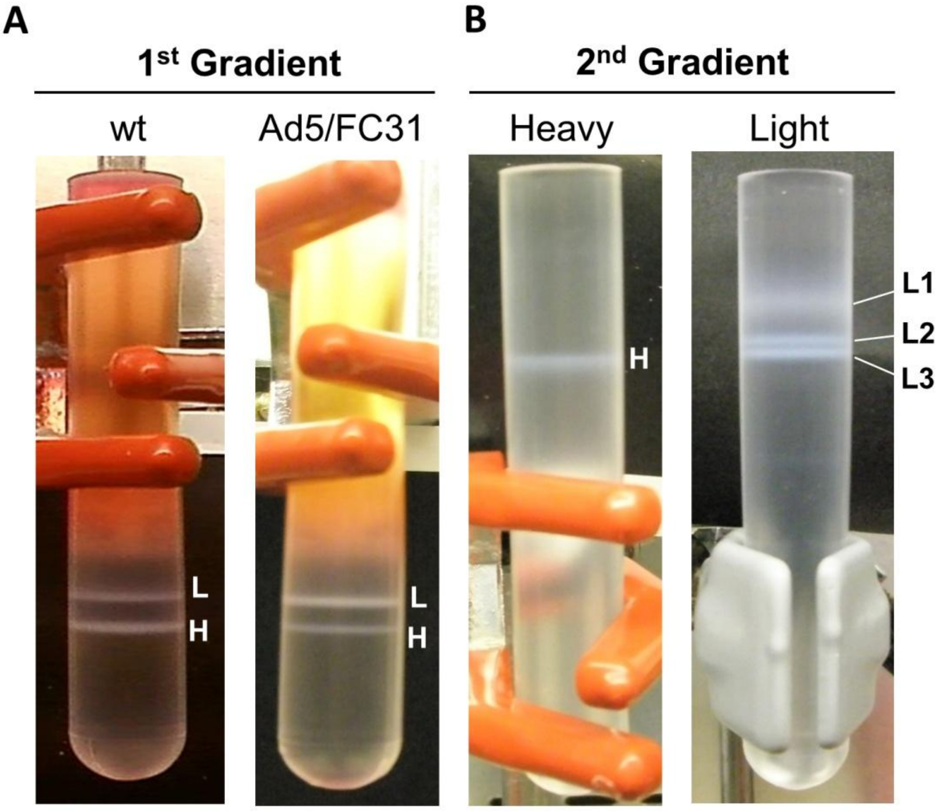

Figure 30: Purification of Ad5/FC31 light particles by double CsCl gradient centrifugaton. (A) The result of the first gradient is shown for Ad5 wt and the Ad5/FC31 mutant, as indicated. Ad5 wt purified at 36 hpi; Ad5/FC31 purified at 56 hpi. **L:** light density band; **H:** high density band. **(B)** Result of the second CsCl gradient centrifugation for the Ad5/FC31 heavy **(H)** and light bands. The light band from the first gradient separates into three distinct bands **(L1 to L3)** in the second one.

4.2.1 Ad5/FC31 Light Particles Are Not Artefacts Produced During the Purification

It is widely accepted that AdV light particles are assembly intermediates because they appear earlier than heavy particles (144), contain protein precursors (64, 160) and do not have DNA or only fragments (17, 29, 145, 160). However, Edvardsson, et al. (36) demonstrated that cores were released from light density particles, suggesting that they could be artefacts produced by degradation during the purification. To examine the possibility that the particles in the Ad5/FC31 L2 and L3 bands were artifacts, we obtained ultrathin sections of infected cells and measured the average electron density of viral particles present in the nucleus (section 3.13) at late times post-infection. This analysis indicated that capsids with electro-clear interior exist in both Ad5 wt and Ad5/FC31 infected cells, but the proportion of electro-clear particles is higher in Ad5/FC31 (**Figure 31**). That is, a larger amount of viral particles lacking the genome is already present in the Ad5/FC31 infected cell, and therefore L2 and L3 particles are genuine assembly products, and not purification artifacts.

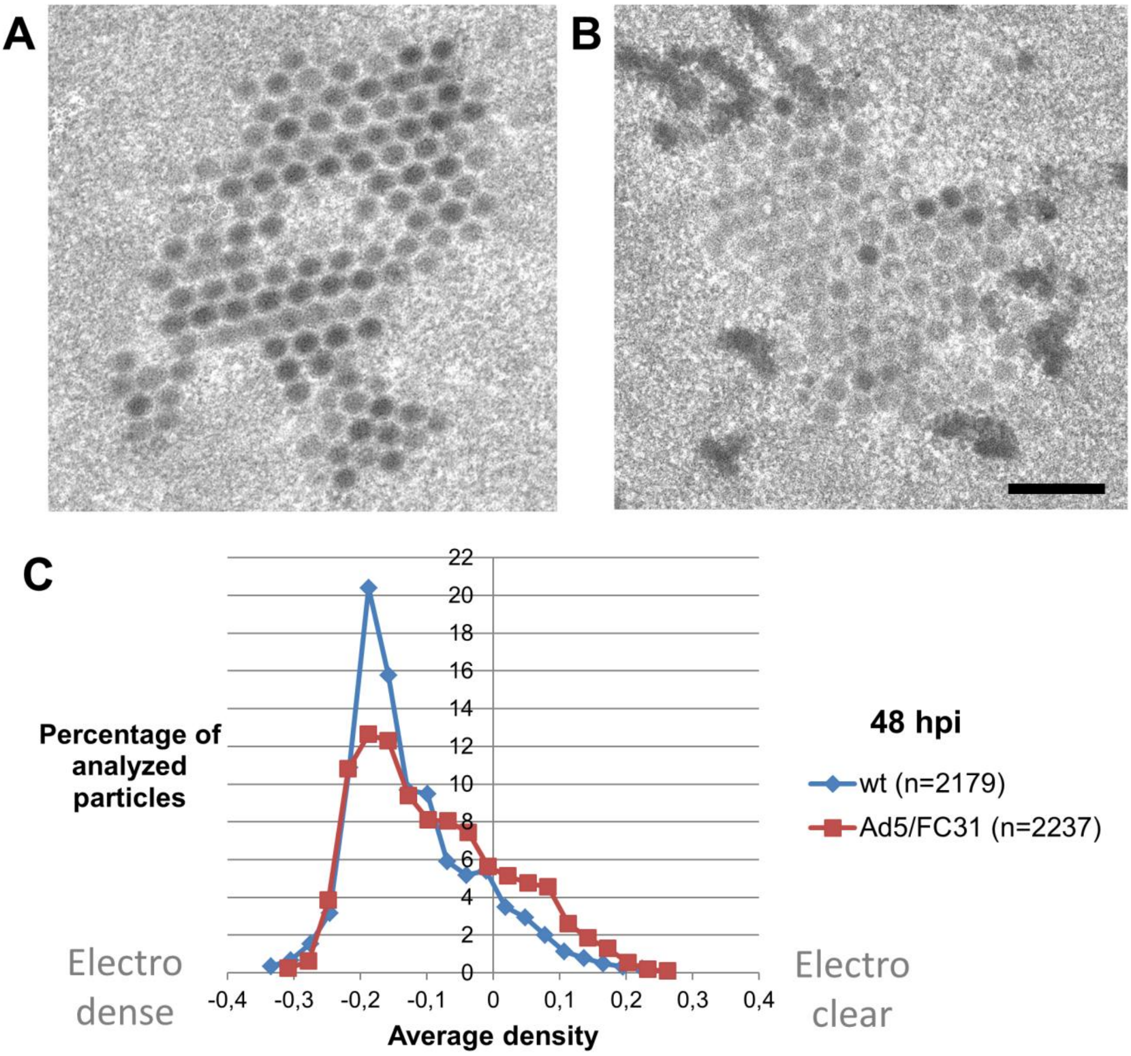

Figure 31: Analysis of particle electron-density in infected cells indicates that Ad5/FC31 L2 and L3 particles are not purification artifacts. Viral particle arrays in ultrathin sections of Epon-embedded HEK293 cells infected with Ad5 wt **(A)** or Ad5/FC31 virus **(B)** at 36 and 56 hpi respectively. The proportion of DNA-containing, electron dense (dark) particles is larger in (A) than in (B). The bar represents 250 nm. **(C)** Histogram quantifying percentage of viral particles *vs*. electron density level at 48 hpi. While in Ad5 wt there is a clearly dominant electron-dense population, for Ad5/FC31 the histogram shows more populated electro-clear (low pixel density) bins corresponding to light, genome lacking particles.

4.2.2 Molecular Characterization of Viral Particles in Ad5/FC31 L2 and L3.

Denaturing protein electrophoresis and Western blot assays were carried out to characterize and compare the protein content of Ad5/FC31 L2 and L3 bands with light and heavy bands of wt and Ad2 *ts1* (section 3.1), a thermosensitive mutant producing only young virions which contains the precursor version of all AVP targets (section 1.5). These assays showed that L2 and L3 particles contain the packaging/scaffold protein L1 52/55k in two different stages of proteolytic maturation (**Figure 32 A and B**). In both cases, bands corresponding to the full length protein and some proteolytic fragments were present. However, in L2 the full length species was clearly the most abundant, while in L3 up to three different proteolysis products were observed, in larger amounts than the full length protein. Similarly, L2 contained only the precursor version of polypeptide VI (pVI), while L3 contained both the mature version (VI) and the maturation intermediate iVI, generated when pVI is cleaved at only one of two possible sites (46). These results indicate that L2 and L3 represent two different stages of the AdV proteolytic maturation, with L3 being more processed than L2. Both L2 and L3 contained the putative packaging ATPase IVa2, but they lacked core protein V.

The lack of V (a core protein) in Ad5/FC31 L2 and L3 bands would indicate that these particles do not have DNA. DNA extractions from $1.5x10^{11}$ (Ad5/FC31 L2 or L3) or $3.6x10^{10}$ (Ad5/FC31 heavy) particles (section 3.10) were performed to assess this point. DNA concentration estimated by absorbance at 260 nm indicated a total mass of extracted DNA of 110 ng for Ad5/FC31 L2, 500 ng for Ad5/FC31 L3, and 985 ng for Ad5/FC31 heavy particles. However, 260/280 absorbance ratios (0.91 for L2, 1.38 for L3 and 1.7 for heavy particles) suggested that the real amount of DNA extracted from the light particles was lower. This aspect was confirmed by electrophoresis of the purified DNA in 0.8% agarose gels (**Figure 32C**). Volumes loaded were 25 µl for L2 and L3 (the maximum well capacity), and 7.9 µl for heavy particles. Although these volumes contained nominal DNA amounts of 55, 250 and 150 ng for L2, L3 and heavy particles respectively, no detectable bands were observed for L2, and only a weak band in L3. The viral origin of this band was corroborated by southern blot (**Figure 32C**) (section 3.12).

The AdV maturation protease is inactive in the absence of DNA (13, 46, 84, 85, 88). Therefore, the fact that L2 and L3 particles have undergone part of the maturation cleavages but are devoid of genome indicates that packaging must have started, but not succeeded. It is possible that L2 and L3 particles have lost their partially encapsidated genomes due to inefficient tethering of the DNA to the packaging proteins, caused by the exogenous sequences flanking the packaging signal in Ad5/FC31. Since L3 particles have undergone more extensive proteolytic processing than L2 (**Figure 32 A and B**), it follows that they retained their genomes for a longer time (more efficiently) than the L2 particles. Therefore, Ad5/FC31 L2 and L3 particles are not assembly intermediates but abortive assembly products where packaging and maturation were truncated at different stages of the process.

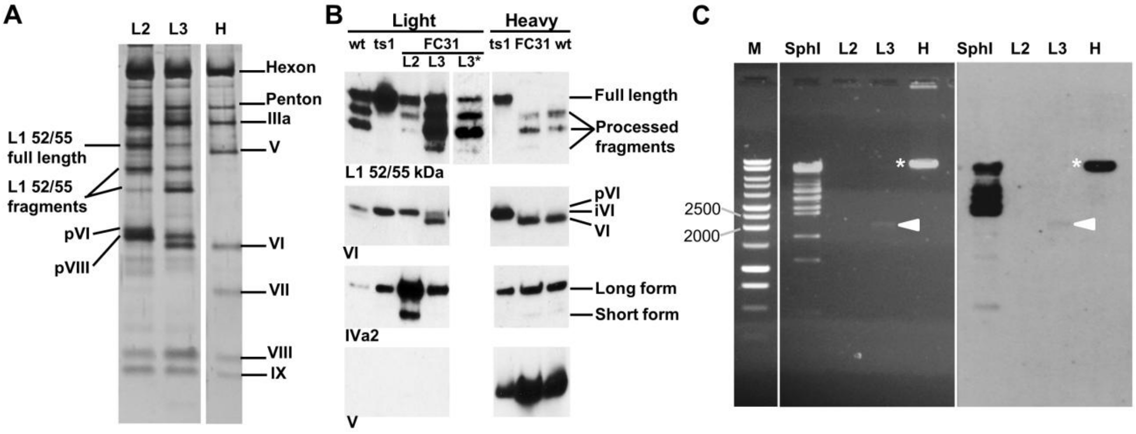

Figure 32: Molecular characterization of Ad5/FC31 light particles. **(A)** Silver-stained denaturing electrophoresis showing the proteins present in **L2, L3** and heavy (**H**, mature virions) Ad5/FC31 particles purified at 56 hpi. **(B)** Purified viral particles analyzed by Western blot against selected AdV proteins. Particles from the light and heavy CsCl gradient bands of Ad5 wt, Ad5/FC31, and Ad2 *ts1*, were probed with the indicated antibodies. Similar amounts of viral particles (~6x10^9 vp, as estimated by the intensity of the hexon band in silver stained gels) were loaded in each well. In the Western blot for L1 52/55k, the L3 lane is shown with two different exposures (L3 and L3*) for better appreciation of the different bands. Signal for a previously described short isoform of the putative packaging ATPase IVa2 is also observed in some cases, most notably in the Ad5/FC31 L2 particles (98). **(C)** Analysis of DNA extracted from purified Ad5/FC31 light (L2 and L3) and heavy particles, as indicated. A non-denaturing electrophoresis in a 0.8% agarose gel (left) and a Southern blot probed with digested viral genomes of Ad2 *ts1* (right) are shown. A **star (*)** indicates the position of the 35 kpb viral genome; **arrows** indicate a fragment between 2.5 and 2 kbp. SphI: Ad2 *ts1* genome digested with SphI enzyme. **M.** 1 kb DNA ladder (section 3.11)

4.2.3 Structure of Ad5/FC31 L2 and L3 Particles.

L2 and L3 particles were examined by conventional negative staining electron microscopy (see section 3.8) (**Figure 33A**). L2 particles presented the typical aspect of AdV light particles, with a dark center indicating that the staining agent penetrates the protein shell and fills the absent core space (28, 93, 163). On the contrary, L3 particles were indistinguishable from heavy particles in spite of lacking viral genome and associated core proteins. This observation indicates that these capsids are sealed and the staining agent cannot penetrate. Cryo-EM images (**Figure 33B**) showed that, in agreement with the negative staining observations, some L2 particles seemed to lack capsid fragments, while L3 particles in general looked intact. The Ad5/FC31 L3 genome-less, structurally complete capsids would be the first authentic AdV virus-like particles (VLPs) described, and as such an ideal candidate for the development of epitope display-based vaccines with low biosafety hurdles. In addition, the fact that sealed genome-less particles can exist corroborates the idea that they are assembly dead ends, because no DNA translocation into the capsid could occur after sealing. Cryo-EM 3D maps for the Ad5/FC31 light particles were obtained at 12.3 Å resolution for L2 and 12.5 Å for L3[1] (**Figure 35C**) and are analyzed in the next sections. They also corroborated the structural integrity of the L3 particles (**Figure 41**)

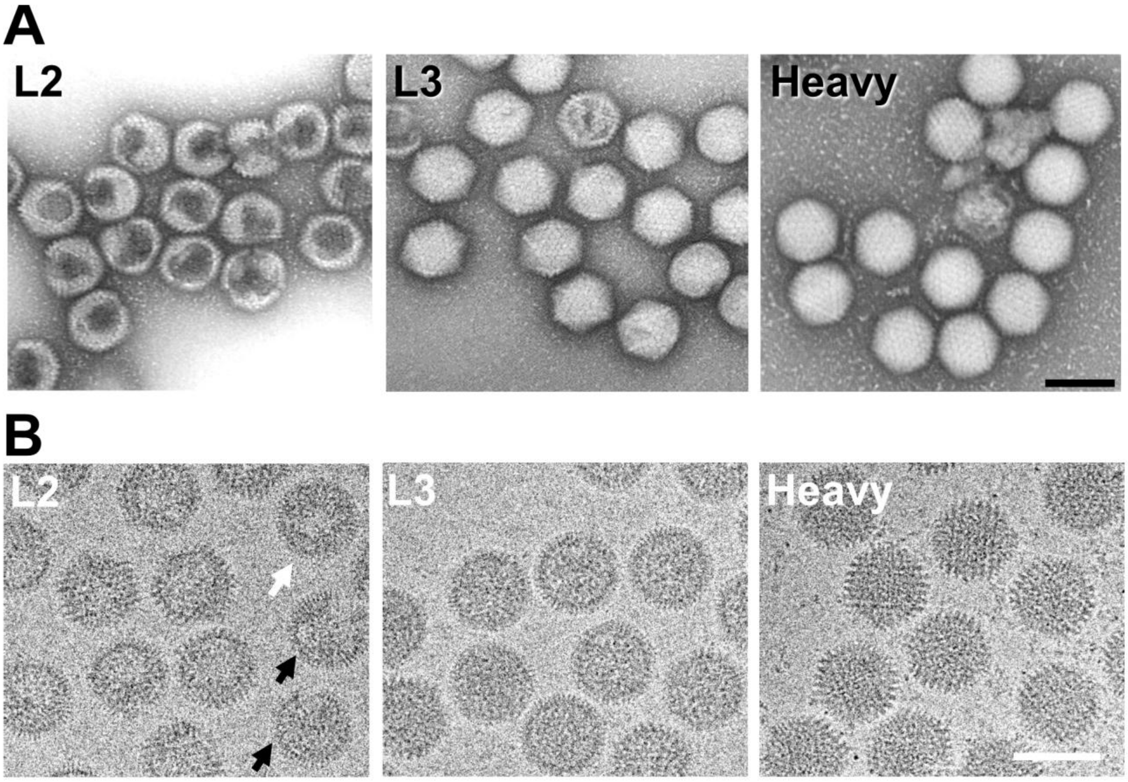

Figure 33: Structural characterization of Ad5/FC31 L2 and L3 particles. **(A)** Negative staining EM images showing the overall structure of Ad5/FC31 L2, L3 and heavy particles. The bar represents 100 nm. **(B)** Representative cryo-EM micrographs of Ad5/FC31 L2, L3 and heavy particles. The bar represents 100 nm. In L2, a particle with a continuous layer of internal density is indicated with a white arrow, and disrupted particles are indicated with black arrows.

---

[1] Image processing was carried out by Dr. Carmen San Martín.

4.2.4 Comparing the Structures of Ad5/FC31 Light Particles and the Two Alternative Models for Mature Ad5.

The structure of the icosahedral Ad5 capsid was solved at high resolution (~3.5 Å) by both X-ray crystallography and cryo-EM (76, 119). However the location of some of the minor coat proteins is still a subject of debate (19, 120) (section 1.3.1). One issue is the location of polypeptide IIIa. In the cryo-EM study, polypeptide IIIa is assigned to a pinwheel feature located beneath the vertices, in association with polypeptide VIII (76) (**Figure 34A**). An internal location for IIIa is also supported by other structural studies (129, 131, 132, 135); biochemical evidence indicating that IIIa interacts with the genome-bound maturation protease and the genome itself (13, 82); and the observation that IIIa is released together with other internal vertex components in the early stages of virus entry (49). In the X-ray study however, polypeptide IIIa is assigned to a 4-helix bundle located on the outer surface of the capsid, at the icosahedral edges (120) (**Figure 2**). This feature had been assigned to the C-terminal domain of polypeptide IX in the cryo-EM high resolution analysis (76) and previous peptide mapping studies (39). In turn, according to the latest X-ray model, the pinwheel feature under the vertices would be composed by shell proteins VI and VIII, and core polypeptide V (120) (**Figure 34A**).

Since Ad5/FC31 L2 and L3 particles lack polypeptide V (**Figure 32B**), comparing their cryo-EM maps with the X-ray and cryo-EM models could help settle the current controversy between them. Accordingly, both models were fitted into the L2 and L3 maps and the pinwheel region was analyzed. In the X-ray model (PDB ID 4CWU) (120), 72 of the 368 residues in protein V were traced in two fragments (208-219 and 236-295). A short helix formed by the smaller fragment, together with residues 236 to 273, form a more or less compact, globular domain, while the rest of the traced residues adopt an extended structure. Fitting the X-ray model into the L2 and L3 cryo-EM maps showed that only a part of the extended arm (residues 273-285) protrudes from the density of L2 and L3 maps; while the globular domain is completely covered by it (**Figure 34B**). Therefore, more than 80% of the traced region of polypeptide V is covered by density in maps of particles lacking this protein. As a control, the pinwheel region of the Ad2 *ts1* mutant, which contains protein V, was also analyzed. The fitting indicated the same results as in Ad5/FC31 L2 and L3 (**Figure 34B**). These results provide evidence to support the cryo-EM model and reject the assignation of protein V in the pinwheel proposed by the X-ray model. Accordingly, the cryo-EM model will be used for interpretation of the L2 and L3 maps in the rest of the sections.

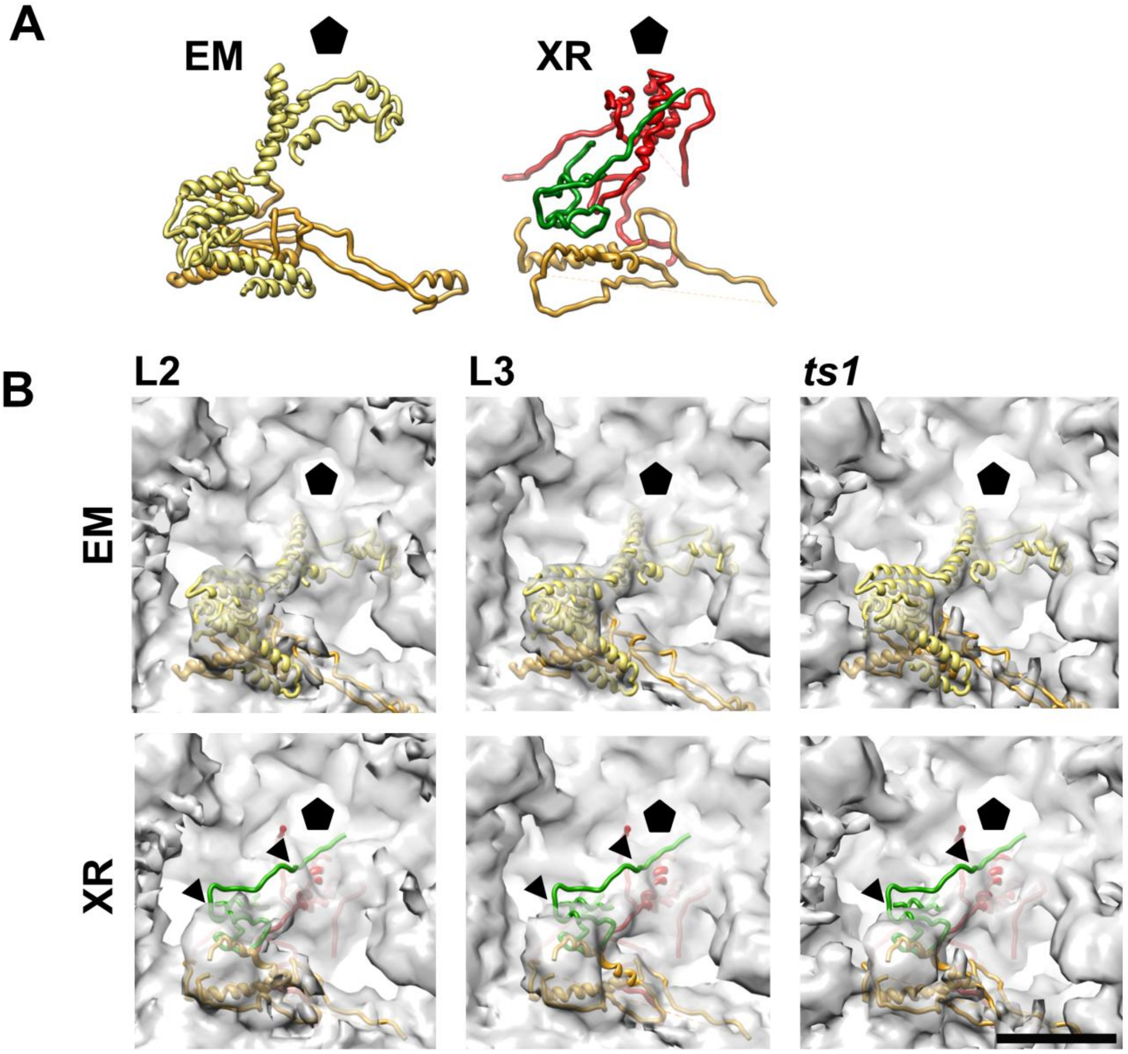

Figure 34: Comparison of L2 and L3 particles lacking polypeptide V with the two available models for the full Ad5 virion. (A) Ribbon representation of the proteins assigned to the pinwheel feature located beneath the vertex region in the cryo-EM **(EM**, PDB ID: 3IYN**)** and X-ray (**XR**, PDB ID: 4CWU) models of full, mature Ad5. Polypeptide IIIa is depicted in yellow, V in green, VI in red, and VIII in orange. **(B)** The pinwheel proteins from the cryo-EM or X-ray Ad5 model are shown fitted into the Ad5/FC31 L2 and L3 cryo-EM maps, as indicated. For comparison, atomic models were also fitted to a previously published cryo-EM map of Ad2 *ts1* mutant (100), filtered to the same resolution as the Ad5/FC31 light particle maps. This mutant, stalled at the immature state, contains the fully packaged genome and core proteins, including V. The view is from inside the capsid, along a 5-fold symmetry axis. Most of the polypeptide V residues modeled in the X-ray study (except those in the stretch limited by two arrowheads, residues 273-285) are well covered by density in the cryo-EM maps of particles lacking this protein. The cryo-EM maps (in semi-transparent gray) are contoured at 1.4σ above the average density (1.46σ for *ts1*). The position of the 5-fold axis is indicated by a black pentagon. The bar represents 50 Å.

4.2.5 Differences between Mature Ad5 and Ad5/FC31 Incomplete Particles

Cryo-EM images showed that the Ad5/FC31 L2 and L3 particles contained some heterogeneous material inside the capsids, in spite of these particles lacking the genome and core proteins (**Figure 33B**). In L2, the contents tended to be close to the inner capsid surface and occasionally appeared as a continuous layer (**Figure 33B,** white arrow). In the cryo-EM reconstructions, these contents appeared as a weak density layer inside the capsid shell (**Figure 35**). The layer density was weak but stronger than noise, consistent with contents heterogeneous and disordered. Radial average profiles of the 3D maps (**Figure 35B**) indicated that in L2 the internal density was stronger directly beneath the capsid (between 220 and 320 Å radii). Conversely, in L3 the shell adjacent to the capsid presented a density minimum, while the strongest gray values for the disordered contents were found at lower radii (170 to 270 Å). These results indicate that, although disordered, the material present in L2 has to be interacting with the inner capsid surface because it is preferentially located there. This interaction would be lost in L3.

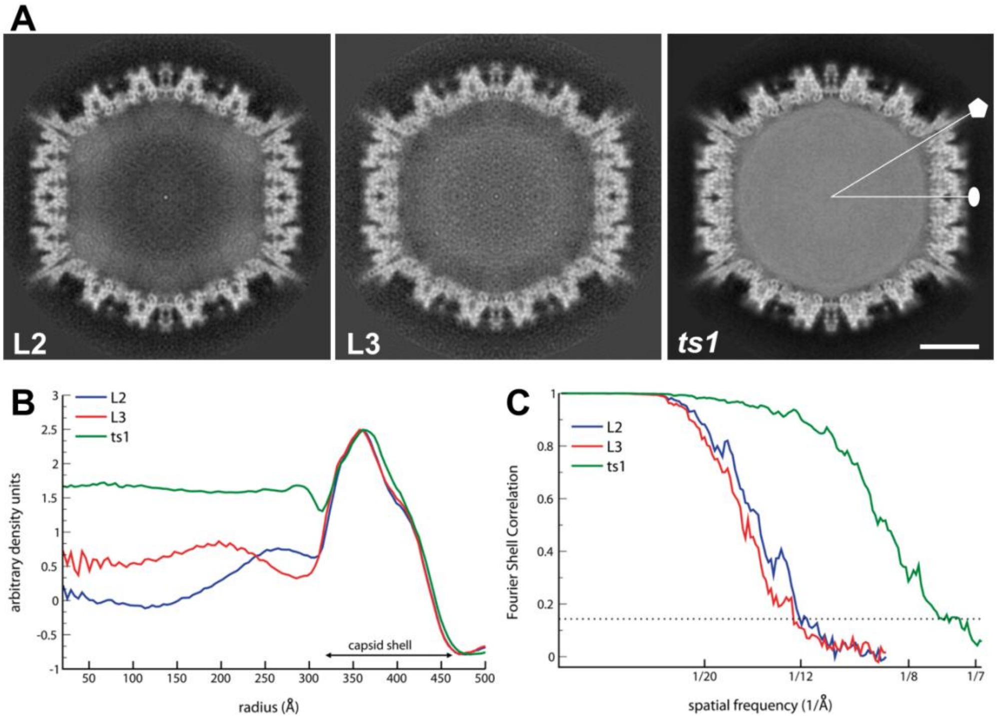

Figure 35: Cryo-EM reconstructions of Ad5/FC31 L2 and L3 particles. **A.** Central sections of the Ad5/FC31- L2 and L3 maps, as indicated. The view is along a 2-fold symmetry axis. A central section of the Ad2 *ts1* mutant map (100) is also shown for comparison, with the positions of one 5-fold and one 2-fold icosahedral symmetry axes indicated by a white pentagon and white oval, respectively. All maps are low-pass filtered at 12.3 Å resolution, and higher density is shown in white. The bar represents 200 Å. **B.** Radial average profiles of the Ad5/FC31-L2 and L3 maps, compared to that of the full Ad2 *ts1* map. **C.** Resolution curves for all maps used in this study. The FSC=0.143 threshold is indicated by a dotted line.

Difference maps calculated by subtracting a map created from the Ad5 cryo-EM model (76)(filtered at 12.3 Å) from the L2 or L3 maps revealed density present in Ad5/FC31 light particles but not in the EM model for mature Ad5 (**Figure 36**). On the external part of the capsid, extra density corresponded to fiber and hexon loops which are not traced in the Ad5 high resolution model (**Figure 36 A-D**) because they are flexible. Also, extra densities were found inside of L2 and L3 capsids. These densities correspond to the weak shells directly observable in the maps (**Figure 35**). In L2, the extra densities were located on the inner capsid surface and they were stronger beneath the vertices (**Figure 36A and B,** thin arrow; and **36E and F**). This observation indicates the presence of a disordered material in L2 particles, which does not follow icosahedral symmetry but binds preferentially to internal vertex components. Also, at the same threshold (1.5σ above the map average density) small densities were detectable in the inner hexon cavity and directly on the inner hexon surface (**Figure 36B,** thick arrow and arrowhead respectively). At very low threshold (0.75σ), these densities completely filled the hexon cavity and merged with the other described extra densities giving rise to an 80 nm thick inner shell (**Figure 36B,** right hand side panel). Unlike in L2, in L3 the region beneath vertices lacked extra density (**Figure 36C** circle; and **36D-G**). The other features described for L2 were also present in L3; densities in the inner hexon cavity and on the inner hexon surface (**Figure 36D,** thick arrow and arrow head respectively). As in L2, at low threshold the L3 extra densities filled all hexon cavities and connected with each other on the inner capsid surface forming a network that contacts hexons at multiple points, but not the pinwheel proteins beneath the vertex (**Fig. 36 E, F and G**). A thicker layer of weak density appears at more internal radii, disconnected from the icosahedral shell and the difference densities on the inner capsid surface (**Figure 36D and F,** right hand side panels).

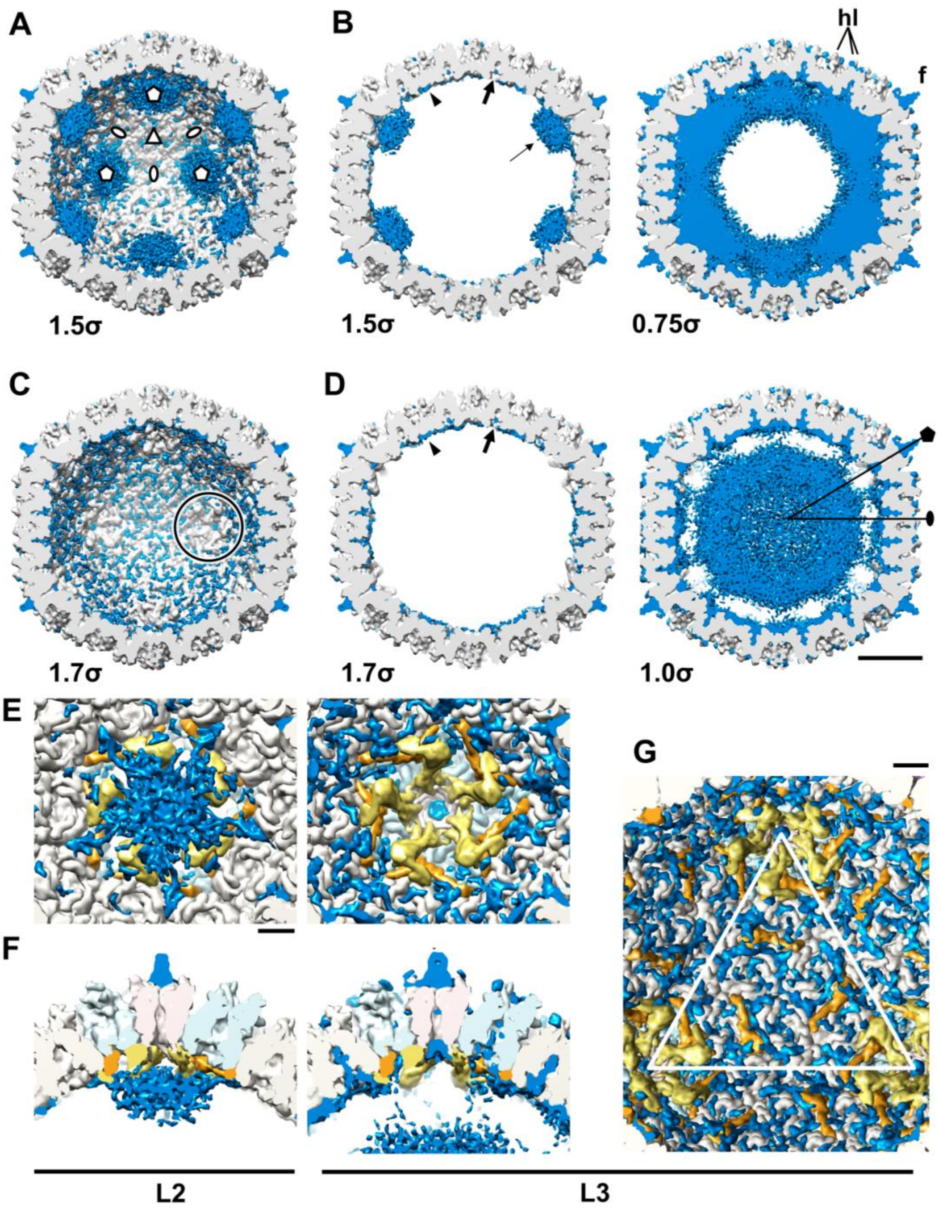

Figure 36: Difference maps calculated by subtracting Ad5 from Ad5/FC31-L2 (A and B); and Ad5 from Ad5/FC31-L3 (C and D). The Ad5 wt map (gray) is contoured at 1 standard deviation above the average map density (1σ), and the difference maps (blue) are contoured at the indicated thresholds, chosen to show similar features in L2 and L3. The highest contour levels reveal the strongest differences. **A and C** show the back half of the viral particle cut open for visualization of the internal difference density. In **B and D** only a slab is shown, for further clarity. The view is along a 2-fold symmetry axis. Pentagons, triangles and ovals indicate the positions of the 5-fold, 3-fold and 2-fold icosahedral symmetry axes. The circle in (C) indicates the lack of extra density beneath the vertex in L3; arrowheads indicate extra-densities on the inner capsid surface; thick arrows point to extra-density in the entrance of the hexon cavity; the thin arrow in (A) points to extra-density beneath the vertex in L2; hl: hexon loops; f: fiber. **E, F and G** show details of the L2 and L3 difference maps, with the various proteins in the Ad5 wt cryo-EM model in different colors: IIIa in yellow, VIII in orange, penton base in pale pink, peripentonal hexons in pale cyan, and other hexons in pale tan. The view in (E) is from inside the particle along a 5-fold axis; (F) shows a section across the vertex, and (G) shows a complete facet (delineated with a white triangle) as seen from inside the L3 particle. Difference maps in (E-G) are contoured at 1.6σ except for panel L3 in (F), which is at 1.2σ. The bar represents 100 Å for (A-D), and 50 Å for (E-G).

Discussion

5. Discussion

This thesis addresses the problem of AdV assembly and packaging. In spite of numerous previous studies, these mechanisms are still not fully understood. Two models have been proposed for AdV assembly and packaging: concerted and sequential (section 1.8). Studying Ad5/FC31light particles and comparing Ad5 wt and Ad5/FC31 infected cells, new information on this problem has been obtained.

5.1 Adenovirus Assembly Occurs in the PRZ in a Concerted Manner

In the first part of this thesis, the fate of viral components involved in assembly and packaging was followed during the infection. Immuno-fluorescence and immuno-EM assays indicated that both packaging and assembly factors were located in the region previously defined as the PRZ (**Figure 37A**). Viral particles were observed in this area too. These observations indicate that the PRZ is the AdV factory. EM images of assembly intermediates in infected cells showed that the capsid grows around cores budding from DNA bundles. This kind of images support the concerted assembly and packaging model, where capsid and core are assembled simultaneously (**Figure 37B**).

If we compare the Adenovirus factory with other viral factories, it is possible to find some similarities with the factories of large dsDNA viruses. In Baculovirus, assembly occurs at the edge of the intrastromal spaces (section 1.7), located in the virogenic stroma (VS). In sections of Baculovirus infected cells, the VS looks like the DNA bundles observed in AdV infections (**Figure 7C and D**). The Mimivirus factory originates from replication centers, as shown here for Adenovirus. Also, the Mimivirus capsid is assembled on the DNA which comes from of the replication zone, Starting from a single vertex (90) (**Figure 7B**). A similar assembly mechanism has been described for African Swine Fever Virus (ASFV) (143). Electron tomography images of Mimivirus and ASFV infected cells (90, 143) suggest that viral DNA is engulfed by a partially assembled capsid. Here, AdV assembly intermediates have also been observed engulfing the DNA (**Figure 26D and 27 D-E**). Both ASFV and Mimivirus contain a membrane. The open membrane, which holds the viral DNA, is progressively coated by the viral capsid to form an icosahedral particle. In Adenovirus, there is no internal membrane, but the L1 52/55 kDa protein would serve as a base to assemble the capsid around the core, because this protein would connect them.

It is relevant that the work presented here reveals an assembly mechanism for AdV similar to that of Mimivirus or ASFV, since all these viruses are structurally related: they all belong to the AdV-PRD1 linage, according to the classification based on the double jellyroll fold of their coat proteins (8, 73). The structural similarity found in the viral particles raised the question of a common evolution ancestry for these viruses, that would be also reflected in aspects of their assembly mechanism.

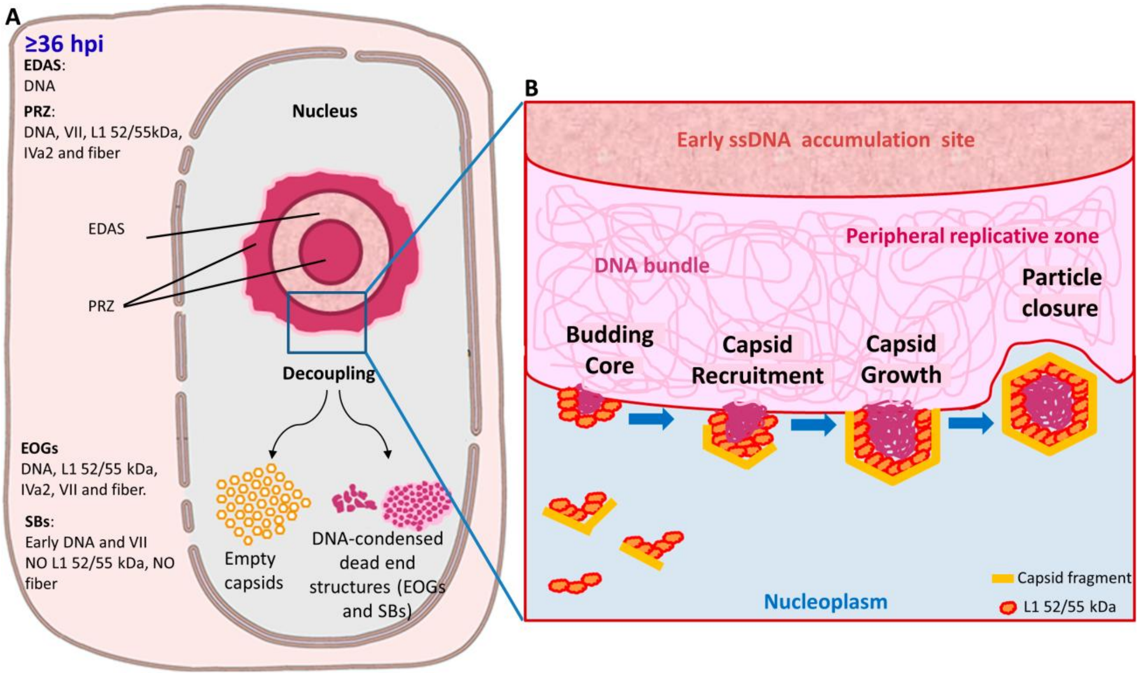
A
≥36 hpi
EDAS:
DNA
PRZ:
DNA, VII, L1 52/55kDa, IVa2 and fiber
Nucleus
EDAS
PRZ
Decoupling
EOGs
DNA, L1 52/55 kDa, IVa2, VII and fiber.
SBs:
Early DNA and VII
NO L1 52/55 kDa, NO fiber
Empty capsids
DNA-condensed dead end structures (EOGs and SBs)
B
Early ssDNA accumulation site
Peripheral replicative zone
DNA bundle
Particle closure
Budding Core
Capsid Recruitment
Capsid Growth
Capsid fragment
L1 52/55 kDa
Nucleoplasm

Figure 37: Proposed AdV assembly pathway. A. General scheme of an infected cell showing the localization of assembly factors in the structures produced by AdV. Only when the capsid and core assembly are correctly coordinate by interaction of the packaging factors L1 52/55 kDa and IVa2 with the viral genome, the virions are assembled. When there is a defective interaction, the capsid and core are assembled independently giving rise to dead end products: empty capsids and EOGs/SBs. **B.** Model for Adenovirus concerted assembly and packaging based on the data present in this thesis.

5.2 Adenovirus Assembly Requires the Coordination of Two Independent Routes

Alba, et al. (2) showed that the Ad5/FC31 mutant has a packaging delay and produces large amounts of light particles. In this thesis, the molecular characterization of the Ad5/FC31 light particles indicated that they started, but failed to complete packaging. Therefore, the light particles produced by Ad5/FC31 are dead ends in this virus morphogenesis. The cell studies also revealed that EOGs and SBs are more abundant in Ad5/FC31 than in Ad5 wt infections. All together, the results presented are consistent with an assembly process with two independent routes (**Figure 37A**): one for capsids, and another one for cores. Only when both pathways are coordinated in time and space the viral particles are produced. Otherwise, dead ends are generated. In the case of Ad5/FC31 there is a decoupling of these pathways.

Both SBs and EOGs contain viral DNA and core proteins, and are more condensed than the DNA bundles; these observations suggest that they would be dead end products of the core assembly pathway. Inmuno-EM assays show that EOGs and SBs have a similar composition. It is possible that both structures share a common origin, but have a different development grade. EOGs could be the precursors of speckles in the SBs. This idea is supported by EM images where some SBs contain elongated speckles similar in shape to EOGs (**Figure 29**), and could explain the presence of some SBs in wt. In general, the incorrect coupling of the core and capsid assembly pathways would produce EOGs in both wt and Ad5/FC31; and these structures contained in PRZs would be condensing more with time to generate SBs. Some SBs with ring shape (**Figure 12D**), similar to early PRZs, support this idea. EOGs would be dead end products produced regularly in wt infections and only in extreme cases these structures would evolve into SBs, as indicated by the fact that few SBs are observed in wt. In Ad5/FC31, these extreme cases are more frequent by the mutation present in this virus. The dead end product of the capsid pathways would be the light density particles, also more abundant in Ad5/FC31. These were analyzed in the second part of this thesis.

5.3 Structures of Incomplete Particles and Implications for Adenovirus Assembly

The Ad5/FC31 mutant produces two kinds of light density particles: L2 and L3. They represent two different stages of maturation and both lack viral genome. Cryo-EM maps of L2 and L3 showed extra densities that can be interpreted with the help of the particle molecular characterization and previous knowledge. The main difference between L2 and L3 is the processing degree of proteins VI and L1 52/55 kDa (**figure 32B**). L1 52/55 kDa is indispensable for packaging (50), can form oligomers (99), and binds to shell (IIIa) (82) and core components (VII, dsDNA and AVP)(99, 102, 166). Polypeptide VI binds to hexon and dsDNA (47, 86), and its C-terminal peptide is a cofactor for AVP (46). Studies with the *ts147* mutant, which is defective for hexon nuclear import, suggested that VI binds to the internal cavity of the hexon trimer (161). In the AdV capsid, protein VI is not icosahedrally ordered and only weak density for small fragments of VI has been observed in previous structural studies (76, 120). Both L1 52/55 kDa and protein VI are processed by AVP, but the first one suffers a much more drastic processing with up to 14 potential cleavages (section 1.5) (**Figure 4**) which disrupt its links with capsid and core (99), leading to its eventual removal from the mature particle. On the other hand, polypeptide VI is cleaved only in two sites; removing 33 and 11 residues from its N- and C-termini respectively (section 1.5) (**Figure 4**); and it remains in the mature particle (131, 142). The only structural change observed for VI upon maturation is a lower degree of icosahedral ordering in the hexon-interacting region (100, 140).

These considerations suggest that the densities in common in the L2 and L3 difference maps (within hexon cavities and the network of weak density on the inner hexon surface, **Figure 36A-D**) would correspond to polypeptide VI (**Figure 38, red symbols**). This assignment is consistent with previous studies about the localization of short VI fragments within or close to the hexon cavity (76, 100, 120, 140). The network in contact with the inner hexon surface would correspond to rest of the polypeptide VI, which would not be easily visualized in 3D studies of genome-containing particles. The core would produce noise, hiding the signal of this network.

The rest of the differences, making up the thick shell connected to the capsid in L2 but disconnected in L3 (**Figure 36B and D**), would correspond to L1 52/55 kDa (**Figure 38, blue symbols**). The presence of extra density beneath the vertices (**Figure 36A-B and E-F**) is consistent with studies reporting the interaction of L1 52/55 kDa with IIIa (located beneath the vertices) (82), and with IVa2 (reported to be at a single vertex (26, 51)). However, the L2 images did not indicate the interaction of L1 52/55 kDa at a special single vertex. The formation of a thick shell starting from a preferential interaction with the vertices is consistent with the L1 52/55k homo-oligomerization properties (99). The results presented here suggest that full length L1 52/55 kDa protein is required to establish interactions with IIIa, because the extra densities beneath the vertices in L2 are absent in L3, where L1 52/55 kDa is partially processed. Also, the ability to oligomerize with itself would be lost when L1 52/55 KDa was processed by AVP (99) and therefore the thick shell crumbles away and falls to the center of the empty capsid (**Figure 38**). The L2 and L3 structures provide, for the first time, information about the localization of a packaging factor in the AdV capsid.

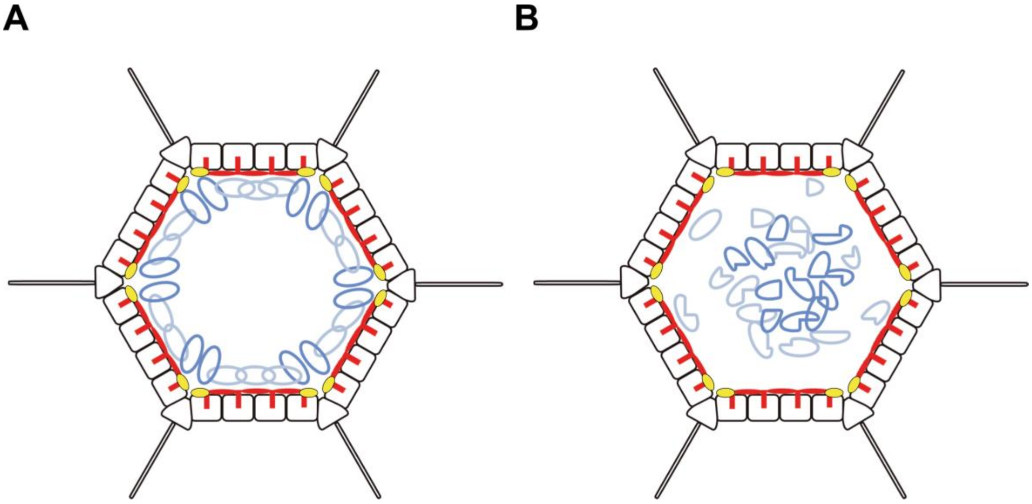

Figure 38: Schematics depicting the interpretation of the Ad5/FC31 L2 and L3 difference maps. Cartoons showing a cross section of the L2 **(A)** and L3 **(B)** particles with symbols for pVI/VI in red and L1 52/55k in blue, using a darker shade for copies bound to the vertex region (IIIa, yellow).

In inmuno-labeling assays on infected cells, L1 51/55 kDa was found in DNA bundles (**Figure 20**), budding cores (**Figure 27**) and in empty and open capsids (**Figure 21C-D and I-H; 27B**). These results agree with the two pool model (section 1.8.2): one pool of packaging proteins in the capsid (most likely beneath the vertex) and another one in the core (bound to Ψ). The L1 52/55 kDa located beneath the vertex could be used as an anchor point for the first interaction between capsid and core during assembly, because it is known that this protein can interact with itself (99). In immuno-labeling assays, L1 52/55 kDa also appears as an arch pattern close to PRZ (**Figure 20B**) and inside viral particles (**Figure 21D and J**). Homo-oligomers of this protein would be responsible for this kind of pattern. These observations match with the assignation of L1 52/55 kDa to the thick shell located on the inner capsid surface of the L2 particle map (**Figure 38A**). These results suggest that during assembly L1 52/55 kDa would form a thick shell, preferentially interacting with the vertex proteins, ready to act as a tether with the budding core. When the L3 structure, which is more processed than L2, was analyzed, this thick shell of L1 52/55 kDa was not found, indicating that when maturation starts L1 52/55 kDa is cleaved and the tether disappears. The *ts1* mutant, which is a maturation mutant, is not infectious because the genome cannot be properly uncoated during the infection (92, 100, 101), showing that the L1 52/55 kDa conectivity is necessary during assembly but has to disappear to allow successful virus propagation.

The existence of DNA-lacking and partially processed light particles also indicates that maturation and packaging occur simultaneously. DNA is a cofactor for AVP, so partial maturation in these particles must have taken place because in some moment they had viral DNA, but lost it before completing packaging/assembly and therefore the maturation stopped.

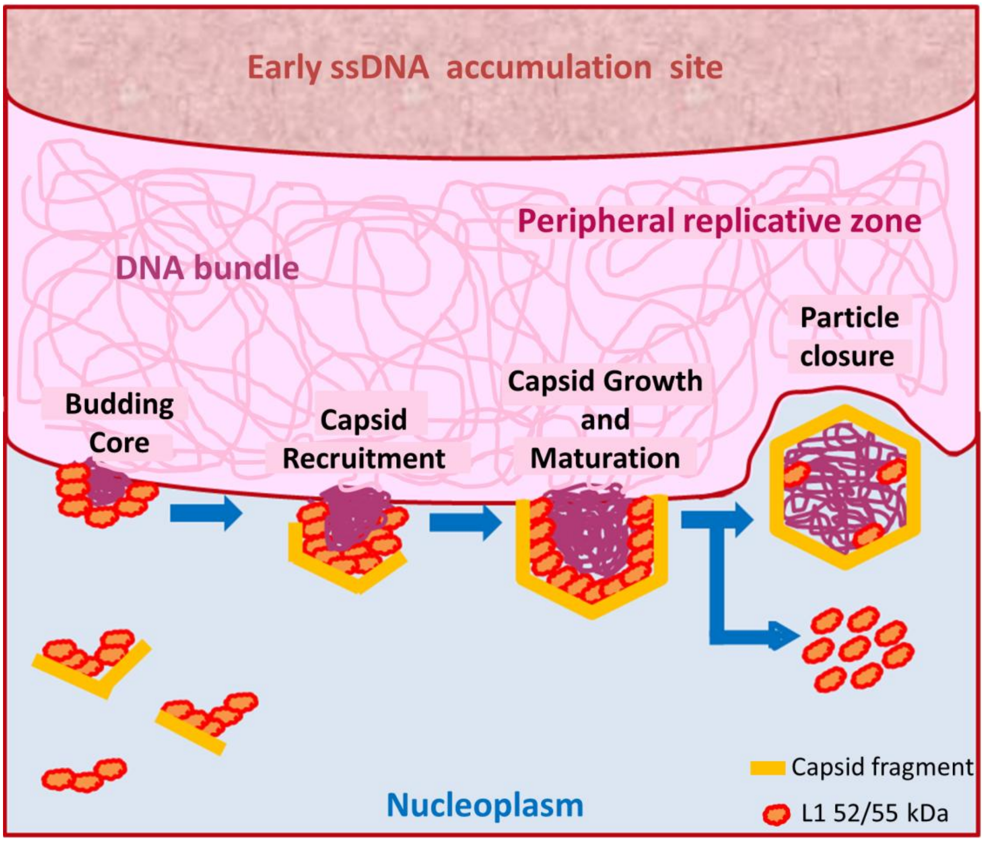
Early ssDNA accumulation site
Peripheral replicative zone
DNA bundle
Particle closure
Capsid Growth and Maturation
Budding Core
Capsid Recruitment
Capsid fragment
L1 52/55 kDa
Nucleoplasm

Figure 39: Revised AdV assembly model based on the information provides by incomplete particles. The two pools of L1 52/55 kDa interact and bind the nascent core and capsid fragment. During the capsid assembly around to core, L1 52/55 kDa hold together the core and capsid. Simultaneously, AVP starts the proteolytic process releasing L1 52/55 kDa before the capsid is sealed.

The Ad5/FC31 light particle study provides new data to add to the assembly model proposed in section 4.1.6 (**Figure 38B**), where the exact localization and the assembly way (concerted) was revealed. With the new results, a more specific model can be proposed (**Figure 39**): packaging proteins IVa2 and L1 52/55 kDa (also possibly L4 22k), located in the DNA bundles, bind to Ψ. The viral DNA would start its condensation by the action of core proteins. At the same time, in areas close to the PRZ, full length L1 52/55k would bind to IIIa/IVa2 at one vertex of a nascent capsid, growing from there a disordered shell made up by more L1 52/55k molecules. The two pools of L1 52/55 kDa (in capsid and core) interact binding the two pools of IVa2 that would help complete the interaction between capsid and core. The thick L1 52/55K shell would act as a velcro, tethering the incoming genome to the nascent capsid. As capsid assembly proceeds around the core, proteolytic processing starts releasing L1 52/55k from the capsid shell, the genome and other L1 52/55k molecules. The L1 52/55 kDa fragments would be removed from the particle before capsid assembly is completed.

5.4 Origin of Ad5/FC31 Light Particles

With this new model, and taking into account the information obtained from the studies on light particles and infected cells, it is possible to propose an origin for the Ad5/FC31 light particles. It has been reported that in the first 36 hpi Ad5/FC31 does not produce a clear heavy band because a cellular protein interferes with the correct interaction between packaging proteins and Ψ (1). During this time, capsids could not start assembling around DNA because Ψ is hidden and there is no interaction between packaging pools of the vertex and core. When the unknown cellular protein is depleted, Ψ becomes free and the two pools of packaging proteins would be able to interact correctly and bind core and capsid. The union between capsid and core by L1 52/55 kDa would be sufficiently stable to allow the beginning of particle assembly and maturation. Nevertheless, Ad5/FC31 still produces more empty particles than Ad5 wt: L2 and L3 which have started but failed to complete packaging. The reason for this behavior could be the presence of the exogenous *attB* sequence close to Ψ, which could destabilize the interactions between capsid and core through IVa2, L4 22 kDa and L1 52/55 kDa. It is known that IVa2 and L4 22 kDa bind to a specific site of Ψ (165) forming a complex together with L1 52/55 kDa. It is possible that this complex requires a specific three-dimensional structure during assembly. The presence of the *attB* sequence could prevent the formation of this structure on Ψ. The L2 and L3 particles could be produced when the interaction between capsid and core is not sufficiently stable throughout assembly. L2 particles would lose the interaction with the budding core at earlier times than L3, producing the differences found in proteolytic processing. At 56 hpi, both L2 and L3 particles, as well as mature virions are present in the infected cell. This means that the instability produced by *attB* is overcome in some cases and mature particles are produced.

5.5 Other Contributions of this Thesis

The Ad5/FC31 light particle structures helped to solve the controversy regarding location of minor coat proteins raised by disagreements in the interpretation of wt Ad5 crystallographic and cryo-EM high resolution maps (76, 120). Analyzing the pinwheel feature located beneath the vertex region in these particles, which lack core polypeptide V, no density was missing at the localization proposed for V in the X-ray model. Therefore, this analysis supports the cryo-

EM high resolution structure. Also, this work showed for the first time structurally, genome less AdV particles: the L3 particles. They are authentic VLPs that could be used as biosafe platforms for display of epitopes of biomedical interest.

5.6 Remaining questions

Although this thesis provides information to support the mechanism and exact localization for AdV assembly, some questions remain unanswered. Is there a special vertex in the capsid where assembly starts? If the answer were positive: is L1 52/55 kDa bound preferentially to this vertex? and IVa2? Why does IVa2 bind ATP if it would not act as a packaging motor? One possibility is that IVa2 could be acting by translocating DNA from the bundle to the budding core. Why does DNA contained in some L3 particles have a specific size? A possible answer to this question is that the small DNA fragments present in L3 are abortive replication products. If replication aborts were packaged, the maturation process would not be complete. AVP travels along viral DNA while processing the precursors (molecular-sled model, section 1.5), but in the presence of short DNA fragments AVP could not reach all the precursors present in the particle.

New experimental work will be required to answer the remaining questions. However, the results obtained in the two sections of this research (infected cells and light particles), are consistent between them and support a concerted assembly model for Ad5. In this model, L1 52/55 kDa plays an important role recruiting capsid fragments onto budding cores and keeping the interaction between them during particle assembly.

Conclusions

6 Conclusions

This thesis addresses the problem of AdV assembly and packaging using two strategies, following assembly factors in infected cells, and studying light particles produce by the Ad5/FC31 mutant. The main conclusions obtained are:

Concerning AdV assembly in the cell:

- Tracking assembly factors (viral DNA, packaging, core and capsid proteins) by inmuno-labeling in fluorescence and electron microscopy reveled that these factors meet in the DNA replicative area called PRZ.
- The presence of assembly intermediates and factors in the PRZ indicates that AdV assembly occurs there. Therefore the PRZ is the AdV factory.
- The AdV assembly mechanism involves two pathways, one for capsid proteins and another for viral DNA and core proteins. Viral particles are assembled only when these pathways are coupled.
- When there is a decoupling between the two pathways, abortive structures are produced: empty capsids, SBs and EOGS. The last two are dead end products of the core pathway.
- AdV assembly and packaging are simultaneous, as proposed by the concerted model. L1 52/55 kDa binds to viral DNA and capsid proteins (two pools) while the core proteins begin to condense the viral genome. Protein L1 52/55 kDa recruits and binds capsid fragments to nascent cores, acting as a velcro to keep both joined. Capsid assembly proceeds around the core, which is still connected to DNA bundles.

Concerning the structure of Ad5/FC31 light particles:

- The structure and composition of two types of light particles (L2 and L3) has been characterized, finding that they represent two different stages of the AdV proteolytic maturation, with L3 being more processed than L2. Both types of particles lack genome and core proteins.
- The light particles of Ad5/FC31 have started but not completed packaging. Therefore these particles would not be assembly intermediates but assembly abortions.
- L3 particles, which lack the viral genome and are sealed, would be the first authentic Ad5 virus-like particles (VLPs).
- The structures of L2 and L3 particles provide evidence to support the cryo-EM model and reject the assignation of protein V in the pinwheel proposed by the X-ray model.

- The structures of L2 and L3 particles provide the first information on the localization of protein L1 52/55 kDa. The full length protein forms a shell on the inner capsid surface with more density beneath the vertices. This shell is disrupted during maturation. Full length L1 52/55 kDa preferably located beneath the vertex could engage the virus genome during assembly.

Conclusiones

Esta tesis aborda el problema del ensamblaje y encapsidación del genoma de AdV usando dos estrategias para su estudio: siguiendo los componentes involucrados en el ensamblaje y encapsidación del genoma viral dentro de células infectadas, y estudiando las partículas ligeras producidas por el mutante Ad5/FC31. Las principales conclusiones obtenidas son las siguientes:

En relación con el ensamblaje de AdV en el interior celular:

- El rastreo de los factores de ensamblaje (ADN viral y proteínas de encapsidación, del core y de la cápside) por inmuno-marcaje en microscopia de fluorescencia y electrónica revelo que estos factores coinciden en el área de replicación del genome viral llamada PRZ.
- La presencia de los factores e intermediarios de ensamblaje en la PRZ indica que es allí donde tiene lugar el ensamblaje de AdV. Por lo tanto, la PRZ es la factoría de AdV.
- El mecanismo de ensamblaje de AdV involucra dos rutas, una para proteínas de la cápside y otra para el ADN viral y proteínas del core. Las partículas virales se ensamblan correctamente sólo si ambas rutas están acopladas.
- Cuando hay un desacoplamiento entre estas dos rutas se producen estructuras abortivas: cápsides vacías, cuerpos moteados y granulos electro opacos. Las últimas son productos abortivos de la ruta del core.
- El ensamblaje y encapsidación del genoma son simultáneos, como propone el modelo concertado. La proteína L1 52/55 kDa se une al ADN viral y a proteinas de la cápside, mientras que las proteínas del core empiezan a condensar el genoma viral. La proteína L1 52/55 kDa recluta y enlaza los fragmentos de cápside a los cores nacientes, actuando como un velcro que mantiene unidas ambas estructuras. El ensamblaje de la cápside prosigue alrededor del core que aún sigue unido a la madeja de ADN.

En relación con la estructura de las partículas ligeras:

- Se ha caracterizado la estructura y composición de dos partículas ligeras (L2 y L3), encontrando que representan dos diferentes estadíos de maduración proteolítica, siendo L3 más procesada que L2. Los dos tipos de partículas carecen de genoma viral y proteínas del core.

- Las partículas ligeras de Ad5/FC31 habían empezado pero no completaron la encapsidación del ADN. Por lo tanto estas partículas no serían intermediarios de ensamblaje sino abortos de ensamblaje.
- Las partículas L3, que carecen de genoma viral y están cerradas, serían las primeras auténticas partículas pseudo-virales (VLPs) de AdV humano descritas.
- La estructura de las partículas L2 y L3 proporciona evidencia para apoyar el modelo de crio-microscopía eléctronica y rechazar la asignación de la proteína V en el pinwheel (localizada debajo del vertice) propuesta por el modelo de rayos-X.
- Las estructuras de las partículas L2 y L3 proporcionan por primera vez información sobre la localización de L1 52/55 kDa. La forma completa de esta proteína forma una capa sobre la superficie interna de la cápside con más densidad debajo de los vértices. Esta capa se desorganiza durante la maduración. La forma completa de L1 52/55 kDa que preferiblemente se localiza debajo de los vértices podría capturar el genoma del virus durante el ensamblaje.

References

8. References

1. **Alba R.** 2007. Caracterización del sistema *attB/attP*-ΦC31 para la producción de adenovirus gutless. Universitat Autònoma de Barcelona, Bellaterra.
2. **Alba R, Cots D, Ostapchuk P, Bosch A, Hearing P, Chillon M.** 2011. Altering the Ad5 packaging domain affects the maturation of the Ad particles. PloS one **6:**e19564.
3. **Alba R, Hearing P, Bosch A, Chillon M.** 2007. Differential amplification of adenovirus vectors by flanking the packaging signal with attB/attP-PhiC31 sequences: implications for helper-dependent adenovirus production. Virology **367:**51-58.
4. **Ali H, LeRoy G, Bridge G, Flint SJ.** 2007. The adenovirus L4 33-kilodalton protein binds to intragenic sequences of the major late promoter required for late phase-specific stimulation of transcription. J Virol **81:**1327-1338.
5. **Anderson CW, Young ME, Flint SJ.** 1989. Characterization of the adenovirus 2 virion protein, mu. Virology **172:**506-512.
6. **Arnberg N.** 2012. Adenovirus receptors: implications for targeting of viral vectors. Trends in pharmacological sciences **33:**442-448.
7. **Backstrom E, Kaufmann KB, Lan X, Akusjarvi G.** 2010. Adenovirus L4-22K stimulates major late transcription by a mechanism requiring the intragenic late-specific transcription factor-binding site. Virus research **151:**220-228.
8. **Bamford DH, Grimes JM, Stuart DI.** 2005. What does structure tell us about virus evolution? Current opinion in structural biology **15:**655-663.
9. **Benevento M, Di Palma S, Snijder J, Moyer CL, Reddy VS, Nemerow GR, Heck AJ.** 2014. Adenovirus composition, proteolysis, and disassembly studied by in-depth qualitative and quantitative proteomics. The Journal of biological chemistry **289:**11421-11430.
10. **Bergelson JM, Cunningham JA, Droguett G, Kurt-Jones EA, Krithivas A, Hong JS, Horwitz MS, Crowell RL, Finberg RW.** 1997. Isolation of a common receptor for Coxsackie B viruses and adenoviruses 2 and 5. Science **275:**1320-1323.
11. **Berk AJ.** 2007. Adenoviridae: The Viruses and Their Replication, p. 3177. *In* Knipe DM, Howley PM (ed.), Fields Virology, Fifth edition ed, vol. II. Lippincott Williams &Wilkins, Philadelphia.
12. **Besse S, Puvion-Dutilleul F.** 1994. High resolution localization of replicating viral genome in adenovirus-infected HeLa cells. European journal of cell biology **63:**269-279.
13. **Blainey PC, Graziano V, Perez-Berna AJ, McGrath WJ, Flint SJ, San Martin C, Xie XS, Mangel WF.** 2013. Regulation of a viral proteinase by a peptide and DNA in one-dimensional space: IV. viral proteinase slides along DNA to locate and process its substrates. The Journal of biological chemistry **288:**2092-2102.
14. **Braithwaite AW, Russell IA.** 2001. Induction of cell death by adenoviruses. Apoptosis : an international journal on programmed cell death **6:**359-370.
15. **Brown MT, McGrath WJ, Toledo DL, Mangel WF.** 1996. Different modes of inhibition of human adenovirus proteinase, probably a cysteine proteinase, by bovine pancreatic trypsin inhibitor. FEBS letters **388:**233-237.
16. **Burckhardt CJ, Suomalainen M, Schoenenberger P, Boucke K, Hemmi S, Greber UF.** 2011. Drifting motions of the adenovirus receptor CAR and immobile integrins initiate virus uncoating and membrane lytic protein exposure. Cell host & microbe **10:**105-117.
17. **Burlingham BT, Brown DT, Doerfler W.** 1974. Incomplete particles of adenovirus. I. Characteristics of the DNA associated with incomplete adenovirions of types 2 and 12. Virology **60:**419-430.
18. **Cai Y, Long Z, Qiu J, Yuan M, Li G, Yang K.** 2012. An ac34 deletion mutant of Autographa californica nucleopolyhedrovirus exhibits delayed late gene expression and a lack of virulence in vivo. J Virol **86:**10432-10443.
19. **Campos SK.** 2014. New structural model of adenoviral cement proteins is not yet concrete. Proceedings of the National Academy of Sciences **111:**E4542-E4543.
20. **Condit RC, Moussatche N.** 2015. The vaccinia virus E6 protein influences virion protein localization during virus assembly. Virology **482:**147-156.
21. **Cots D, Bosch A, Chillon M.** 2013. Helper dependent adenovirus vectors: progress and future prospects. Current gene therapy **13:**370-381.
22. **Cuervo A, Daudén MI, Carrascosa JL.** 2013. Nucleic Acid Packaging in Viruses, p. 361-394. *In* Mateu M (ed.), Structure and Physics of Viruses. Springer.
23. **Chatterjee PK, Vayda ME, Flint SJ.** 1986. Adenoviral protein VII packages intracellular viral DNA throughout the early phase of infection. The EMBO journal **5:**1633-1644.

24. **Chen S, McMullan G, Faruqi AR, Murshudov GN, Short JM, Scheres SH, Henderson R.** 2013. High-resolution noise substitution to measure overfitting and validate resolution in 3D structure determination by single particle electron cryomicroscopy. Ultramicroscopy **135:**24-35.
25. **Cheng L, Huang X, Li X, Xiong W, Sun W, Yang C, Zhang K, Wang Y, Liu H, Huang X, Ji G, Sun F, Zheng C, Zhu P.** 2014. Cryo-EM structures of two bovine adenovirus type 3 intermediates. Virology **450-451:**174-181.
26. **Christensen JB, Byrd SA, Walker AK, Strahler JR, Andrews PC, Imperiale MJ.** 2008. Presence of the adenovirus IVa2 protein at a single vertex of the mature virion. J Virol **82:**9086-9093.
27. **Chroboczek J, Viard F, D'Halluin JC.** 1986. Human adenovirus 2 temperature-sensitive mutant 112 contains three mutations in the protein IIIa gene. Gene **49:**157-160.
28. **D'Halluin JC, Milleville M, Boulanger PA, Martin GR.** 1978. Temperature-sensitive mutant of adenovirus type 2 blocked in virion assembly: accumulation of light intermediate particles. J Virol **26:**344-356.
29. **Daniell E.** 1976. Genome structure of incomplete particles of adenovirus. J Virol **19:**685-708.
30. **Daniell E, Groff DE, Fedor MJ.** 1981. Adenovirus chromatin structure at different stages of infection. Molecular and cellular biology **1:**1094-1105.
31. **de Castro IF, Volonte L, Risco C.** 2013. Virus factories: biogenesis and structural design. Cellular microbiology **15:**24-34.
32. **de la Rosa-Trevin JM, Oton J, Marabini R, Zaldivar A, Vargas J, Carazo JM, Sorzano CO.** 2013. Xmipp 3.0: an improved software suite for image processing in electron microscopy. Journal of structural biology **184:**321-328.
33. **Dery CV, Toth M, Brown M, Horvath J, Allaire S, Weber JM.** 1985. The structure of adenovirus chromatin in infected cells. The Journal of general virology **66 (Pt 12):**2671-2684.
34. **Dobbelstein M.** 2004. Replicating adenoviruses in cancer therapy. Current Topics in Microbiology and Immunology **273:**291-334.
35. **Draper SJ, Heeney JL.** 2010. Viruses as vaccine vectors for infectious diseases and cancer. Nat Rev Microbiol **8:**62-73.
36. **Edvardsson B, Everitt E, Jornvall H, Prage L, Philipson L.** 1976. Intermediates in adenovirus assembly. J Virol **19:**533-547.
37. **Erickson KD, Bouchet-Marquis C, Heiser K, Szomolanyi-Tsuda E, Mishra R, Lamothe B, Hoenger A, Garcea RL.** 2012. Virion assembly factories in the nucleus of polyomavirus-infected cells. PLoS pathogens **8:**e1002630.
38. **Ewing SG, Byrd SA, Christensen JB, Tyler RE, Imperiale MJ.** 2007. Ternary complex formation on the adenovirus packaging sequence by the IVa2 and L4 22-kilodalton proteins. J Virol **81:**12450-12457.
39. **Fabry CM, Rosa-Calatrava M, Moriscot C, Ruigrok RW, Boulanger P, Schoehn G.** 2009. The C-terminal domains of adenovirus serotype 5 protein IX assemble into an antiparallel structure on the facets of the capsid. J Virol **83:**1135-1139.
40. **Flint SJ, Enquist LW, Racaniello VR, Skalka AM.** 2009. Principles of Virology, third ed, vol. I. ASM Press, Washington.
41. **Franqueville L, Henning P, Magnusson M, Vigne E, Schoehn G, Blair-Zajdel ME, Habib N, Lindholm L, Blair GE, Hong SS, Boulanger P.** 2008. Protein crystals in Adenovirus type 5-infected cells: requirements for intranuclear crystallogenesis, structural and functional analysis. PloS one **3:**e2894.
42. **Goldsmith CS, Miller SE.** 2009. Modern uses of electron microscopy for detection of viruses. Clinical microbiology reviews **22:**552-563.
43. **Goncalves MA, de Vries AA.** 2006. Adenovirus: from foe to friend. Rev Med Virol **16:**167-186.
44. **Grable M, Hearing P.** 1990. Adenovirus type 5 packaging domain is composed of a repeated element that is functionally redundant. J Virol **64:**2047-2056.
45. **Graham FL, Smiley J, Russell WC, Nairn R.** 1977. Characteristics of a human cell line transformed by DNA from human adenovirus type 5. The Journal of general virology **36:**59-74.
46. **Graziano V, Luo G, Blainey PC, Perez-Berna AJ, McGrath WJ, Flint SJ, San Martin C, Xie XS, Mangel WF.** 2013. Regulation of a viral proteinase by a peptide and DNA in one-dimensional space: II. adenovirus proteinase is activated in an unusual one-dimensional biochemical reaction. The Journal of biological chemistry **288:**2068-2080.
47. **Graziano V, McGrath WJ, Suomalainen M, Greber UF, Freimuth P, Blainey PC, Luo G, Xie XS, Mangel WF.** 2013. Regulation of a viral proteinase by a peptide and DNA in one-

dimensional space: I. binding to DNA and to hexon of the precursor to protein VI, pVI, of human adenovirus. The Journal of biological chemistry **288:**2059-2067.

48. **Greber UF, Webster P, Weber J, Helenius A.** 1996. The role of the adenovirus protease on virus entry into cells. The EMBO journal **15:**1766-1777.
49. **Greber UF, Willetts M, Webster P, Helenius A.** 1993. Stepwise dismantling of adenovirus 2 during entry into cells. Cell **75:**477-486.
50. **Gustin KE, Imperiale MJ.** 1998. Encapsidation of viral DNA requires the adenovirus L1 52/55-kilodalton protein. J Virol **72:**7860-7870.
51. **Gustin KE, Lutz P, Imperiale MJ.** 1996. Interaction of the adenovirus L1 52/55-kilodalton protein with the IVa2 gene product during infection. J Virol **70:**6463-6467.
52. **Halbert DN, Cutt JR, Shenk T.** 1985. Adenovirus early region 4 encodes functions required for efficient DNA replication, late gene expression, and host cell shutoff. J Virol **56:**250-257.
53. **Hammarskjold ML, Winberg G.** 1980. Encapsidation of adenovirus 16 DNA is directed by a small DNA sequence at the left end of the genome. Cell **20:**787-795.
54. **Harrach B, Benko M, Both G, Brown M, Davison A, Echevarría M, Hess M, Jones M, Kajon A, Lehmkuhl H, Mautner V, Mittal S, Wadell G.** 2011. Family Adenoviridae, p. 95-111. *In* King A, Adams M, Carstens E, Lefkowitz E (ed.), Virus Taxonomy: Classification and Nomenclature of Viruses. Ninth Report of the International Committee on Taxonomy of Viruses. Elsevier, San Diego.
55. **Haruki H, Gyurcsik B, Okuwaki M, Nagata K.** 2003. Ternary complex formation between DNA-adenovirus core protein VII and TAF-Ibeta/SET, an acidic molecular chaperone. FEBS letters **555:**521-527.
56. **Haruki H, Okuwaki M, Miyagishi M, Taira K, Nagata K.** 2006. Involvement of template-activating factor I/SET in transcription of adenovirus early genes as a positive-acting factor. J Virol **80:**794-801.
57. **Hassell JA, Weber J.** 1978. Genetic analysis of adenovirus type 2. VIII. Physical locations of temperature-sensitive mutations. J Virol **28:**671-678.
58. **Hasson TB, Ornelles DA, Shenk T.** 1992. Adenovirus L1 52- and 55-kilodalton proteins are present within assembling virions and colocalize with nuclear structures distinct from replication centers. J Virol **66:**6133-6142.
59. **Hasson TB, Soloway PD, Ornelles DA, Doerfler W, Shenk T.** 1989. Adenovirus L1 52- and 55-kilodalton proteins are required for assembly of virions. J Virol **63:**3612-3621.
60. **Hearing P, Samulski RJ, Wishart WL, Shenk T.** 1987. Identification of a repeated sequence element required for efficient encapsidation of the adenovirus type 5 chromosome. J Virol **61:**2555-2558.
61. **Henry CJ, Atchison RW.** 1971. Paracrystal formation in cell cultures infected with adenovirus type 2. J Virol **8:**842-849.
62. **Henry LJ, Xia D, Wilke ME, Deisenhofer J, Gerard RD.** 1994. Characterization of the knob domain of the adenovirus type 5 fiber protein expressed in Escherichia coli. J Virol **68:**5239-5246.
63. **Honda T, Saitoh H, Masuko M, Katagiri-Abe T, Tominaga K, Kozakai I, Kobayashi K, Kumanishi T, Watanabe YG, Odani S, Kuwano R.** 2000. The coxsackievirus-adenovirus receptor protein as a cell adhesion molecule in the developing mouse brain. Brain research. Molecular brain research **77:**19-28.
64. **Ishibashi M, Maizel JV, Jr.** 1974. The polypeptides of adenovirus. V. Young virions, structural intermediate between top components and aged virions. Virology **57:**409-424.
65. **Ishov AM, Maul GG.** 1996. The periphery of nuclear domain 10 (ND10) as site of DNA virus deposition. The Journal of cell biology **134:**815-826.
66. **Kato SE, Chahal JS, Flint SJ.** 2012. Reduced infectivity of adenovirus type 5 particles and degradation of entering viral genomes associated with incomplete processing of the preterminal protein. J Virol **86:**13554-13565.
67. **Kelkar SA, Pfister KK, Crystal RG, Leopold PL.** 2004. Cytoplasmic dynein mediates adenovirus binding to microtubules. J Virol **78:**10122-10132.
68. **Khittoo G, Weber J.** 1977. Genetic analysis of adenovirus type 2. VI. A temperature-sensitive mutant defective for DNA encapsidation. Virology **81:**126-137.
69. **Khittoo G, Weber JM.** 1981. The nature of the DNA associated with incomplete particles of adenovirus type 2. The Journal of general virology **54:**343-355.
70. **Komatsu T, Haruki H, Nagata K.** 2011. Cellular and viral chromatin proteins are positive factors in the regulation of adenovirus gene expression. Nucleic acids research **39:**889-901.

71. **Komatsu T, Nagata K.** 2012. Replication-uncoupled histone deposition during adenovirus DNA replication. J Virol **86:**6701-6711.

72. **Koonin EV, Senkevich TG, Chernos VI.** 1993. Gene A32 product of vaccinia virus may be an ATPase involved in viral DNA packaging as indicated by sequence comparisons with other putative viral ATPases. Virus genes **7:**89-94.

73. **Krupovic M, Bamford DH.** 2008. Virus evolution: how far does the double beta-barrel viral lineage extend? Nat Rev Microbiol **6:**941-948.

74. **Leen AM, Rooney CM.** 2004. Adenovirus as an emerging pathogen in immunocompromised patients. British Journal of Haematology **128:**135-144.

75. **Lenk R, Storch T, Maizel JV, Jr.** 1980. Cell architecture during adenovirus infection. Virology **105:**19-34.

76. **Liu H, Jin L, Koh SB, Atanasov I, Schein S, Wu L, Zhou ZH.** 2010. Atomic structure of human adenovirus by cryo-EM reveals interactions among protein networks. Science **329:**1038-1043.

77. **Liu H, Naismith JH, Hay RT.** 2003. Adenovirus DNA Replication, p. 131-164. *In* Doerfler W, Böhm P (ed.), Adenovirusses: Model and Vectors in Virus-Host Interactions. Virion-Structure,Viral Replication and Host-Cell Interactions. Springer, Berlin.

78. **Ludtke SJ, Baldwin PR, Chiu W.** 1999. EMAN: semiautomated software for high-resolution single-particle reconstructions. Journal of structural biology **128:**82-97.

79. **Lunt R, Vayda ME, Young M, Flint SJ.** 1988. Isolation and characterization of monoclonal antibodies against the adenovirus core proteins. Virology **164:**275-279.

80. **Lutz P, Puvion-Dutilleul F, Lutz Y, Kedinger C.** 1996. Nucleoplasmic and nucleolar distribution of the adenovirus IVa2 gene product. J Virol **70:**3449-3460.

81. **Lutz P, Rosa-Calatrava M, Kedinger C.** 1997. The product of the adenovirus intermediate gene IX is a transcriptional activator. J Virol **71:**5102-5109.

82. **Ma HC, Hearing P.** 2011. Adenovirus structural protein IIIa is involved in the serotype specificity of viral DNA packaging. J Virol **85:**7849-7855.

83. **Majhen D, Calderon H, Chandra N, Fajardo CA, Rajan A, Alemany R, Custers J.** 2014. Adenovirus-based vaccines for fighting infectious diseases and cancer: progress in the field. Human gene therapy **25:**301-317.

84. **Mangel WF, McGrath WJ, Toledo DL, Anderson CW.** 1993. Viral DNA and a viral peptide can act as cofactors of adenovirus virion proteinase activity. Nature **361:**274-275.

85. **Mangel WF, Toledo DL, Brown MT, Martin JH, McGrath WJ.** 1996. Characterization of three components of human adenovirus proteinase activity in vitro. The Journal of biological chemistry **271:**536-543.

86. **Matthews DA, Russell WC.** 1995. Adenovirus protein-protein interactions: molecular parameters governing the binding of protein VI to hexon and the activation of the adenovirus 23K protease. The Journal of general virology **76 (Pt 8):**1959-1969.

87. **Maul GG.** 1998. Nuclear domain 10, the site of DNA virus transcription and replication. BioEssays : news and reviews in molecular, cellular and developmental biology **20:**660-667.

88. **McGrath WJ, Baniecki ML, Li C, McWhirter SM, Brown MT, Toledo DL, Mangel WF.** 2001. Human adenovirus proteinase: DNA binding and stimulation of proteinase activity by DNA. Biochemistry **40:**13237-13245.

89. **Medina-Kauwe LK.** 2003. Endocytosis of adenovirus and adenovirus capsid proteins. Advanced drug delivery reviews **55:**1485-1496.

90. **Mutsafi Y, Shimoni E, Shimon A, Minsky A.** 2013. Membrane assembly during the infection cycle of the giant Mimivirus. PLoS pathogens **9:**e1003367.

91. **Novoa RR, Calderita G, Arranz R, Fontana J, Granzow H, Risco C.** 2005. Virus factories: associations of cell organelles for viral replication and morphogenesis. Biology of the cell / under the auspices of the European Cell Biology Organization **97:**147-172.

92. **Ortega-Esteban A, Perez-Berna AJ, Menendez-Conejero R, Flint SJ, San Martin C, de Pablo PJ.** 2013. Monitoring dynamics of human adenovirus disassembly induced by mechanical fatigue. Sci Rep **3:**1434.

93. **Ostapchuk P, Almond M, Hearing P.** 2011. Characterization of Empty adenovirus particles assembled in the absence of a functional adenovirus IVa2 protein. J Virol **85:**5524-5531.

94. **Ostapchuk P, Anderson ME, Chandrasekhar S, Hearing P.** 2006. The L4 22-kilodalton protein plays a role in packaging of the adenovirus genome. J Virol **80:**6973-6981.

95. **Ostapchuk P, Hearing P.** 2008. Adenovirus IVa2 protein binds ATP. J Virol **82:**10290-10294.

96. **Ostapchuk P, Yang J, Auffarth E, Hearing P.** 2005. Functional interaction of the adenovirus IVa2 protein with adenovirus type 5 packaging sequences. J Virol **79:**2831-2838.

97. **Ostberg S, Tormanen Persson H, Akusjarvi G.** 2012. Serine 192 in the tiny RS repeat of the adenoviral L4-33K splicing enhancer protein is essential for function and reorganization of the protein to the periphery of viral replication centers. Virology **433:**273-281.

98. **Pardo-Mateos A, Young CS.** 2004. A 40 kDa isoform of the type 5 adenovirus IVa2 protein is sufficient for virus viability. Virology **324:**151-164.

99. **Peréz-Berná AJ, Mangel WF, McGrath WJ, Graziano V, Flint J, San Martin C.** 2014. Processing of the l1 52/55k protein by the adenovirus protease: a new substrate and new insights into virion maturation. J Virol **88:**1513-1524.

100. **Perez-Berna AJ, Marabini R, Scheres SH, Menendez-Conejero R, Dmitriev IP, Curiel DT, Mangel WF, Flint SJ, San Martin C.** 2009. Structure and uncoating of immature adenovirus. Journal of molecular biology **392:**547-557.

101. **Peréz-Berná AJ, Ortega-Esteban A, Menendez-Conejero R, Winkler DC, Menendez M, Steven AC, Flint SJ, de Pablo PJ, San Martin C.** 2012. The role of capsid maturation on adenovirus priming for sequential uncoating. The Journal of biological chemistry **287:**31582-31595.

102. **Perez-Romero P, Tyler RE, Abend JR, Dus M, Imperiale MJ.** 2005. Analysis of the interaction of the adenovirus L1 52/55-kilodalton and IVa2 proteins with the packaging sequence in vivo and in vitro. J Virol **79:**2366-2374.

103. **Perez-Vargas J, Vaughan RC, Houser C, Hastie KM, Kao CC, Nemerow GR.** 2014. Isolation and Characterization of the DNA and Protein Binding Activities of Adenovirus Core Protein V. J Virol.

104. **Pettersen EF, Goddard TD, Huang CC, Couch GS, Greenblatt DM, Meng EC, Ferrin TE.** 2004. UCSF Chimera--a visualization system for exploratory research and analysis. Journal of computational chemistry **25:**1605-1612.

105. **Pettersson U, Philipson L, Hoglund S.** 1967. Structural proteins of adenoviruses. I. Purification and characterization of the adenovirus type 2 hexon antigen. Virology **33:**575-590.

106. **Pettersson U, Philipson L, Hoglund S.** 1968. Structural proteins of adenoviruses. II. Purification and characterization of the adenovirus type 2 fiber antigen. Virology **35:**204-215.

107. **Pombo A, Ferreira J, Bridge E, Carmo-Fonseca M.** 1994. Adenovirus replication and transcription sites are spatially separated in the nucleus of infected cells. The EMBO journal **13:**5075-5085.

108. **Prage L, Pettersson U, Hoglund S, Lonberg-Holm K, Philipson L.** 1970. Structural proteins of adenoviruses. IV. Sequential degradation of the adenovirus type 2 virion. Virology **42:**341-358.

109. **Puvion-Dutilleul F.** 1991. Simultaneous detection of highly phosphorylated proteins and viral major DNA binding protein distribution in nuclei of adenovirus type 5-infected HeLa cells. The journal of histochemistry and cytochemistry : official journal of the Histochemistry Society **39:**669-680.

110. **Puvion-Dutilleul F, Bachellerie JP, Visa N, Puvion E.** 1994. Rearrangements of intranuclear structures involved in RNA processing in response to adenovirus infection. Journal of cell science **107 (Pt 6):**1457-1468.

111. **Puvion-Dutilleul F, Besse S, Pichard E, Cajean-Feroldi C.** 1998. Release of viruses and viral DNA from nucleus to cytoplasm of HeLa cells at late stages of productive adenovirus infection as revealed by electron microscope in situ hybridization. Biology of the cell / under the auspices of the European Cell Biology Organization **90:**5-38.

112. **Puvion-Dutilleul F, Chelbi-Alix MK, Koken M, Quignon F, Puvion E, de The H.** 1995. Adenovirus infection induces rearrangements in the intranuclear distribution of the nuclear body-associated PML protein. Experimental cell research **218:**9-16.

113. **Puvion-Dutilleul F, Legrand V, Mehtali M, Chelbi-Alix MK, de The H, Puvion E.** 1999. Deletion of the fiber gene induces the storage of hexon and penton base proteins in PML/Sp100-containing inclusions during adenovirus infection. Biology of the cell / under the auspices of the European Cell Biology Organization **91:**617-628.

114. **Puvion-Dutilleul F, Pichard E.** 1992. Segregation of viral double-stranded and single-stranded DNA molecules in nuclei of adenovirus infected cells as revealed by electron microscope in situ hybridization. Biology of the cell / under the auspices of the European Cell Biology Organization **76:**139-150.

115. **Puvion-Dutilleul F, Puvion E.** 1990. Analysis by in situ hybridization and autoradiography of sites of replication and storage of single- and double-stranded adenovirus type 5 DNA in lytically infected HeLa cells. Journal of structural biology **103:**280-289.

116. **Puvion-Dutilleul F, Puvion E.** 1990. Replicating single-stranded adenovirus type 5 DNA molecules accumulate within well-delimited intranuclear areas of lytically infected HeLa cells. European journal of cell biology **52:**379-388.

117. **Puvion-Dutilleul F, Puvion E.** 1991. Sites of transcription of adenovirus type 5 genomes in relation to early viral DNA replication in infected HeLa cells. A high resolution in situ hybridization and autoradiographical study. Biology of the cell / under the auspices of the European Cell Biology Organization **71:**135-147.

118. **Puvion-Dutilleul F, Roussev R, Puvion E.** 1992. Distribution of viral RNA molecules during the adenovirus type 5 infectious cycle in HeLa cells. Journal of structural biology **108:**209-220.

119. **Reddy VS, Natchiar SK, Stewart PL, Nemerow GR.** 2010. Crystal structure of human adenovirus at 3.5 A resolution. Science **329:**1071-1075.

120. **Reddy VS, Nemerow GR.** 2014. Structures and organization of adenovirus cement proteins provide insights into the role of capsid maturation in virus entry and infection. Proc Natl Acad Sci U S A **111:**11715-11720.

121. **Reich NC, Sarnow P, Duprey E, Levine AJ.** 1983. Monoclonal antibodies which recognize native and denatured forms of the adenovirus DNA-binding protein. Virology **128:**480-484.

122. **Rekosh DM, Russell WC, Bellet AJ, Robinson AJ.** 1977. Identification of a protein linked to the ends of adenovirus DNA. Cell **11:**283-295.

123. **Robinson CM, Singh G, Lee JY, Dehghan S, Rajaiya J, Liu EB, Yousuf MA, Betensky RA, Jones MS, Dyer DW, Seto D, Chodosh J.** 2013. Molecular evolution of human adenoviruses. Scientific Reports **3:**1-7.

124. **Rohrmann GF.** 2013. The Baculovirus replication cycle: Effects on cells and insects, Baculovirus Molecular Biology: Third Edition, Bethesda (MD).

125. **Rosa-Calatrava M, Grave L, Puvion-Dutilleul F, Chatton B, Kedinger C.** 2001. Functional analysis of adenovirus protein IX identifies domains involved in capsid stability, transcriptional activity, and nuclear reorganization. J Virol **75:**7131-7141.

126. **Rosa-Calatrava M, Puvion-Dutilleul F, Lutz P, Dreyer D, de The H, Chatton B, Kedinger C.** 2003. Adenovirus protein IX sequesters host-cell promyelocytic leukaemia protein and contributes to efficient viral proliferation. EMBO reports **4:**969-975.

127. **Rowe WP, Huebner RJ, Gilmore LK, Parrot RH, Ward TG.** 1953. Isolation of a cytopathogenic agent from human adenoids undergoing spontaneous degeneration in tissue culture. Proccedings of the Society for Experimental Biology and Medicine **84:**570-573.

128. **Russell WC.** 2000. Update on adenovirus and its vectors. The Journal of general virology **81:**2573-2604.

129. **Saban SD, Silvestry M, Nemerow GR, Stewart PL.** 2006. Visualization of α-helices in a 6 Å resolution cryoEM structure of adenovirus allows refinement of capsid protein assignments. J Virol **80:**12049-12059.

130. **Samad MA, Komatsu T, Okuwaki M, Nagata K.** 2012. B23/nucleophosmin is involved in regulation of adenovirus chromatin structure at late infection stages, but not in virus replication and transcription. The Journal of general virology **93:**1328-1338.

131. **San Martin C.** 2012. Latest insights on adenovirus structure and assembly. Viruses **4:**847-877.

132. **San Martín C, Glasgow JN, Borovjagin A, Beatty MS, Kashentseva EA, Curiel DT, Marabini R, Dmitriev IP.** 2008. Localization of the N-terminus of minor coat protein IIIa in the adenovirus capsid. J Mol Biol **383:**923-934.

133. **Scheres SH.** 2012. RELION: implementation of a Bayesian approach to cryo-EM structure determination. Journal of structural biology **180:**519-530.

134. **Scheres SH, Chen S.** 2012. Prevention of overfitting in cryo-EM structure determination. Nature methods **9:**853-854.

135. **Scheres SHW, Marabini R, Lanzavecchia S, Cantele F, Rutten T, Fuller SD, Carazo JM, Burnett RM, San Martín C.** 2005. Classification of single-projection reconstructions for cryo-electron microscopy data of icosahedral viruses. J Struct Biol **151:**79-91.

136. **Schmid SI, Hearing P.** 1997. Bipartite structure and functional independence of adenovirus type 5 packaging elements. J Virol **71:**3375-3384.

137. **Schneider CA, Rasband WS, Eliceiri KW.** 2012. NIH Image to ImageJ: 25 years of image analysis. Nature methods **9:**671-675.

138. **Seki T, Dmitriev I, Kashentseva E, Takayama K, Rots M, Suzuki K, Curiel DT.** 2002. Artificial extension of the adenovirus fiber shaft inhibits infectivity in coxsackievirus and adenovirus receptor-positive cell lines. J Virol **76:**1100-1108.

139. **Shinagawa M, Iida Y, Matsuda A, Tsukiyama T, Sato G.** 1987. Phylogenetic relationships between adenoviruses as inferred from nucleotide sequences of inverted terminal repeats. Gene **55:**85-93.
140. **Silvestry M, Lindert S, Smith JG, Maier O, Wiethoff CM, Nemerow GR, Stewart PL.** 2009. Cryo-electron microscopy structure of adenovirus type 2 temperature-sensitive mutant 1 reveals insight into the cell entry defect. J Virol **83:**7375-7383.
141. **Singh M, Shmulevitz M, Tikoo SK.** 2005. A newly identified interaction between IVa2 and pVIII proteins during porcine adenovirus type 3 infection. Virology **336:**60-69.
142. **Snijder J, Benevento M, Moyer CL, Reddy V, Nemerow GR, Heck AJ.** 2014. The Cleaved N-Terminus of pVI Binds Peripentonal Hexons in Mature Adenovirus. Journal of molecular biology.
143. **Suarez C, Andres G, Kolovou A, Hoppe S, Salas ML, Walther P, Locker JK.** 2015. African swine fever virus assembles a single membrane derived from rupture of the endoplasmic reticulum. Cellular microbiology.
144. **Sundquist B, Everitt E, Philipson L, Hoglund S.** 1973. Assembly of adenoviruses. J Virol **11:**449-459.
145. **Tibbetts C.** 1977. Viral DNA sequences from incomplete particles of human adenovirus type 7. Cell **12:**243-249.
146. **Tormanen H, Backstrom E, Carlsson A, Akusjarvi G.** 2006. L4-33K, an adenovirus-encoded alternative RNA splicing factor. The Journal of biological chemistry **281:**36510-36517.
147. **Tribouley C, Lutz P, Staub A, Kedinger C.** 1994. The product of the adenovirus intermediate gene IVa2 is a transcriptional activator of the major late promoter. J Virol **68:**4450-4457.
148. **Trotman LC, Mosberger N, Fornerod M, Stidwill RP, Greber UF.** 2001. Import of adenovirus DNA involves the nuclear pore complex receptor CAN/Nup214 and histone H1. Nature cell biology **3:**1092-1100.
149. **Tyler RE, Ewing SG, Imperiale MJ.** 2007. Formation of a multiple protein complex on the adenovirus packaging sequence by the IVa2 protein. J Virol **81:**3447-3454.
150. **Valentine RC, Pereira HG.** 1965. Antigens and structure of the adenovirus. Journal of molecular biology **13:**13-20.
151. **Van der Vliet PC.** 1995. Adenovirus DNA replication. Curr Top Microbiol Immunol **199 (Pt 2):**1-30.
152. **van Oostrum J, Burnett RM.** 1985. Molecular composition of the adenovirus type 2 virion. J Virol **56:**439-448.
153. **van Raaij MJ, Louis N, Chroboczek J, Cusack S.** 1999. Structure of the human adenovirus serotype 2 fiber head domain at 1.5 A resolution. Virology **262:**333-343.
154. **Vayda ME, Rogers AE, Flint SJ.** 1983. The structure of nucleoprotein cores released from adenovirions. Nucleic acids research **11:**441-460.
155. **Walters RW, Freimuth P, Moninger TO, Ganske I, Zabner J, Welsh MJ.** 2002. Adenovirus fiber disrupts CAR-mediated intercellular adhesion allowing virus escape. Cell **110:**789-799.
156. **Weber JM, Dery CV, Mirza MA, Horvath J.** 1985. Adenovirus DNA synthesis is coupled to virus assembly. Virology **140:**351-359.
157. **Webster A, Hay RT, Kemp G.** 1993. The adenovirus protease is activated by a virus-coded disulphide-linked peptide. Cell **72:**97-104.
158. **Wickham TJ, Filardo EJ, Cheresh DA, Nemerow GR.** 1994. Integrin alpha v beta 5 selectively promotes adenovirus mediated cell membrane permeabilization. The Journal of cell biology **127:**257-264.
159. **Wiethoff CM, Wodrich H, Gerace L, Nemerow GR.** 2005. Adenovirus protein VI mediates membrane disruption following capsid disassembly. J Virol **79:**1992-2000.
160. **Winberg G, Wadell G.** 1977. Structural polypeptides of adenovirus type 16 incomplete particles. J Virol **22:**389-401.
161. **Wodrich H, Guan T, Cingolani G, Von Seggern D, Nemerow G, Gerace L.** 2003. Switch from capsid protein import to adenovirus assembly by cleavage of nuclear transport signals. The EMBO journal **22:**6245-6255.
162. **Wohl BP, Hearing P.** 2008. Role for the L1-52/55K protein in the serotype specificity of adenovirus DNA packaging. J Virol **82:**5089-5092.
163. **Wu K, Guimet D, Hearing P.** 2013. The adenovirus L4-33K protein regulates both late gene expression patterns and viral DNA packaging. J Virol **87:**6739-6747.
164. **Wu K, Orozco D, Hearing P.** 2012. The adenovirus L4-22K protein is multifunctional and is an integral component of crucial aspects of infection. J Virol **86:**10474-10483.

165. **Yang TC, Maluf NK.** 2012. Cooperative heteroassembly of the adenoviral L4-22K and IVa2 proteins onto the viral packaging sequence DNA. Biochemistry **51:**1357-1368.
166. **Zhang W, Arcos R.** 2005. Interaction of the adenovirus major core protein precursor, pVII, with the viral DNA packaging machinery. Virology **334:**194-202.
167. **Zhang W, Imperiale MJ.** 2000. Interaction of the adenovirus IVa2 protein with viral packaging sequences. J Virol **74:**2687-2693.

Appendices

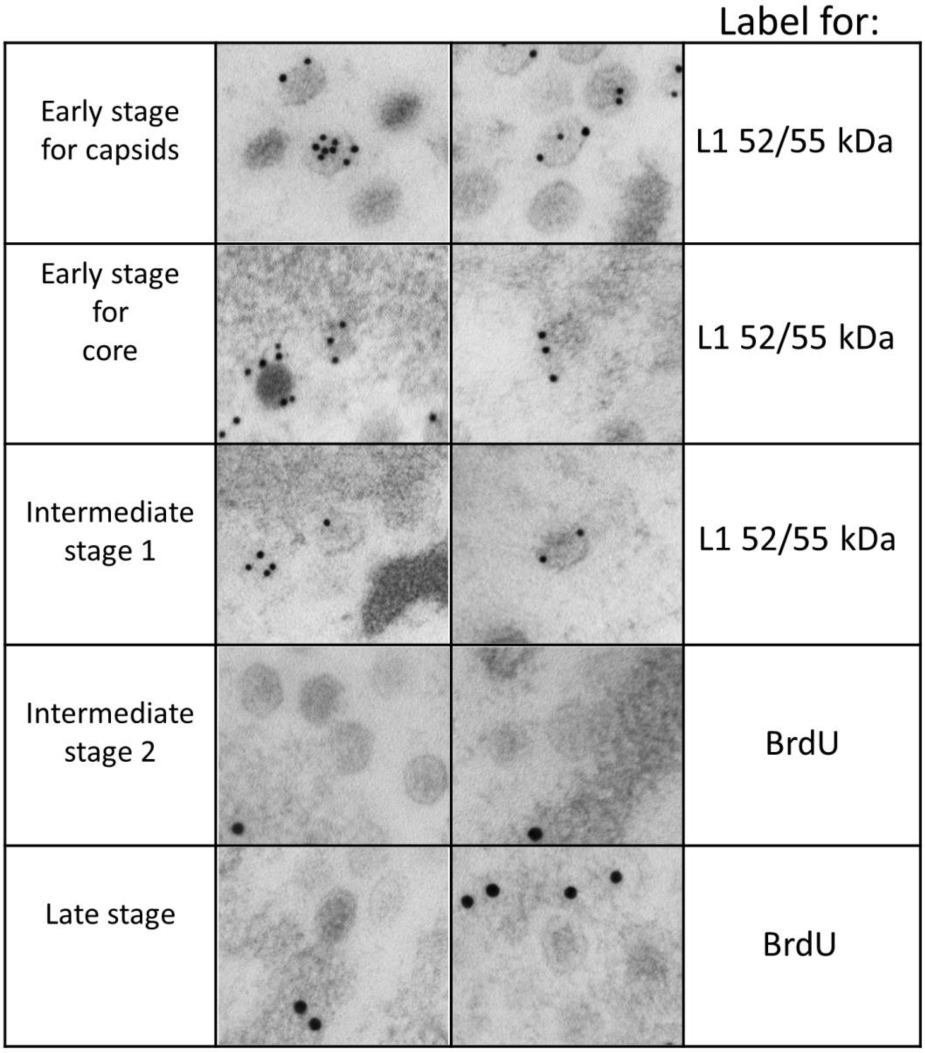
Label for:
Early stage for capsids
L1 52/55 kDa
Early stage for core
L1 52/55 kDa
Intermediate stage 1
L1 52/55 kDa
Intermediate stage 2
BrdU
Late stage
BrdU

Figure 40: Examples of different events in the AdV assembly model. Cells infected with Ad5/FC31 (48 hpi) and labeled against L1 52/55 kDa and BrdU. In the first stage, capsid caps are assembled. They contain L1 52/55 kDa, which would be used like a velcro to bind to other L1 52/55 kDa molecules or other packaging elements in the core. While in the DNA bundle, small condensations appear, also containing L1 52/55 kDa. In the intermediate stage 1, the caps bind to these condensations through L1 52/55kDa. The capsid goes on growing around the budding core (intermediate stage 2). Finally, in the late stage it is possible to observe almost complete capsids containing the core but still connected to the DNA bundles.

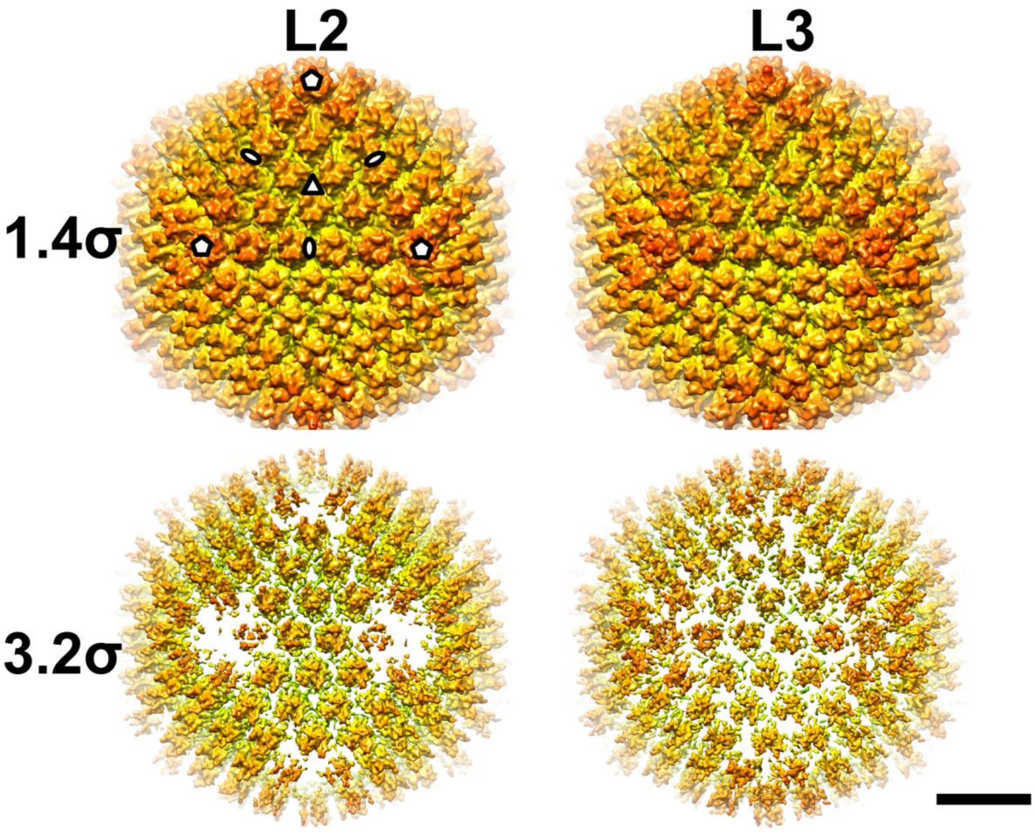

Figure 41: Occupancy of vertex proteins in Ad5/FC31 L2 and L3. Surface rendering of the L2 and L3 cryo-EM maps contoured at 1.4 and 3.2 standard deviations above the average map density, as indicated, and colored by radius. At 3.2σ only the strongest densities are conserved. In L3 these include the pentons, but in L2 the penton and part of the peripentonal hexon density are lost, indicating lower occupancy with respect to the rest of the capsomers. The scale bar represents 200 Å. Pentagons, ovals and a triangle indicate the positions of the 5-fold, 2-fold and 3-fold axes in one facet.

Publications

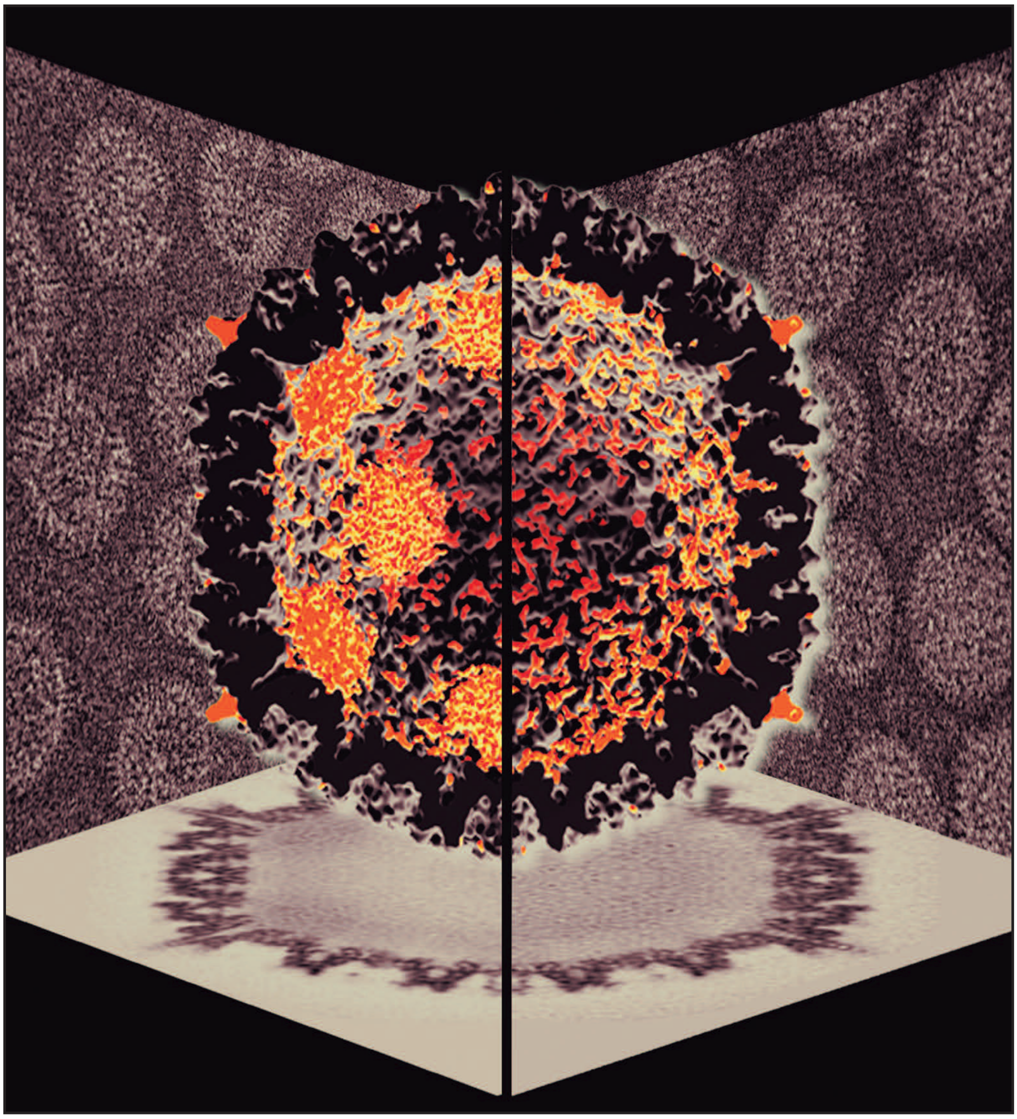

Published
Twice Monthly
by the
American
Society
for
Microbiology

Journal of Virology

AMERICAN
SOCIETY FOR
MICROBIOLOGY

JVI

OCTOBER 2015, VOLUME 89, NUMBER 20

Cover photograph (Copyright © 2015, American Society for Microbiology. All Rights Reserved.): Structural studies of incomplete human adenovirus particles show the localization of packaging protein L1 52/55k and how this localization changes during maturation. Difference maps (orange surfaces) between cryo-EM structures of the mature virion and two types of genome-lacking particles show that full-length L1 52/55k interacts preferentially with the inner vertex components (left). After partial processing by the maturation protease, this interaction is lost (right). *(See related article in September 2015, vol. 89, no. 18, p. 9653–9664.)*

Under Review

Mechanics of viral chromatin reveals the pressurization of human adenovirus

A. Ortega-Esteban[1], G. N. Condezo[2], A. J. Pérez-Berná[2†], M. Chillón[3], S. J. Flint[4], D. Reguera[5], C. San Martín[2], P. J. de Pablo[1]*

[1] Departamento de Física de la Materia Condensada, Universidad Autónoma de Madrid, 28049 Madrid (Spain)

[2] Department of Macromolecular Structure and NanoBioMedicine Initiative, Centro Nacional de Biotecnología (CNB-CSIC). Darwin 3, 28049 Madrid (Spain)

[3] Institut Català de Recerca i Estudis Avançats (ICREA), CBATEG-Department of Biochemistry and Molecular Biology, Universitat Autonoma Barcelona, Bellaterra Barcelona, 08010, Spain

[4] Department of Molecular Biology, Princeton University, Princeton, NJ 08544, USA

[5] Departament de Física Fonamental, Facultat de Física, Universitat de Barcelona, Martí i Franqués 1, 08028 Barcelona, Spain

[†] Present address: ALBA Synchrotron Light Source, MISTRAL Beamline Experiments Division, 08290 Cerdanyola del Vallès, Barcelona, Spain

*Corresponding author: p.j.depablo@uam.es